Development and Implementation of an Alternative Method for Complete Characterization of Surface-Breaking Cracks using Ultrasonic Rayleigh Waves

by

Bhupesh VERMA

MANUSCRIPT-BASED THESIS PRESENTED TO ÉCOLE DE TECHNOLOGIE SUPÉRIEURE IN PARTIAL FULFILLMENT FOR THE DEGREE OF DOCTOR OF PHILOSOPHY
Ph.D.

MONTREAL, "APRIL 8^{th}, 2024"

ÉCOLE DE TECHNOLOGIE SUPÉRIEURE
UNIVERSITÉ DU QUÉBEC

BOARD OF EXAMINERS

THIS THESIS HAS BEEN EVALUATED

BY THE FOLLOWING BOARD OF EXAMINERS

Mr. Pierre Bélanger, Thesis supervisor
Department of Mechanical Engineering, École de Technologie Supérieure

Mr. Ricardo Izquierdo, Chair, Board of Examiners
Department of Electrical Engineering, École de Technologie Supérieure

Mr. Martin Viens, Member of the Jury
Department of Mechanical Engineering, École de Technologie Supérieure

Mr. Zheng Fan, External Independent Examiner
School of Mechanical and Aerospace Engineering, Nanyang Technological University, Singapore

THIS THESIS WAS PRESENTED AND DEFENDED

IN THE PRESENCE OF A BOARD OF EXAMINERS AND THE PUBLIC

ON FEBRUARY 20^{th}, 2024

AT ÉCOLE DE TECHNOLOGIE SUPÉRIEURE

ACKNOWLEDGEMENTS

I would like to sincerely thank **Professor Pierre Bélanger** for providing me with the opportunity to undertake a project under his guidance. His constant encouragement, support, and motivation have been invaluable throughout my research journey. The knowledge and values I have gained from him will continue to guide me throughout my entire life.

I also want to express my gratitude to my MS thesis supervisor, **Professor Prabhu Rajagopal** at IIT Madras, for trusting in my work and recommending me for the PhD position at ETS Montreal.

Special thanks to my jury members, Professor Ricardo Izquierdo and Martin Viens, for their valuable suggestions that have elevated this work to a meaningful level with positive outcomes.

I am immensely grateful to all the members of PULETS for their invaluable contributions, assistance, and collaboration. A heartfelt thank you to Jorge for his help and support in getting me started with Pogo software and experiments. I would also like to extend my appreciation to Lucas for his assistance in conducting experiments and engaging in insightful discussions. Special thanks to Ricardo, Baptiste, Aubin, Sevan, Aurélien, Laura, Tony, and Adrien for generously sharing their expertise and knowledge with me

I would like to express my gratitude to my friends Satyendra Kumar Mishra and Prashant Dhondapure for being a source of support during my time in Canada. Their presence made my PhD journey far more enjoyable and fulfilling.

Finally, I want to express my deep love and gratitude to my parents, sisters, and my wife (Chitra) for their encouragement, understanding, and unwavering support. Last but not least, I thank everyone who has helped me directly or indirectly in all my activities here at ETS Montreal, Canada.

Développement et mise en œuvre d'une méthode alternative pour la caractérisation complète des fissures de surface en utilisant les ondes ultrasonores de Rayleigh

Bhupesh VERMA

RÉSUMÉ

Cette thèse se concentre sur le développement d'une nouvelle méthode pour caractériser les fissures de surface en utilisant des ondes de Rayleigh, offrant une alternative aux approches actuelles de contrôle non destructifs (CND). Les fissures de surface sont courantes dans de nombreuses industries, et les méthodes traditionnelles telles que le contrôle par courants de Foucault (CCF) présentent des inconvénients, nécessitant un étalonnage complexe et des inspecteurs hautement qualifiés. Le CCF rencontre également des défis dans les inspections de grandes surfaces, exigeant de nombreux balayages et ayant une profondeur de pénétration limitée, affectant la plage de détection. Un intérêt de recherche récent s'est développé autour de la méthode de dimensionnement des fissures avec les ondes de Rayleigh excitées avec un sabot en raison de son excitabilité unidirectionnelle et de sa capacité à balayer de grandes surfaces avec quelques emplacements de sonde. Cependant, des défis surviennent car les caractéristiques d'ondes de Rayleigh générées par les extrémités de fissure sont souvent faibles et masquées par le bruit et elles s'atténuent souvent avant d'atteindre la sonde réceptrice en raison du couplant à l'interface entre le sabot et la pièce. Par conséquent, dimensionner la profondeur de fissures est difficile en utilisant une configuration d'écho-impulsion si un sabot est utilisé. De plus, la flexibilité pour générer des ondes de Rayleigh sur différents guides d'ondes en utilisant le même sabot est limitée, car l'angle du sabot dépend de la longueur d'onde des ondes de Rayleigh. Cette thèse aborde ces problèmes en introduisant une méthode alternative d'excitation des ondes de Rayleigh en utilisant un transducteur multiélément conventionnel, offrant des capacités similaires à la technique de sabot mais surmontant ses limitations. Cette nouvelle méthode est ensuite étendue pour innover une approche de dimensionnement des fissures de surface basée sur un mode spécifique d'onde de Rayleigh converti provenant de la pointe d'une fissure, reposant uniquement sur les informations de temps de vol (TOF). De plus, une nouvelle méthode est introduite pour acquérir la capture complète de la matrice des ondes de Rayleigh (FMC), qui est ensuite utilisée avec l'algorithme d'imagerie de la méthode de focalisation totale (TFM) pour générer des images de fissures de surface. Cette approche complète permet la caractérisation complète des fissures de surface, y compris l'estimation de la longueur et de la profondeur en une seule mesure, une capacité absente dans les méthodes de CND existantes. Les performances des méthodes proposées sont démontrées par des simulations par éléments finis et des expériences. Les résultats de cette étude montrent un dimensionnement précis de la longueur et de la profondeur de la fissure avec une marge d'erreur de 5%. En conclusion, la thèse suggère que la méthode de caractérisation des fissures de surface présentée a le potentiel d'être une alternative appropriée aux méthodes actuelles de CND.

Mots-clés: imagerie des ondes de Rayleigh, réseau phasé, méthode d'excitation, dimensionnement des fissures de surface, FMC-TFM

Development and Implementation of an Alternative Method for Complete Characterization of Surface-Breaking Cracks using Ultrasonic Rayleigh Waves

Bhupesh VERMA

ABSTRACT

This thesis focuses on developing a new method for characterizing surface cracks using Rayleigh waves, providing an alternative to current nondestructive testing (NDT) approaches. Surface cracks are common in many industries, and traditional methods like eddy current testing (ECT) for crack sizing have drawbacks, requiring a complex calibration and highly trained inspectors. ECT also faces challenges in large-area inspections, demanding additional scanning arrangements and having limited penetration depth, affecting detection range. Recent research interest has grown in the wedge technique-based Rayleigh wave crack sizing method due to its unidirectional excitability and capacity to scan large areas with few probe locations. However, challenges arise as Rayleigh wave features generated at crack tips are often weak and masked by noise and they mostly attenuate before reaching the receiving probe due to the couplant at the wedge-test specimen interface. Consequently, sizing the crack depth is difficult using a pulse-echo setup. Moreover, the flexibility to generate Rayleigh waves on different waveguides using the same wedge is limited, as the wedge angle depends on the Rayleigh wave wavelength. This thesis addresses these issues by introducing an alternative Rayleigh wave excitation method using a conventional phased array transducer, offering capabilities similar to the wedge technique but overcoming its limitations. This new method is then extended to innovate a surface crack sizing approach based on a specific mode-converted Rayleigh wave originating from the crack tip, relying solely on time-of-flight (TOF) information. Moreover, a novel method is introduced for acquiring Rayleigh wave full matrix capture (FMC), which is then utilized with the total focusing method (TFM) imaging algorithm to generate images of surface cracks. This comprehensive approach allows for the complete characterization of surface cracks, including length and depth estimation in a single measurement—a capability lacking in existing NDT methods. The performance of the proposed methods is demonstrated through finite element simulations and experiments. The findings of this thesis demonstrate accurate sizing of the crack length and depth within a 5% error margin. In conclusion, the study suggests that the presented surface crack characterization method has the potential to be a suitable alternative to current NDT methods.

Keywords: Rayleigh wave imaging, Phased array, Excitation method, Surface crack sizing, FMC-TFM

TABLE OF CONTENTS

LIST OF TABLES

LIST OF FIGURES

LIST OF ABBREVIATIONS

ECT	Eddy Current Testing
EMAT	Electro Magnetic Acoustic Transducer
FEM	Finite Element Method
FMC	Full Matrix Capture
HSTFM	Half Skip Total Focusing Method
IDT	Interdigital Transducers
IRT	Infrared Thermography
MPI	Magnetic Particle Inspection
NDE	Nondestructive Evaluation
NDT	Nondestructive Testing
PAUT	Phased Array Ultrasonic Testing
PT	Penetrant Testing
PWI	Plane Wave Imaging
ROI	Region of Interest
SAFT	Synthetic Aperture Focusing Technique
SNR	Signal-to-Noise Ratio
SBCs	Surface-breaking cracks
TFM	Total Focusing Method
TOF	Time of Flight

UT	Ultrasonic Testing
L	Longitudinal wave
S	Shear wave

LIST OF SYMBOLS AND UNITS OF MEASUREMENTS

A_1 , B_1	Arbitrary constant
λ, μ	Lamé constants
λ_R	Rayleigh wave wavelength
c	Wave velocity
c_l	Longitudinal wave velocity
C_R	Rayleigh wave velocity
c_t	Shear wave velocity
d_e	Distance between emitter to pixel
d_r	Distance between pixel to receiver
H	Hilbert transform
$I(x, y)$	Image intensity
k	Wave number
N	Number of elements in the phased array transducer
ω	Angular frequency
ϕ	Scalar potential
ν	Possion's ratio
ρ	Material density
S_{ij}	Time trace signals from all potential transmitter-receiver pairs
t_{ij}	Arrival time of Rayleigh waves traveling from the emitter (i) to the pixel P, and then returning to the receiver (j)

$\vec{u}$	Displacement vector
u	Displacement component along the y-axis
v	Displacement component along the z-axis
$\vec{\psi}$	Vector potential
x_i	Spatial position of i^{th} emitter in the x-direction
x_j	Spatial position of j^{th} receiver in the x-direction
(x_p, y_p)	The coordinates of pixels within the ROI
∇^2	Three dimensional Laplace operator

INTRODUCTION

Solid structures, used across various industries including aerospace, power plants, railways, and petrochemicals face harsh operational and environmental conditions that can generate surface discontinuities. These discontinuities, if left unaddressed, may convert into stable cracks imposing limitations on the service life of components and, in worst cases, leading to catastrophic failures. Such failures can have a substantial impact on both the environment and the economy. To avoid these risks and ensure structural safety and reliability, regular inspections are of vital importance.

Nondestructive testing (NDT) techniques offer a potential solution, allowing for the inspection of components while in service without hampering their functionality and properties. Various NDT techniques, such as penetrant testing (PT), magnetic particle inspection (MPI), eddy current testing (ECT), thermography (IRT), and ultrasonic testing (UT), are commonly employed. However, each method has its limitations. For instance, MPI is confined to ferromagnetic materials, and the need for demagnetization after each test is a requirement. Similarly, ECT faces challenges in conducting large area inspections due to the requirement for additional scanning arrangements, demands complex calibration for accurate depth and length sizing, and has limited penetration depth. PT has constraints related to careful surface preparation and is not suitable for sub-surface cracks. Moreover, PT is recognized as a potentially polluting method and regulatory attention has been drawn to its environmental impact, necessitating the removal of pollutants post-inspection, leading to concerns about subsequent sedimentation. This has prompted a search for alternative approaches.

UT, known for its flexibility, offers various inspection configurations. Among these, ultrasonic Rayleigh waves present unique characteristics, being the simplest form of ultrasonic guided waves with their energy concentrated to within a few wavelengths of the surface on which they propagate. This makes Rayleigh waves highly sensitive to surface and near-surface

discontinuities. Additionally, their ability to propagate over long-distance allows for efficient inspections of large areas with minimal probe locations. Therefore, the use of Rayleigh waves presents an attractive and suitable solution for characterizing surface cracks. Hence, the choice was made to utilize ultrasonic Rayleigh waves for the current study.

The generation of Rayleigh waves can be accomplished using various methods, among which the most accepted and widely employed wedge technique stands out. Recent years have seen more research interest in utilizing Rayleigh waves for surface crack detection and sizing, using the wedge technique for wave excitation and detection. However, this method is not without its drawbacks, as Rayleigh waves undergo transmission loss at the interfaces of the wedge. Additionally, the flexibility to excite Rayleigh waves on different waveguides using a single wedge is limited due to the dependence of the wedge angle on the Rayleigh wave wavelength. The features of Rayleigh waves generated at crack tips often face challenges, appearing weak and obscured by signal noise, and they mostly attenuate before reaching the receiving transducer due to the couplant between the wedge face and test specimen surface. As a result, the sizing of crack depth remains unattainable in a pulse-echo setup.

Furthermore, despite a significant body of research dedicated to surface crack detection and characterization using Rayleigh waves, existing studies are limited to sizing either surface crack length or depth independently. None of these studies offers a comprehensive characterization method that allows for simultaneous estimation of both surface crack length and depth in a single measurement. Therefore, it is essential to develop an alternative approach for Rayleigh wave generation and detection, capable of overcoming the limitations associated with the wedge technique. Moreover, this new approach of generation and detection should extend to innovating a method for the complete characterization of surface-breaking cracks, facilitating combine estimation of both crack length and depth in a single measurement. Overall, this initiative also seeks to provide an appropriate alternative to existing NDT techniques, such as ECT or PT.

This thesis, therefore, aims to develop a new NDT method for characterizing surface cracks using Rayleigh waves, offering an alternative to current NDT methods. The collaborative aspect of this project involves Siemens Energy Canada as the industrial partner, enhancing the practicality and real-world applicability of the proposed method. The research is structured into two main sections:

- To begin with, a comprehensive literature review was undertaken to identify the limitations of the wedge technique, which is currently considered the most efficient method for generating Rayleigh waves. Consequently, the primary focus of this research is on developing an alternative method for exciting Rayleigh waves. This novel approach is designed to replicate the excitation capabilities inherent in the wedge technique, including selective and unidirectional Rayleigh wave generation and propagation. This is achieved using a conventional phased array transducer, and all without the need for a wedge. Notably, the proposed method not only provides comparable excitation capabilities to those associated with the wedge technique but also enhances flexibility by allowing excitation on different waveguide materials using the same phased array transducer and using a wide range of frequencies as well.
- Subsequently, the study utilizes the new Rayleigh wave excitation approach to innovate a method for characterizing surface cracks. This method provides the simultaneous estimation of surface crack length and depth in a single measurement—an ability lacking in existing NDT methods. The idea is for this method to serve as a suitable alternative to existing methods for the complete characterization of surface cracks.

The subsequent structure of the thesis is as follows: Chapter 1 provides a background on the theory of Rayleigh wave propagation, followed by a thorough literature review within the scope of the current research. This is followed by an identification of gaps in previous work and the definition of objectives for this research. The subsequent three chapters showcase the articles

published and submitted during the research. Finally, the last section offers conclusions drawn from this work and outlines its future direction.

CHAPTER 1

THEORY OF RAYLEIGH WAVE PROPAGATION AND LITERATURE REVIEW

1.1 Background: Ultrasonic waves

Ultrasonic inspection is one of the most widely used NDT techniques for both flaw detection and material characterization. In standard ultrasonic inspection, high-frequency acoustic waves ranging from 0.1 to 30 MHz are transmitted into a material, propagating as mechanical waves. As these ultrasonic waves interact with geometric or material irregularities, their energy is either reflected, diffracted, or refracted. The reflected and transmitted waves carry the signal information, including amplitude and time of flight. Utilizing this information crack location, size, and orientation can be inferred. Acoustic bulk waves, commonly employed in inspection, exist as longitudinal waves (L) and shear waves (S) within the bulk of a homogeneous elastic medium. Interaction of these bulk waves with boundaries results in mode conversion between longitudinal and shear waves. The superposition of these waves, due to multiple reflections from the boundaries, leads to constructive interference and the potential formation of ultrasonic-guided wave modes. The fundamental distinction between bulk and guided waves lies in their travel paths: guided waves either propagate at the boundary (known as surface waves or Rayleigh waves (Rayleigh (1888)) or travel within the medium enclosed by the structure's boundaries (known as a Lamb wave (Lamb (1917)). Additionally, certain wave modes are also guided by the interface between two media, such as Stoneley waves at a solid-solid interface or Scholte waves at a liquid-solid interface. In contrast, bulk waves travel within the material's bulk, away from the boundary.

Bulk waves and guided waves are governed by the same set of partial differential equations, which is also known as the wave equation. The principal difference in the mathematical solution of these two waves is that there is no requirement for boundary conditions in the case of bulk waves. Conversely, a guided wave problem must adhere to both the governing equations and physical boundary conditions at the structure's boundaries, such as the traction-free surfaces of the bounded medium. The fundamental principles of guided waves are very well discussed

and documented in many classical textbooks (Eason (1975), Auld (1990), Rose (1999)). Given that this work focuses on understanding the interaction of Rayleigh waves with surface defects, a thorough understanding of how they generate, propagate, and interact with discontinuities is necessary. Therefore, a detailed review of guided waves is omitted, and only the key characteristics of Rayleigh waves are explored in this chapter.

The subsequent sections of this chapter begin by introducing the theory of ultrasonic Rayleigh wave propagation. Following this, a thorough review of the literature within the scope of this research is presented. By evaluating recent contributions from researchers in the field of surface crack characterization using Rayleigh waves, gaps in previous work are identified. Finally, the objectives are defined, and the contributions from this research work are stated.

1.1.1 Rayleigh waves

The existence of Rayleigh waves was first described long ago in 1885 by Rayleigh (1888). Rayleigh waves are one among the various ultrasonic guided wave modes, which exist on the surface of a semi-infinite solid. Rayleigh waves exhibit a unique behavior where longitudinal and shear displacements of a particle are closely coupled, propagating at a common velocity, which is distinct from the longitudinal and shear acoustic plane wave velocity. The energy of Rayleigh waves is concentrated within approximately one wavelength (λ_R) beneath the surface along their path, with energy diminishing as depth increases. This characteristic makes Rayleigh waves particularly suitable for detecting surface and sub-surface discontinuities. Before being able to use Rayleigh waves for the detection and sizing of surface discontinuities, a thorough understanding of the theory of Rayleigh wave propagation is essential. The equation governing Rayleigh wave propagation is well-documented in various textbooks (Auld (1990), Eason (1975), Rose (1999), Viktorov (1967)). In the subsequent sub-section, we briefly derive this equation, closely following the treatment given in Rose (1999).

1.1.2 Rayleigh wave propagation

Let's examine the polarization of a wave within the sagittal (yz) plane, where the surface normal aligns with the z-axis, and the propagation occurs in the y-direction, depicted in Figure 1.1. In this configuration, the velocity and displacement components are oriented in the y and z directions.

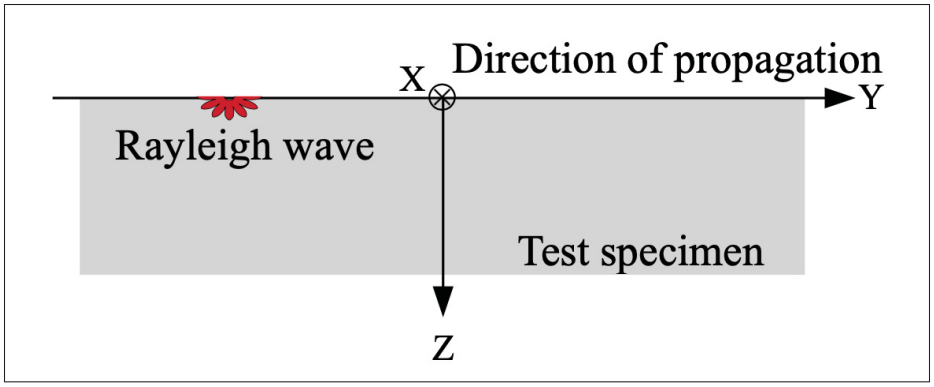

Figure 1.1 Coordinate system and Rayleigh wave propagation in the region where z > 0 on a semi-space medium

Navier's differential equation of motion for an isotropic elastic medium (neglecting body forces) is expressed as follows:

$$(\lambda + \mu)\nabla\nabla\vec{u} + \mu\nabla^2\vec{u} = \rho\frac{\partial^2\vec{u}}{\partial t^2} \tag{1.1}$$

where $\vec{u}$ represents the three-dimensional displacement field, ρ is the material density, and λ and μ are two material constants also known as Lamé constants. The symbol ∇^2 denotes the three-dimensional Laplace operator.

The displacement vector $\vec{u}$ can be expressed through the Helmholtz decomposition as the gradient of a scalar and the curl of the zero divergence vector:

$$\vec{u} = \nabla\phi + \nabla\times\vec{\psi} \tag{1.2}$$

Inserting the potential function, as given in Equation 1.2, into Navier's governing wave Equation 1.1 results in the separation of the equation of motion into two distinct equations-one for longitudinal waves and another for shear waves:

$$\begin{aligned} \nabla^2\phi &= c_l^2 \frac{\partial^2 \phi}{\partial t^2} \\ \nabla^2\vec{\psi} &= c_t^2 \frac{\partial^2 \vec{\psi}}{\partial t^2} \end{aligned} \tag{1.3}$$

where c_l and c_t are longitudinal and shear wave velocities.

The harmonic solution for Equation 1.3, representing the propagation of a bulk wave with angular frequency ω in the y-direction (refer to Figure 1.1), can be written as:

$$\begin{aligned} \phi &= F_1(z)e^{i(ky-\omega t)} \\ \vec{\psi} &= F_2(z)e^{i(ky-\omega t)} \end{aligned} \tag{1.4}$$

By substituting Equation 1.4 into Equation 1.3 and omitting the impractical part of the solution that does not attenuate, we obtain the following expression:

$$\begin{aligned} \phi &= A_1 e^{-kqz} e^{i(ky-\omega t)} \\ \psi &= B_1 e^{-ksz} e^{i(ky-\omega t)} \end{aligned} \tag{1.5}$$

where

$$q = \sqrt{1 - \left(\frac{c}{c_l}\right)^2}, s = \sqrt{1 - \left(\frac{c}{c_t}\right)^2}, c = \frac{\omega}{k} \tag{1.6}$$

and A_1 and B_1 are arbitrary constants. The expressions for the displacement components u and v along the y and z axis respectively, can be written as:

$$\begin{aligned} u &= k(iA_1 e^{-kqz} - B_1 s e^{-ksz}) e^{i(ky-\omega t)} \\ v &= k(-A_1 q e^{-kqz} - iB_1 e^{-ksz}) e^{i(ky-\omega t)} \end{aligned} \tag{1.7}$$

From Equation 1.7, and on the basis of Hooke's law stress components can be derived as:

$$\begin{aligned} \sigma_{yy} &= \mu k^2 (A_1(s^2 - 2q^2 - 1) e^{-kqz} - 2iB_1 s e^{-ksz}) e^{i(ky-\omega t)} \\ \sigma_{zz} &= \mu k^2 (A_1(1 + s^2) e^{-kqz} + 2iB_1 s e^{-ksz}) e^{i(ky-\omega t)} \\ \sigma_{yz} &= \mu k^2 (-2iA_1 q e^{-kqz} + 2B_1(1 + s^2) e^{-ksz}) e^{i(ky-\omega t)} \end{aligned} \tag{1.8}$$

Now imposing the boundary condition $\sigma_{zz} = \sigma_{yz} = 0$ for $z = 0$, relation bwtween A_1 and B_1 can be obtained:

$$A_1 = \frac{-2is}{1 + s^2} B_1 \tag{1.9}$$

with some algebraic manipulation, the Rayleigh wave velocity equation is given as

$$\eta^6 - 8\eta^4 + 8(3 - 2\zeta^2)\eta^2 + 16(\zeta^2 - 1) = 0 \tag{1.10}$$

where

$$\begin{aligned} \eta &= \frac{c}{c_t} \\ \zeta &= \frac{c_t}{c_l} = \sqrt{\frac{1 - 2\nu}{2(1 - \nu)}} \end{aligned} \tag{1.11}$$

Equation 1.10 represents the Rayleigh wave velocity equation, which possesses six roots. However, only one of these, denoted as η_R, corresponds to the existence of the Rayleigh wave. η_R is solely a function of the Poisson's ratio, ν, and is independent of frequency, indicating that

Rayleigh waves are nondispersive. Within the permissible range of Poisson's ratio ($0 < \nu < 0.5$), the Rayleigh wave velocity ranges from 87% to 96% of the shear wave velocity.

1.1.3 Rayleigh wave excitation and reception

Rayleigh wave excitation and reception are possible through various methods, broadly classified as contact and non-contact methods, and are comprehensively reviewed in (Chakrapani & Bond (2018)). Non-contact methods offer the benefit of not requiring a couplant for inspections. However, for accurate crack sizing, achieving the required maximum operating frequency or bandwidth can be challenging. Laser-based methods are common but they are expensive due to the high-cost equipment involved as well safety concerns are major constraints. The use of piezoelectric transducers is therefore widespread due to their affordability. This serves as the basis for choosing a piezoelectric transducer for the excitation and reception of Rayleigh waves in the current work. The simplest approach involves placing a longitudinal or shear wave transducer in contact with the specimen's surface using a couplant (Rose (1999)), but this lacks control over transmitted waves, making it inefficient (Chakrapani & Bond (2018)). Various piezoelectric transducer methods for Rayleigh wave generation have been developed, including comb transducers (Penttinen & Luukkala (1974); Hurley (1999); Zhang, Cheng, Li & Kundu (2022)) and interdigital transducers (IDT) (Na & Blackshire (2010); Moulzolf, Behanan, Pollard, Lad & da Cunha (2013)). Comb transducers use an array of elements with a pitch matching the Rayleigh wavelength. Overlapping two comb transducers creates an IDT. However, adapting to frequency or material changes demands a new transducer (Chakrapani & Bond (2018)). A flexible fixture was designed to overcome this limitation (Barnard (2007)), but the generation of other plate modes along with Rayleigh waves brings complexity to signal processing.

The wedge technique provides better Rayleigh wave excitation and detection efficiency compared to other methods (Chakrapani & Bond (2018); Rose (1999)). It involves converting longitudinal waves into Rayleigh waves through refraction at the wedge-test specimen interface as illustrated in Figure 1.2. While ensuring Rayleigh waves transmit in only one direction, the coupling condition is not constant, necessitating a couplant. However, Rayleigh wave features generated

at crack tips are often weak, masked by noise, and attenuate before reaching the receiving probe due to the couplant. Consequently, sizing crack depth is challenging using a pulse-echo setup with the wedge technique. Moreover, despite being considered the most efficient and accepted, transmission losses at the wedge interfaces (Ohara *et al.* (2017); Zhang, Li & Jeong (2017)) and inflexibility for different waveguides using the same wedge pose challenges (Chakrapani & Bond (2018)). Therefore, the development of an alternative Rayleigh wave excitation method that ensures unidirectional and selective excitation and offers sufficient flexibility for various materials using the same transducer is a primary focus of this research. Additionally, it should also offer excitability using a broad range of frequencies.

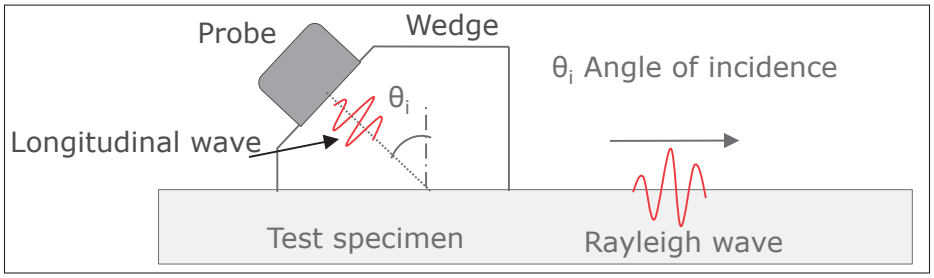

Figure 1.2 Cross-sectional view illustrating the generation of Rayleigh waves using the wedge technique

1.2 Phased-array ultrasonic testing (PAUT)

Phased Array Ultrasonic Testing (PAUT) has become well established, finding a significant surge in its application across diverse industries for nondestructive evaluation (NDE) in recent years. It offers greater flexibility compared to mono-element transducer-based conventional UT. The fundamental principle of conventional UT is briefed at the beginning of this chapter and can be referenced in classical textbooks like (Cheeke (2012); Rose (1999)). Within the scope of the current research focus, this section presents multi-element transducers, commonly referred to as phased array transducers, which will play a pivotal role in the transmission and reception of Rayleigh waves throughout the project. Additionally, it provides an overview of the

corresponding wave transmission scheme and imaging technique that will be employed later in this study.

Unlike mono-element transducers, phased array transducers consist of multiple piezoelectric elements, each with individual transmission and reception control. By introducing appropriate delays between the emissions of each element, an oriented and focused wavefront can be steered in the desired depth and direction. Leveraging this flexibility, a linear time delay is designed and implemented to a conventional linear phased array in this project, achieving equivalent Rayleigh wave excitation capabilities to what is present when using the wedge technique. Phased array transducers offer an additional benefit in that they can gather comprehensive defect information by illuminating the defect from a broad range of angles. Following this, the collected data can undergo processing to facilitate imaging through the application of various post-processing techniques such as synthetic aperture focussing technique (SAFT) (Seydel (1982)), total focusing method (TFM) (Holmes, Drinkwater & Wilcox (2005)), inverse wave-field extrapolation (Portzgen, Gisolf & Blacquiere (2006)), the wave number algorithm (Hunter, Drinkwater & Wilcox (2008)), and plane wave imaging (PWI) (Le Jeune, Robert & Prada (2016)). While all these methods aim to generate high-resolution images, TFM exhibits superior relative performance and is widely acknowledged as the "gold standard" in the field of NDT.

Phased array probes come in various configurations, including linear probes (the most common), matrix probes, annular probes, curved, focused, etc. Initially, a linear phased array is employed in this project to develop a wedge-free Rayleigh wave excitation method. Subsequently, this excitation method is expanded to encompass a matrix phased array transducer for acquiring Rayleigh wave FMC, followed by the TFM imaging technique to visualize a surface crack. Since commercial phased array transducers are utilized, the design and construction aspects of the probes are not detailed here, but such information can be found in textbooks like (Schmerr (2015)). The wave transmission and imaging techniques employed in this study are briefly presented in the following subsection.

1.2.1 Full matrix capture (FMC)

FMC is an ultrasonic data acquisition scheme, that offers comprehensive time domain signal information, including amplitude and time of flight (Sutcliffe, Weston, Dutton, Charlton & Donne (2012)). The underlying principle of the FMC process is depicted in Figure 1.3. In the FMC acquisition approach, each element within the array transducer is sequentially excited, followed by reception at all elements. As a result, a N-element array generates a matrix containing a total of $N \times N$ time trace signals, each corresponding to a potential transmitter-receiver combination. The FMC matrix, with dimensions $l \times N \times N$ (where l represents the length of the time trace signal), is gaining popularity due to its advantage of including all ultrasonic data from the inspection. This allows for the execution of imaging or beamforming methods either in real-time or in the post-processing of the FMC data. The only drawback lies in the substantial amount of data to be stored and processed, a trade-off compensated by its inherent flexibility (Holmes *et al.* (2005)).

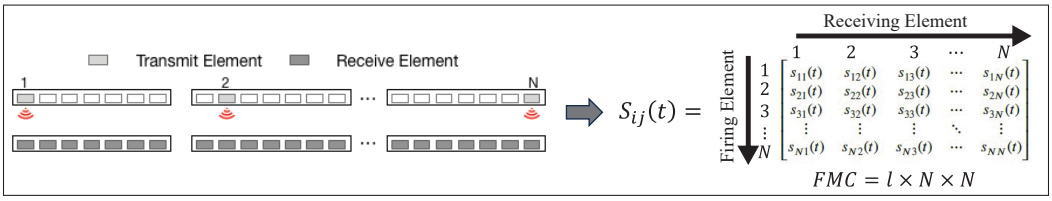

Figure 1.3 Illustration of full matrix capture process

1.2.2 Total focusing method (TFM)

TFM is an advanced post-processing algorithm designed to generate images of a specific region of interest (ROI) within a test specimen using FMC data, as introduced by Holmes *et al.* (2005). Initially applied to produce cross-sectional images with bulk waves, the TFM algorithm has more recently been employed for capturing surface crack images utilizing Rayleigh waves (Hoyle, Sutcliffe, Charlton & Mosey (2019); Ducousso & Reverdy (2020)). This application is based on FMC data obtained using a linear phased array mounted on a wedge to generate Rayleigh waves. However, limitations associated with the wedge technique hinder the widespread application

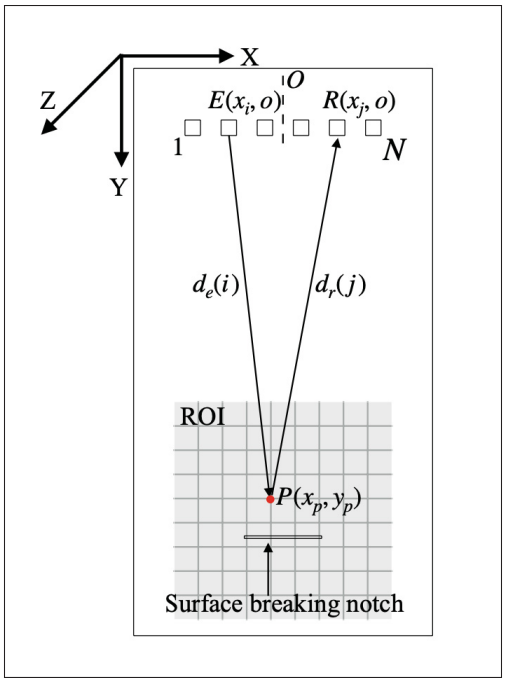

Figure 1.4 Schematic illustrating the principle of Rayleigh wave FMC-TFM imaging (the surface normal aligns with the Z-axis)

of this approach. In this study, we address this issue by introducing a novel Rayleigh wave FMC acquisition approach (presented in Chapter 4). The Rayleigh wave FMC acquired using the proposed method will be utilized for imaging surface cracks through the TFM imaging algorithm, as schematically illustrated in Figure 1.4.

The process starts by dividing the ROI into a grid of pixels. Following this, a coherent summation of signals from all possible transmitter-receiver pairs occurs, resulting in the synthesis of focal points at each pixel location and generating a fully focused image. The intensity of the image at each pixel point P, represented as $I(x, y)$, can be described as:

$$I(x,y) = \left| \sum_{i=1}^{N} \sum_{j=1}^{N} H\left(S_{ij}(t_{ij})\right) \right| \tag{1.12}$$

where H refers to the Hilbert transform, S_{ij} denotes the time trace signals from all potential transmitter-receiver pairs, and t_{ij} represents the arrival time of Rayleigh waves traveling from the emitter (i) to the pixel P, and then returning to the receiver (j). Assuming that Rayleigh waves travel along the path that minimizes travel time, adhering to Fermat's principle, this arrival time can be estimated using the following equation:

$$t_{ij} = \frac{d_e(i) + d_r(j)}{C_R} = \frac{\sqrt{(x_p - x_i)^2 + y_p^2} + \sqrt{(x_p - x_j)^2 + y_p^2}}{C_R} \tag{1.13}$$

where, x_i and x_j denote the spatial positions of i^{th} emitter and j^{th} receiver, respectively, in the x-direction with respect to the origin O, assuming it is at the center of the array. (x_p, y_p) represents the coordinates of pixels within the ROI, and C_R is the Rayleigh wave velocity of the waveguide.

1.3 Review of existing methods for detecting and sizing surface cracks

1.3.1 Magnetic particle inspection (MPI)

Magnetic particle inspection (MPI) is the oldest and most effective NDT method for identifying both surface and subsurface cracks. The process involves magnetizing a test sample, where surface discontinuities create a distortion in the magnetic field, causing a leakage field beyond the sample's surface. Ferrous particles, either dry or wet, are then applied to the sample, accumulating in the region of flux leakage and highlighting an indication of crack mouth (Bowler & Bowler (2002)). Lee *et al.* (2003) conducted finite element simulations to analyze the sensitivity of MPI for defects with various sizes and geometries, leading to an enhanced understanding of the method. A similar study by (Wong *et al.* (2010)) utilized a three-dimensional finite element model to simulate MPI and explore the influence of defect dimensions on magnetic flux density. The research concluded that increased defect depth yields better MPI indications, while defect width has minimal significance. Successful MPI inspection relies on maintaining the magnetic flux density within a specific range; low density may result in no indication,

while high density increases background noise and reduces sensitivity. The complexity of MPI, influenced by numerous parameters, led to the development of typical MPI tests for improved sensitivity (Eisenmann, Enyart, Lo & Brasche (2014)). Studies by Zolfaghari, Zolfaghari & Kolahan (2018) focused on analyzing the detection abilities, reliability, and sensitivity of MPI in identifying surface cracks in welded components, utilizing real samples. However, interpretation of MPI results has traditionally relied on empirical knowledge and experience-based approaches, demanding highly skilled and trained inspectors and increasing inspection costs. Addressing this limitation, Ma, Sun, Zhang & Chen (2016) introduced an automated fluorescent magnetic particle inspection system assisted by machine vision, reducing inspection costs and enhancing repeatability. Despite significant advancements, MPI has inherent limitations, such as applicability only to ferromagnetic materials, requiring demagnetization after each test, and the inability to assess the depth of detected defects.

1.3.2 Penetrant testing (PT)

Penetrant Testing (PT), also known as Liquid Penetrant Testing, is an NDT method often used for detecting surface-accessible defects in solid components, applicable to both ferrous and non-ferrous materials. The basic principle involves applying penetrant to the surface of the testpiece, drawn into surface cracks through capillary action. After allowing sufficient penetration time, the excess amount of penetrant is removed, and a developer, either in dry or liquid form, is applied. The residual penetrant absorbed by the developer indicates the presence of defects on the testpiece's surface (Bray & Stanley (2018)). Fluorescent penetrants are commonly utilized in PT. A major constraint of PT is its applicability solely for detecting surface-breaking cracks. Additionally, a good surface finish is important for easy removal of excess penetrant (Cawley (2001)). In cases of inadequate surface finish, surface preparation is required before each test, leading to increased time consumption and inspection costs. Similar to Magnetic Particle Inspection (MPI), PT result interpretation majorly relies on the operator's empirical knowledge and experience, making the reliability of the method subject to human factors. Moreover, PT is a potentially polluting technique and is currently under scrutiny due to

its environmental impact, along with concerns about the proper sedimentation of pollutants after inspection.

1.3.3 Eddy current testing (ECT)

Eddy current testing (ECT) is a well-established and widely used inspection method for detecting flaws, measuring thickness, and assessing conductivity. It also allows for obtaining defect dimensions through electric impedance change analysis. The material under inspection must be electrically conductive for ECT to be effective. The method involves exciting an alternating current in a coil positioned slightly above the surface to be examined, generating an alternating magnetic field that induces eddy currents in the surface of the test specimen. These induced eddy currents create a magnetic field opposing that of the coil, influencing its electrical impedance. Defects, such as cracks, impede the flow of current, leading to changes in the magnetic field and, consequently, in the coil impedance (Bray & Stanley (2018)). The liftoff, or the distance between the coil and the testpiece surface, is a crucial parameter, determining the sensitivity of the method. An experimental study by Blitz, Willsttäter, Oaten & Hajian (1987) explored sizing surface cracks using ECT with a high liftoff, reporting success in detecting and sizing surface cracks with liftoff values exceeding 12 mm. Research by Bowler & Bowler (2002) introduced a method for determining the size and shape of planar cracks using impedance measurements of a normal coil on simulated cracks. He & Yoshizawa (2002) developed a dual-frequency ECT system, effectively controlling unwanted signals caused by liftoff variance through appropriate excitation frequencies. Studies by Helifa *et al.* (2006) optimized various factors influencing ECT's operation for surface crack detection and sizing. Hur, Choi, Lee, Kim & Han (2010) evaluated the detection and sizing accuracy of ECT using steam generator tubes with circumferential and intergranular attack cracks. Betta, Ferrigno & Laracca (2011) proposed a low-cost handheld ECT instrument for detecting, locating, and characterizing thin defects such as superficial and sub-superficial cracks. An ECT system with a highly sensitive anisotropic magnetoresistive (AMR) sensor was developed by He, Zhang, Shiwa & Moriya (2013) for detecting defects in liquid rocket engine combustion chambers. He, Wang, Kusano,

Kishimoto & Watanabe (2019) reported the development of a new ECT system with a high-sensitivity magnetic sensor, comparing its performance with a traditional ECT system on a 3D-printed titanium alloy sample with surface cracks. In spite of its widespread implementation across various industries, ECT possesses several disadvantages and limitations. Achieving accurate depth and length sizing of surface cracks with ECT is challenging, as it demands complex calibration standards (Van Drunen & Cecco (1984); Fan, Cao, Yang, Li & Tian (2015)). ECT operates as a point test and needs complete scanning for large-area inspections. This aspect makes the process time-consuming and complex, especially when additional scanning arrangements are required to cover expansive surface areas. The method experiences signal losses, particularly in tightly closed cracks like fatigue cracks, further affecting measurement accuracy.

1.3.4 Ultrasonic methods

Detection and sizing of surface-breaking cracks (SBCs) through ultrasonic waves constitute an important aspect of NDT. Both ultrasonic-guided and bulk waves find applications in this area. A comprehensive review of available methods for defect sizing using mono-element transducers was conducted by Doyle & Scala (1978). These methods fall into three categories. The first involves capturing signal information scattered from the cracks and comparing its amplitude to that of a known artificial standard defect to estimate crack depth. The second relies on measuring transit times of waves along crack faces and deducing crack dimensions from these measurements. The third approach utilizes ultrasonic spectroscopic analysis to measure small cracks and map the morphology of crack faces. Considering the primary interest of this research, a detailed review of the state-of-the-art in utilizing ultrasonic Rayleigh waves for surface crack characterization is presented in the next subsection. However, the recent research on bulk waves using ultrasonic arrays for sizing SBCs is cited here.

The characterization of crack-like defects was presented in a study by Zhang, Drinkwater & Wilcox (2010), considering two different approaches. In the first approach, the scattering coefficient matrix (S-matrix) obtained through the inverse back propagation method was utilized for

characterizing small cracks. For larger cracks, the second approach involved direct measurement of features from a high-resolution image obtained using the TFM algorithm. In the TFM algorithm, only direct ray paths between the array and image pixel points are considered, without capturing specular reflection from the crack faces. Consequently, the TFM reconstructed image only shows indications from the tip and root of the cracks. However, the tip indications often exhibit poor SNR, posing challenges for reliable crack depth measurement. A new approach to measure the depth of a small crack using a half-skip configuration of TFM (HSTFM) was introduced by Felice, Velichko & Wilcox (2014), claiming superior reliability in measuring cracks with a depth of less than 1 mm compared to other methods. Similar work conducted by Peng, Bai, Zhang & Drinkwater (2018) aimed to examine the performance of defect characterization using both array image-based and S-matrix-based sizing techniques. The approach demonstrated the capability to size crack depths in the range of 0.78-1.84 wavelengths. In a recent development, a hybrid imaging method using a linear array combining HSTFM and the SAFT was proposed by Saini, Lane, Tu, Xue & Fan (2022). This method provides a high-resolution volumetric image of SBCs, allowing for accurate estimation of the shape and size of the cracks. While ultrasonic arrays have a wide range of applications in characterizing SBCs, they, however, limited to the characterization of SBCs located on inaccessible back surfaces of components.

1.3.5 Rayleigh wave-based methods

The research contributions made by authors in the area of surface crack detection, measurement, and imaging utilizing Rayleigh waves are presented here. Ultrasonic Rayleigh waves have been utilized for in-service NDT inspections of surface cracks on solid parts across various industries for an extended period. The exploration of surface wave techniques for inspecting surface-opening cracks was initially presented by Silk (1976), aiming to identify both the limitations and potential of this approach. The ultrasonic timing method based on TOF of ultrasonic waves to follow the various paths around the crack was used, for measuring the depth of inclined surface defects. The accuracy and reliability of the ultrasonic timing method were further discussed in (Date, Shimada & Ikenaga (1982)). Hévin, Abraham, Pedersen & Campillo (1998) utilized

a numerical model to understand the influence of Rayleigh wave propagation across surface crack geometry in concrete structures. The time-domain signal information obtained from this study was utilized to estimate the depth of the crack. Cook & Berthelot (2001b) successfully detected a small surface crack induced by cyclic loading by analyzing the amplitude of the surface wave pulse scattered from the crack. Several researchers employed a similar approach based on Rayleigh wave characteristics, such as amplitude (Blackshire & Sathish (2002); Aldrin (2004); Arias & Achenbach (2004); Edwards, Dixon & Jian (2006); Zeng, Qi, Liu & Yao (2019); Zhang, Zhao & Pan (2020)), reflection and transmission coefficients (Hassan & Veronesi (2003); Scala (2003); Zhou, Zhang, Zhou, Sun & Wang (2015); Deng *et al.* (2019); Li, Pan, Zhang & An (2020)), and arrival time of mode-converted and transmitted Rayleigh wave signals (Cooper, Dewhurst & Palmer (1986); Jeong (2005); Matsuda, Nakano, Nagai & Hiratsuka (2006); Jian, Fan, Edwards & Dixon (2006); Masserey & Mazza (2007); Yan, Fan, Liu, Zhang & Tao (2018); Xiao, Chen, Yu, Lisevych & Fan (2022); Li *et al.* (2023)) for sizing surface cracks.

Jian, Dixon, Guo & Edwards (2007) utilized the finite element method (FEM) to explore in-plane and out-of-plane displacements of scattered waves at surface cracks, emphasizing their contribution to Rayleigh wave amplitude enhancement in the near field. However, amplitude-based sizing is inconsistent due to variations in the defect signal's amplitude caused by frequency-dependent attenuation related to surface roughness, or coatings. TOF sizing methods, such as Matsuda *et al.* (2006)'s proposal, relying on Rayleigh wave arrival times, offer more reliability in nondestructive evaluation (NDE). Yet, limitations arise from the need for placing the excitation laser and receiver in close proximity to the crack. Various researchers (Jian *et al.* (2006); Masserey & Mazza (2007); Xiao *et al.* (2022)) have used the transmitted Rayleigh wave's arrival time for depth assessment. However, the need for an additional probe or laser interferometry system in a pitch-catch mode to perform inspection introduces complexity to the experimental setup. Moreover, the use of a pitch-catch configuration is suboptimal, particularly for one-sided applications. Dutton, Clough, Rosli & Edwards (2011) utilized a laser-ultrasound approach to study the interaction of Rayleigh waves with angled surface defects and their sizing using the TOF method. Hernandez-Valle, Dutton & Edwards (2014) also

employed a similar laser-generated Rayleigh waves-based technique to explore the sizing of branched defects. Mode-converted Rayleigh waves from the crack tip were considered for depth measurement by other authors (Cooper *et al.* (1986); Jeong (2005); Li *et al.* (2023)). These studies utilized laser ultrasound, which offers benefits like not requiring a couplant and, hence, enabling the possibility of capturing mode-converted Rayleigh waves. However, cost, difficulty of implementation in an industrial setting, and safety concerns associated with laser limit the broad application of the mode-converted Rayleigh wave-based sizing approach for inspections. Moreover, bulk wave modes generation alongside Rayleigh waves in laser ultrasound methods leads to complex signal processing challenges. An electromagnetic acoustic transducer (EMAT) array-based technique has been developed (Xiang, Greenshields, Dixon & Edwards (2020)), offering flexibility through phase delay control but still relying on peak-to-peak amplitude analysis and requiring a pitch-catch setup, adding complexity in the experimental setup. As previously mentioned, although the wedge technique is known for efficient Rayleigh wave generation, however, struggles with reception challenges due to the couplant layer between the wedge and the test specimen interface, hindering the detection of mode-converted Rayleigh wave features from the crack tip. Therefore, there is an ongoing need for an easily implementable and flexible method to detect and size surface cracks, overcoming limitations observed in previous research, particularly focusing on mode-converted Rayleigh waves from the crack tip and relying solely on TOF for sizing.

The focus has been on the sizing of surface crack depth using ultrasonic Rayleigh waves. However, accurate measurement of surface crack length is equally important has gained recent research interest. Studies involving immersion testing configurations have been explored for imaging surface cracks using Rayleigh waves (Ouchi, Sugawara, Ohara & Yamanaka (2015); Shen, Hu, Li & Li (2021)). Linear phased arrays attached to a wedge have been used for surface crack imaging with both linear (Ohara *et al.* (2017); Ohara *et al.* (2022)) and non-linear (Ohara, Nakajima, Tsuji & Mihara (2019)) surface acoustic waves, but these methods are limited to the region directly under the wedge. A surface crack imaging method employing the TFM with FMC data acquired using the wedge technique has shown promise (Hoyle *et al.* (2019);

Ducousso & Reverdy (2020)), although drawbacks include transmission loss at the wedge-test specimen interface and the need for specific wedges when waveguide material changes. A potential solution is a laser ultrasound-based FMC-TFM approach for surface crack imaging (Qian *et al.* (2021)), but safety concerns and costs limit its widespread use. Therefore, an alternative approach, addressing existing limitations with surface crack imaging methods, is essential and a topic of much recent research.

1.4 Gaps in previous research

A comprehensive review of the current body of research on Rayleigh wave excitation techniques and the application of Rayleigh waves for accurate sizing and imaging of surface cracks is conducted. The review identifies substantial gaps in the existing research, which are subsequently outlined. Ultrasonic Rayleigh waves show promise for effective detection and characterization of surface cracks; however, the methods for generating and receiving these waves encounter various limitations. The widely accepted wedge technique, although efficient, faces constraints such as transmission loss at wedge interfaces, the need for material-specific wedges, and challenges in receiving Rayleigh wave information generated at crack tips, restricting its widespread application.

Current methods for sizing surface crack depth rely on Rayleigh wave features, including amplitude, reflection, and transmission coefficients, and the arrival time of transmitted or mode-converted Rayleigh waves from the crack tip. Amplitude-based sizing proves inconsistent due to variations in defect signal amplitudes. At the same time, arrival time-based methods, though more reliable, involve measurement using a pitch-catch setup to capture the TOF of transmitted Rayleigh waves, making experimental configuration complex. Mode-converted Rayleigh wave arrival time methods are based on laser ultrasound techniques, and present safety, and cost concerns. While the wedge technique is known for efficient Rayleigh wave generation, however, faces reception challenges due to the couplant layer between the wedge and the test specimen interface, hindering the detection of mode-converted Rayleigh wave features from the crack tip.

Significant research has been conducted on measuring surface crack length, with FMC-TFM imaging being a prominent approach. However, this method relies on the wedge technique, encountering associated challenges. Moreover, existing methods in the literature primarily focus on measuring either surface crack depth or length, lacking the capability for comprehensive characterization that allows simultaneous measurement of both depth and length in a single assessment.

1.5 Objectives and outline of the present contribution

The primary objective of this research is to develop a new NDT method for characterizing surface cracks using Rayleigh waves, offering an alternative to current NDT methods. To achieve this goal, the research is structured around three sub-objectives, each contributing to a novel article. These articles are briefly introduced here and will be further detailed in the subsequent chapters of this thesis. In addition, a conference paper related to this thesis is included as supplementary content (refer to Appendix I).

- Develop an alternative method for exciting Rayleigh waves, ensuring unidirectional and selective excitation, and providing flexibility to generate Rayleigh waves on various materials using the same transducer. Emphasis is placed on achieving excitability using a wide range of frequencies.
- Apply the newly developed Rayleigh wave excitation method to innovate an easy-to-implement and flexible approach for detecting and sizing surface cracks using pulse-echo Rayleigh waves. The focus is on overcoming limitations observed in previous research, particularly addressing challenges associated with mode-converted Rayleigh waves from the crack tip and relying solely on TOF.
- Expand on the first two studies by developing a method for comprehensively characterizing surface cracks, enabling the simultaneous measurement of both depth and length in a single assessment.

The first article, presented in Chapter 2, introduces an alternative technique for exciting Rayleigh waves. This method employs a conventional ultrasonic phased array transducer. By incorporating

appropriate excitation delays between each piezoelectric element of the array transducer, Rayleigh waves can be effectively generated across a wide range of materials using the same phased array transducer. The article includes a quantitative comparison between the proposed and existing methods. The results illustrate that the proposed method yields better SNR and produces unidirectional and selective Rayleigh waves. Additionally, the findings highlight the potential of this new excitation technique to be used for the development of Rayleigh wave-based inspection methods.

The second article, presented in Chapter 3, focuses on implementing the new Rayleigh excitation method introduced in Chapter 2. This implementation aims to create a wedge-free pulse-echo Rayleigh wave method for sizing surface cracks. The removal of the wedge eliminates a couplant layer, reducing attenuation and allowing the transducer to capture Rayleigh wave features generated at the crack tip. This facilitates surface crack sizing in pulse-echo mode using TOF information. Utilizing the phased array system, an averaging technique applied to the time trace signals from the phased array transducer elements significantly enhances the SNR and minimizes sizing errors by effectively averaging out the other wave modes generated at crack geometries. The obtained results demonstrate accurate sizing with an error margin within 5%.

Finally, the third article, presented in Chapter 4, introduces a novel approach for acquiring FMC of Rayleigh waves using a conventional matrix phased array transducer, without involving a wedge. The absence of a wedge in FMC acquisition enhances flexibility by overcoming the limitations associated with the wedge technique. Furthermore, utilizing Rayleigh wave FMC data, the article explores surface crack imaging through TFM, enabling comprehensive characterization, including simultaneous measurement of crack length and depth in a single assessment—an advancement over current methods. The findings of this study demonstrate precise sizing of the crack length and depth within a 5% error margin. The method proposed in this research holds the potential to be a viable alternative to existing NDT methods.

CHAPTER 2

AN ALTERNATIVE RAYLEIGH WAVE EXCITATION METHOD USING AN ULTRASONIC PHASED ARRAY

Bhupesh Verma[1] , Pierre Bélanger[1]

[1] Département de Génie Mécanique, École de Technologie Supérieure,
1100 Notre-Dame Ouest, Montréal, Québec, Canada H3C 1K3

Article published in the journal « Ultrasonics » in July 2023.

(DOI:https://doi.org/10.1016/j.ultras.2023.107121) .

2.1 Abstract

Ultrasonic Rayleigh waves have been employed for in-service NDT inspection in a wide range of industries for years. The excitation of Rayleigh waves can be achieved using a variety of methods, with the so-called wedge technique being the most widely used. Recent years have seen considerable research interest in surface crack detection and sizing using Rayleigh waves excited and detected with the wedge technique. However, in this method, Rayleigh waves experience transmission loss at the wedge interfaces. Moreover, the flexibility to generate Rayleigh waves on different waveguides using the same wedge is limited, as the wedge angle depends on the Rayleigh wave wavelength. This work demonstrates a method that provides an alternative Rayleigh wave excitation method. In this, a conventional ultrasonic phased array transducer is used. As there is an appropriate excitation delay between each piezoelectric element of the array transducer, Rayleigh waves can be generated in a wide range of materials using the same phased array transducer. The delay can be estimated based on the elementary pitch of the transducer and the Rayleigh wave velocity of the waveguide. The proposed Rayleigh wave excitation method is demonstrated through both experiments and FE simulations. Furthermore, a finite element model is used to better understand the features of the generated waves and to validate them through their characteristics as Rayleigh wave. A quantitative comparison between the proposed and existing methods is also presented. The directivity and beam divergence of the generated Rayleigh waves are quantified. The results obtained from experiments are in

agreement with finite element simulations and demonstrate the possibility of unidirectional and selective excitation of Rayleigh waves through the proposed method. They also highlight the potential for this new excitation method to be used to develop new Rayleigh wave-based inspection methods.

2.2 Introduction

Surface breaking cracks in solid structures used in various industries, including the aerospace, power generation and petrochemical industries, are very common. To avoid any structural degradation and failure, the severity of such cracks must therefore be assessed. Surface cracks can be detected and sized using a variety of available nondestructive testing (NDT) techniques Cawley (2001). Among these, the use of ultrasonic Rayleigh waves to inspect surface discontinuities has recently been gaining increased attention Masserey & Mazza (2007); Xiao *et al.* (2022), thanks to their high sensitivity to surface and near-surface defects.

Rayleigh waves can be excited and received using a wide range of methods, which can broadly be classified as contact and not-contact (as reviewed and summarized in Chakrapani & Bond (2018)). Rayleigh wave-based NDT methods for inspecting surface cracks have been developed using piezoelectric transducers Rose (1999) and non-contact methods, such as those involving air-coupled transducers Chakrapani, Dayal & Barnard (2013); Torello *et al.* (2015), electromagnetic acoustic transducers (EMAT) Isla & Cegla (2017); Deng *et al.* (2019) and lasers Zeng *et al.* (2019); Xiao *et al.* (2022). The main advantage of using non-contact methods is that with them, no couplant is needed to perform inspections. However, when it comes to sizing cracks, the required maximum operating frequency or bandwidth can be difficult to reach. Since the cost of the associated equipment is prohibitive in the case of lasers, the most common methods use piezoelectric transducers. The simplest way to generate Rayleigh waves is to couple a longitudinal or shear wave transducer directly to the surface of a test specimen Rose (1999). In this technique, a couplant is needed between the transducer face and test specimen surface. However, very little control of the transmitted waves is achieved using this method, and therefore, though simple, it is an inefficient way of generating Rayleigh waves Chakrapani & Bond

(2018). A range of other Rayleigh wave generation methods using piezoelectric transducer have been developed in the last few decades, such as methods involving comb transducers Penttinen & Luukkala (1974); Hurley (1999); Zhang *et al.* (2022) and interdigital transducers (IDT) Na & Blackshire (2010); Moulzolf *et al.* (2013). The comb transducer consists of an array of piezoelectric elements with a pitch exactly equal to one Rayleigh wave wavelength. Since the elements are positioned exactly one wavelength apart, the wave generated from the first element travels and superposes with the excitation of the next element, and so on. A pair of comb transducers can be overlapped with a period corresponding to half a Rayleigh wave wavelength, to create an IDT. However, whenever the frequency or the waveguide material changes, a new transducer is required Chakrapani & Bond (2018). To overcome this limitation a fixture was designed to provide the flexibility to adjust the pitch of the fingers, allowing to obtain a range of configurationsBarnard (2007). However, other plate modes are also generated along with Rayleigh waves, thus making the signal processing complex. The wedge technique performs Rayleigh wave excitation and detection better than several other methods Chakrapani & Bond (2018); Rose (1999). The technique is based on the conversion of longitudinal waves into Rayleigh waves through refraction at the interface of the wedge and the test specimen. This method has the benefit of being unidirectional, and thus of transmitting Rayleigh waves in only one direction. However, the coupling condition between the transducer and wedge is not constant, and a couplant is required to ensure transduction. Recent years have seen a considerable research focus on using the wedge technique for surface crack detection and depth measurement Masserey & Mazza (2007), material characterization Zhang, Li, Jeong & Hu (2018), and surface and sub-surface crack imaging Ghosh, Beniwal, Ganguli & Mukherjee (2018); Hoyle *et al.* (2019); Ducousso & Reverdy (2020); Ohara *et al.* (2022). Although the technique is still considered to represent the most efficient Rayleigh wave generation and reception method, transmission losses at the wedge interfaces are observed with it Ohara *et al.* (2017); Zhang *et al.* (2017). In addition, it is not flexible to generate Rayleigh waves on different waveguides as a new wedge is needed when the waveguide material changes Chakrapani & Bond (2018).

The main objective of this paper is to propose an alternative Rayleigh wave excitation method, such as the wedge technique, that ensures a unidirectional and selective excitation. The secondary objective is to achieve sufficient flexibility to adapt the method to a wide range of materials using the same probe, something that is not possible with the wedge technique. A conventional ultrasonic phased array transducer is used in this method. An appropriate linear delay based on the elementary pitch of the transducer and on the Rayleigh wave velocity of the waveguide material is provided between the emission of each piezoelectric element of the array transducer.

The paper is organized as follows: Section 2.3 presents the materials and methods, including a basic overview of the theory used in the estimation of the linear time delay required for the generation of Rayleigh waves. This is followed by a presentation of the method used for FE simulations. Next, the experimental procedure to verify the proposed method and the methods used to assess excited waves are presented. In section 2.4, the results obtained from the FE simulations and experimental studies are presented, analyzed, compared and discussed. Finally, in section 2.5, conclusions are drawn, and directions for further work are presented.

2.3 Materials and methods

2.3.1 Estimation of linear time delay

The Rayleigh wave excitation method presented in this paper is a specific case of the comb excitation method. In a comb transducer, the excitation of the mode can be controlled based on the inter-element space, also known as the pitch of the transducer Penttinen & Luukkala (1974); Rose, Pelts & Quarry (1998). Here, the pitch is equal to or a multiple of the wavelength of the mode to be generated. However, unlike with phase-matched angle beam probes, wave generation using comb transducers is not unidirectional, and therefore, waves travelling in the opposite direction may complicate signal processing. Moreover, the excitation of an individual specific mode is difficult to achieve. As for a given comb transducer with a fixed elementary pitch chosen equal to the wavelength of the targeted wave mode, zones of excitation in the phase velocity dispersion curve depend on the frequency of the input signal. To overcome these

limitations, a phased velocity excitation method was recently proposed by Veit and Bélanger Veit & Bélanger (2020). In their method, a conventional phased array transducer is used, and a time delay is added to each element during excitation to achieve mode control. The present work is an extension of this method for a specific application to Rayleigh waves. This provides a flexible and feasible alternative route for the generation and reception of Rayleigh waves that can be further extended for the future development of Rayleigh wave-based surface crack characterization method. As far as the authors know the research literature to date doesn't have such flexible method for Rayleigh waves.

The rest of this section is primarily based on the approach given in Veit & Bélanger (2020), which is later converted for the excitation of Rayleigh waves. The amplitude A of a transmitted Rayleigh or Lamb mode can be written as:

$$A(x) = X \cdot F(\omega) \cdot C_n(x) \cdot H(\omega) \tag{2.1}$$

where X is the particle displacement, $F(\omega)$ is the frequency response of the elements, $C_n(x)$ is the coupling coefficient between the waveguide surface traction and the targeted wave mode. The parameter $H(\omega)$ on which the amplitude of the transmitted mode depends, can be written as:

$$H(\omega) = \sum_{i=1}^{N} e^{j[\omega(t-t_i)\pm k_x(x-x_i)]} = \frac{sin[N\pi\left(\frac{p}{\lambda} \pm \frac{t_0}{T}\right)]}{sin[\pi\left(\frac{p}{\lambda} \pm \frac{t_0}{T}\right)]} e^{j\left[\omega\left(t-\frac{N-1}{2}t_0\right)\pm k_x(x-x_c)\right]} \tag{2.2}$$

where $\pm$ represents the direction of propagation along the x-axis (see Figure2.1 for axis system), " $-$ " sign corresponds to $+x$ direction and " $+$ " sign corresponds to the $-x$ direction, p is the pitch (element spacing) of the transducer, λ is the wavelength, T is the period and equals to $1/f$, ω is the angular frequency, k_x is the wavenumber along the propagation direction x, N is the number of elements of the array, t_0 is a delay that depends on the pitch and the targeted phased velocity and x_c is the center location of the array transducer.

When $H(\omega)$ is maximized, the amplitude of the transmitted mode $A(x)$ is also maximized regardless of the other parameters. $H(\omega)$ is maximized when $\frac{p}{\lambda} \pm \frac{t_0}{T} = m$, where m is an arbitrary integer. Hence, the wavelength can be written as the expression given in Equation (2.3) and the excited mode can be controlled by choosing the appropriate time delay t_0.

$$\lambda = \frac{p}{m \pm \frac{t_0}{T}} \tag{2.3}$$

Furthermore, if the elementary pitch (p) of the transducer is chosen much smaller than the wavelength (λ) of the targeted mode, the value of the arbitrary integer m becomes very small as the ratio $p/\lambda \ll 1$, hence, the nearest possible value of m is 0. With $m = 0$, Equation (2.3) can be written as:

$$\lambda \cdot f = C_{ph} = \frac{p}{t_0} \tag{2.4}$$

where f is the frequency and C_{ph} is the targeted phase velocity. As a time delay is added to each element, a specific phase velocity can be targeted as a function of the elementary pitch of the transducer (provided p is much smaller than λ).

The idea of the proposed Rayleigh wave excitation method using phased array transducer is based on Equation 2.4. However, having the added advantage of the non-dispersive nature of Rayleigh waves, for the proposed method to work well the criterion of selecting a much smaller elementary pitch compared to the Rayleigh wave wavelength is not required. A preliminary work on this method was presented by the author in Verma & Bélanger (2023). Following the initial work the required time delay t_0 for the excitation of Rayleigh wave was estimated using the fixed elementary pitch p of the transducer and the Rayleigh velocity C_R of the waveguide material, and is given as:

$$t_0 = \frac{p}{C_R} \tag{2.5}$$

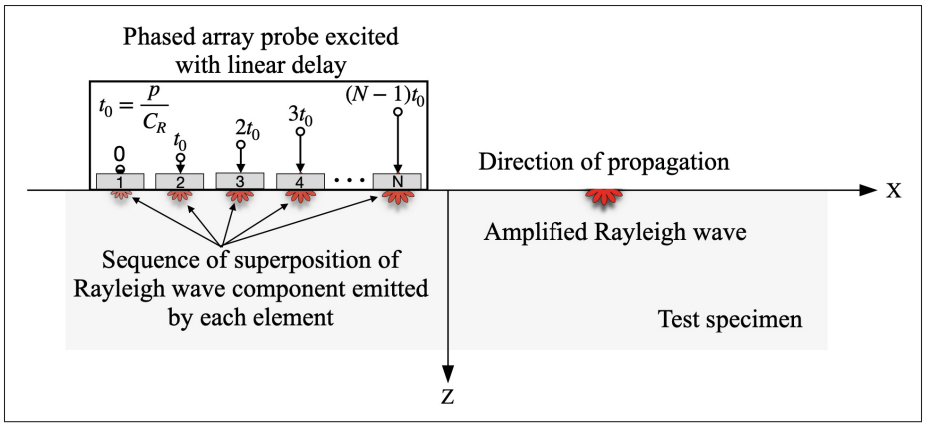

Figure 2.1 Schematic illustration showing the implementation of linear time delay on the elements of the phased array transducer and the sequence of the superposition of Rayleigh wave components generated by each element

The required delay for each element can be written as:

$$t_i = \frac{p * (i-1)}{C_R} \tag{2.6}$$

where t_i is the delay corresponding to the i^{th} element and i ranges from 1 to N, p is the pitch of the transducer, C_R is the velocity of Rayleigh waves in the waveguide. The implementation of the delay estimated using Equation 2.6 during excitation creates a linear delay, as shown schematically in Figure2.1.

The excitation of each element of the phased array probe comprises Rayleigh waves and bulk waves. Since the time delay employed for each element is calculated based on the elementary pitch of the transducer and the Rayleigh wave velocity of the waveguide, the travel time of the Rayleigh wave component generated from a given element is the same as the time delay for emission of the neighboring element. The excitation from each element of the probe are therefore interfering constructively as shown in Figure 2.1. In addition, most of the other wave modes unrelated to Rayleigh waves interfere destructively. Consequently, a clear signal related to the Rayleigh wave energy with no other wave modes also known as a selective Rayleigh wave is transmitted.

2.3.2 Finite Element simulations

Numerical solution techniques such as finite elements, finite differences and boundary elements are very effective and are often required when studying wave propagation and scattering problems. In many recent research articles, the topic of detection and sizing of surface discontinuities using the Rayleigh wave method is examined using numerical techniques such as the finite element method Deng *et al.* (2019); Zeng *et al.* (2019); Xiao *et al.* (2022) and the finite difference method Masserey & Mazza (2007); Masserey & Fromme (2008) and are verified by experiments. Finite Element (FE) simulations were used in the present study. An explicit time domain finite element solver for the linear elastodynamic problem, provided by Pogo, a commercial software application Huthwaite (2014), was used. In explicit time domain FE simulations, the mesh size must be fine enough to provide a converged solution for the elastic wave propagation problem. Thus, 20 elements per shortest wavelength were considered Drozdz, Moreau, Castaings, Lowe & Cawley (2006). To satisfy the stability criterion for the explicit time marching scheme, the step time was chosen based on $\Delta t \leq 0.8\Delta x/C_{max}$ Drozdz *et al.* (2006), where Δx is the size of the smallest element in the finite element mesh and C_{max} is the velocity of the fastest mode. Initially, a 10 mm by 100 mm stainless steel plate (Young's modulus 200 GPa, density 7800 kg/m^3, Poisson's ratio 0.3) was modelled with a mesh consisting of two-dimensional plane strain elements. To avoid the reflections from both ends of the plate, absorbing boundaries were created using the absorbing layers with increase damping (ALID) methodDrozdz *et al.* (2006); Rajagopal, Drozdz, Skelton, Lowe & Craster (2012). The size of the absorbing boundary layers was considered four times the Rayleigh wave wavelength for all the frequencies used in the simulation.

The Rayleigh wave excitation through the method proposed in this paper using a conventional phased array transducer was first simulated. In addition, two other existing Rayleigh wave excitation methods were simulated to allow a comparative study of the proposed and existing methods.

2.3.2.1 Phased array transducer

A conventional phased array probe was simulated. A detailed schematic of the FE model developed is shown in Figure2.2(a). The nodes on the top surface of the plate corresponding to all the elements of the phased array probe were chosen for the excitation. The elementary pitch and element interspace were selected correspond to the phased array probe available in the laboratory. The selected nodes were excited with the required delay for the generation of Rayleigh waves, obtained using Equation 2.6. A 3-cycle Hann windowed toneburst centered at the probe center frequency was used for the excitation. The wave propagating along the surface was received at the three monitoring nodes shown in Figure 2.2(a). In addition, a series of 50 monitoring nodes located 20 mm away from the probe were selected. The monitoring nodes were equally spaced using a step of 0.3 mm.

2.3.2.2 Comb transducer

Figure 2.2(b) presents a schematic of the FE model showing the Rayleigh wave propagation using a comb transducer. A comb transducer comprising 20 piezoelectric elements with an elementary pitch chosen equal to the Rayleigh wavelength of the test specimen at a 3.5 MHz center frequency and an element width equal to 0.42 mm was simulated. The excited nodes were selected accordingly and were all triggered at the same time with a 3-cycle Hann windowed toneburst centered at 3.5 MHz. The out-of-plane displacement of the transmitted waves was captured at the three monitoring nodes depicted in Figure 2.2(b).

2.3.2.3 The wedge technique

In the case of the wedge technique, the implementation of a wedge coupled with the test specimen surface is computationally expensive since the wedge material must also be discretized. To ensure a proper transition between two media, the element size should be selected according to the material with the shortest wavelength, and in this case, that is the wedge. This adds a large number of elements to the FE model, as the longitudinal wave velocity in the wedge material is

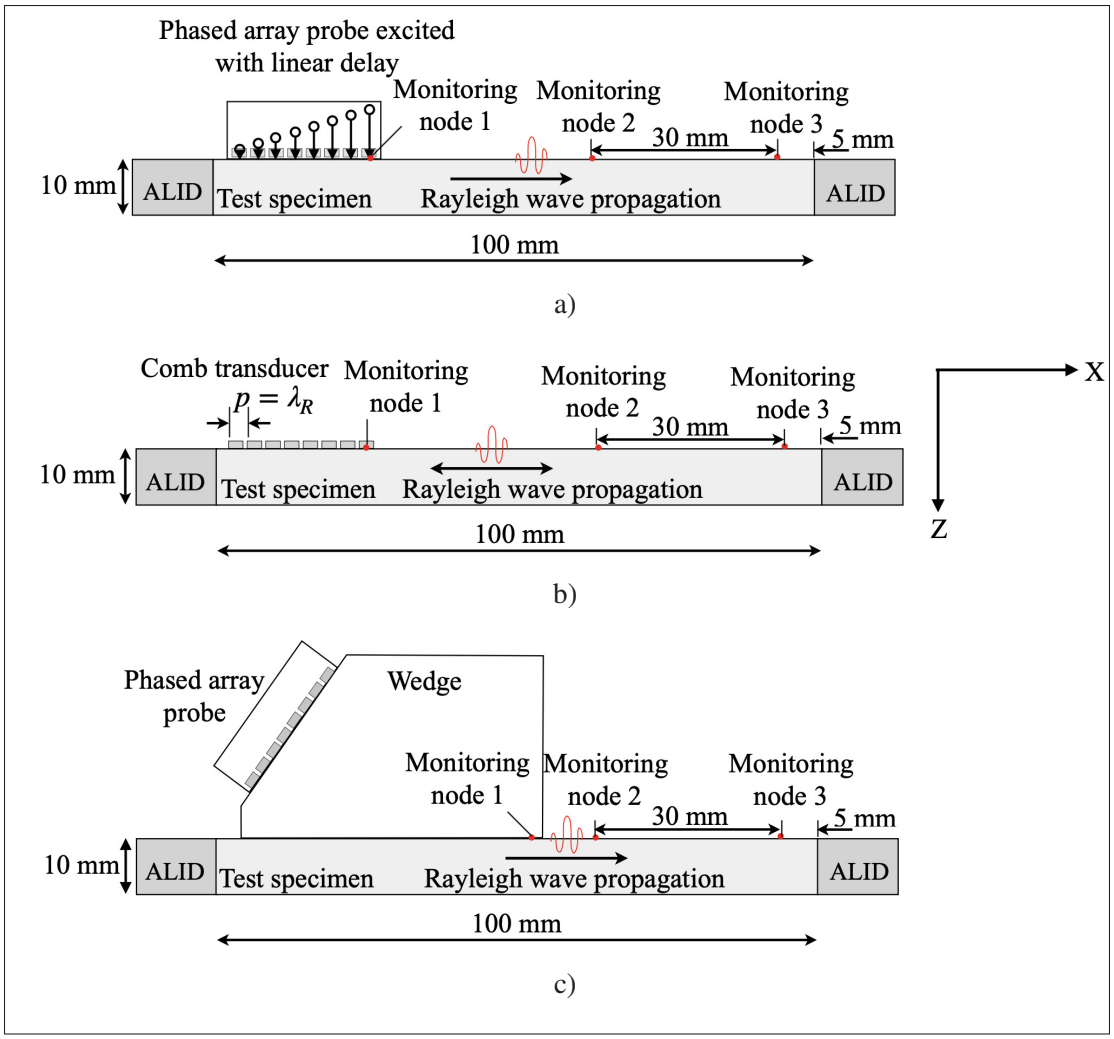

Figure 2.2 Schematic of 2D FE model used to simulate the Rayleigh wave propagation using: (a) a conventional phased array transducer, (b) a comb transducer and (c) the wedge technique

lower than that in the test specimen material. Therefore, in the case of the wedge technique, a hybrid model was used Wilcox *et al.* (2020). Fig 2.2(c) presents a schematic of Rayleigh wave propagation using the wedge technique. A Rexolite (Young's modulus 2.233 GPa, density 1050 kg/m^3, Poisson's ratio 0.42) was used to simulate the wedge and the required incidence angle for the generation of Rayleigh wave was estimated using the Snell's law. First, a 3.5 MHz phased array transducer (see Table 2.1 for the probe parameters) mounted on a wedge was simulated analytically. The time-dependent ultrasonic out-of-plane displacements at the interface between

the wedge and the test specimen were calculated. The output of the analytical simulation was then used as the excitation source in the FE model. All the nodes at the wedge and test specimen interface were selected for an out of plane excitation. The transmitted wave was monitored at the three monitoring nodes shown in Fig 2.2(c).

2.3.3 Experiments

To verify the proposed Rayleigh wave excitation method, experimental measurements were carried out. Rayleigh waves were excited using three different commercial phased array probes, whose parameters are listed in Table 2.1. Experiments were conducted on four different test specimens made of stainless steel, aluminum, low carbon steel and plexiglass. Photographs of the test samples are shown in Figure2.3. Figure2.4 presents a schematic of the typical experimental setup used for the studies conducted in this paper.A Verasonics Vantage 64 LE controller was used for signal generation and to control the emission of each element. A Hann-windowed toneburst at the center frequency was sent to each element, with the required delay for the excitation of Rayleigh waves obtained using Equation 2.6. A very thin layer of oil was used as a couplant between the probe face and the test specimen to ensure coupling. The transmitted waves were received using two different configurations. In the first configuration, as shown in Figure 2.4(a), a laser Doppler vibrometer (Polytec OFV-505, Polytec controller OFV-2570) and a high-definition 4-channel DSO9024H digital oscilloscope was used for the reception. The laser head was mounted on a motorized two-dimensional XY stage to control the scanning along a line before the probe. For a better comparison with the FE simulations, the wave propagating along the surface was received at a series of 50 monitoring points located 20 mm away from the probe, as shown in Figure 2.4(a). The monitoring points were equally spaced using a step of 0.3 mm. In the second configuration, the reception was carried out using the same phased array probe in a pulse-echo mode, as illustrated in Figure 2.4(b).

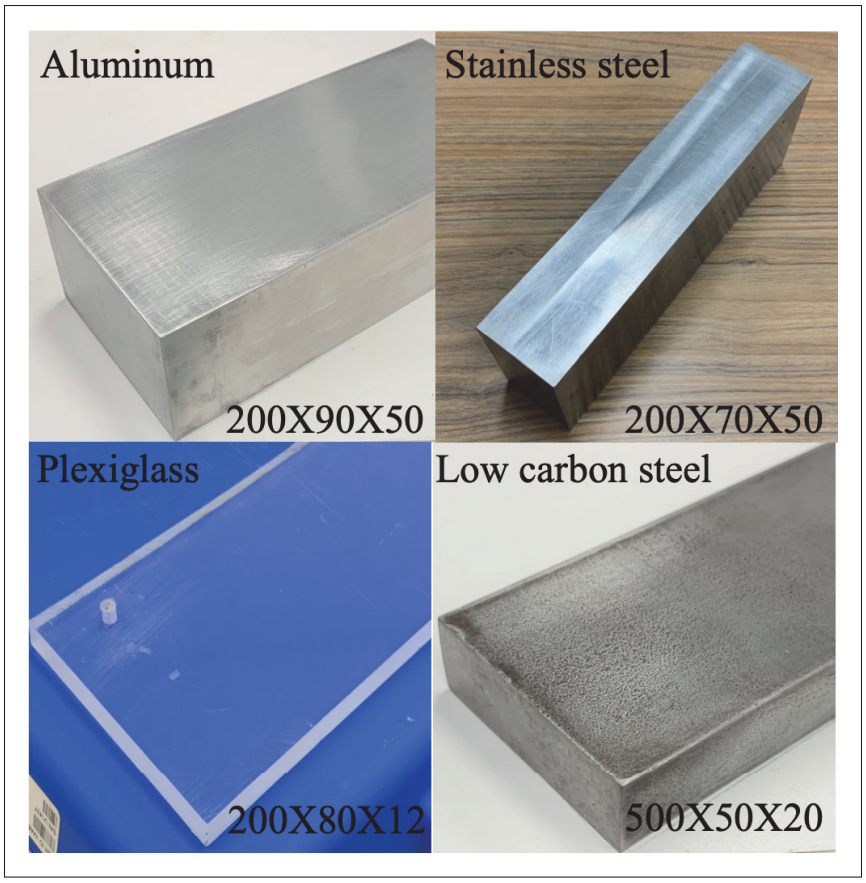

Figure 2.3 Photograph of the test samples used in measurements

Table 2.1 Parameters of the phased array probes used in experiments

Phased array probes			
Parameters	Probe 1	Probe 2	Probe 3
Frequency (MHz)	2.25	3.5	5
Pitch (mm)	1	0.5	0.5
Element count	64	32	64
Aperture (mm)	64	16	32
Elevation (mm)	7	10	10
Bandwidth (%)	83	83	83

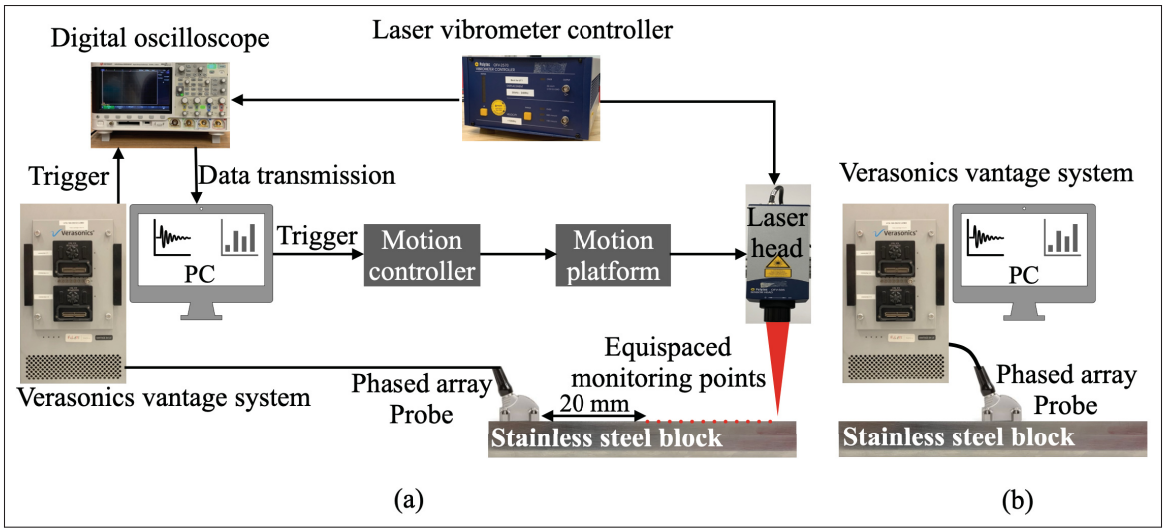

Figure 2.4 Schematic of experimental setup: (a) excitation is achieved through a phased array transducer and a laser Doppler vibrometer is used for the reception; (b) excitation and reception is performed using the same phased array probe in a pulse-echo configuration

2.3.4 Assessment of the generated waves

2.3.4.1 Mode identification and selectivity

The wave generated through the proposed method was verified as a Rayleigh wave primarily on the basis of the measured velocity. The velocity was measured using the time-of-flight (TOF) information of the propagating waves reflected from the two edges across the thickness of the test specimen. A two-dimensional fast Fourier transform (2-D FFT) Alleyne & Cawley (1991) is also a useful tool for identifying propagating modes. Therefore, to further validate the generated wave mode and evaluate the mode selectivity of the proposed method, a 2-D FFT analysis was performed on the displacement field recorded at the monitoring nodes. This analysis was carried out on both experimental and FE simulation measurements. A threshold of -15 dB was considered to visualize the main propagating modes shown on a phase velocity versus frequency plot.

To evaluate the Rayleigh wave selectivity, FE simulations, and experiments were used to perform a quantitative comparison between the proposed and existing excitation methods by measuring the signal-to-noise ratio (SNR). The SNR was measured by taking the ratio of the peak signal to the root mean square (RMS) value of the noise on the background signal. The RMS value of the noise was obtained by calculating the RMS on a range of the time domain signal chosen as noise, shown in Figure 2.8 and 2.9.

2.3.4.2 Ultrasonic beam

Predicting the defect detection and sizing capacity requires knowledge of the directivity and divergence angle of the ultrasonic beam generated through the proposed excitation method. The ultrasonic beam directivity and divergence were studied by extending the initial 2-D FE model to the third dimension. The mesh used in the 3-D FE models consisted of 8-node cubic brick elements. All the nodes corresponding to the element width and the passive aperture of the phased array probe were chosen for the excitation. The probe's passive aperture was 7 mm, a value chosen to facilitate experimental comparisons. The maximum displacement amplitude of the wave propagating along the surface was captured at the monitoring nodes located across a circumferential line with a 35 mm radius and step interval of 10°, as depicted in the schematic shown in Figure2.5. The directivity and divergence obtained from the FE simulations were verified with experimental measurements. Due to the limited width of the test specimen used in the experiments, only the monitoring nodes between positions 90° and 0° shown in Figure2.5 were selected to capture the maximum displacement amplitude of the propagating waves. As the monitoring nodes are symmetric about the axis of symmetry (see Figure 2.5), the same measured displacements were used for the corresponding symmetric monitoring nodes between positions -90° and 0° to ensure a better comparison with the FE simulation results.

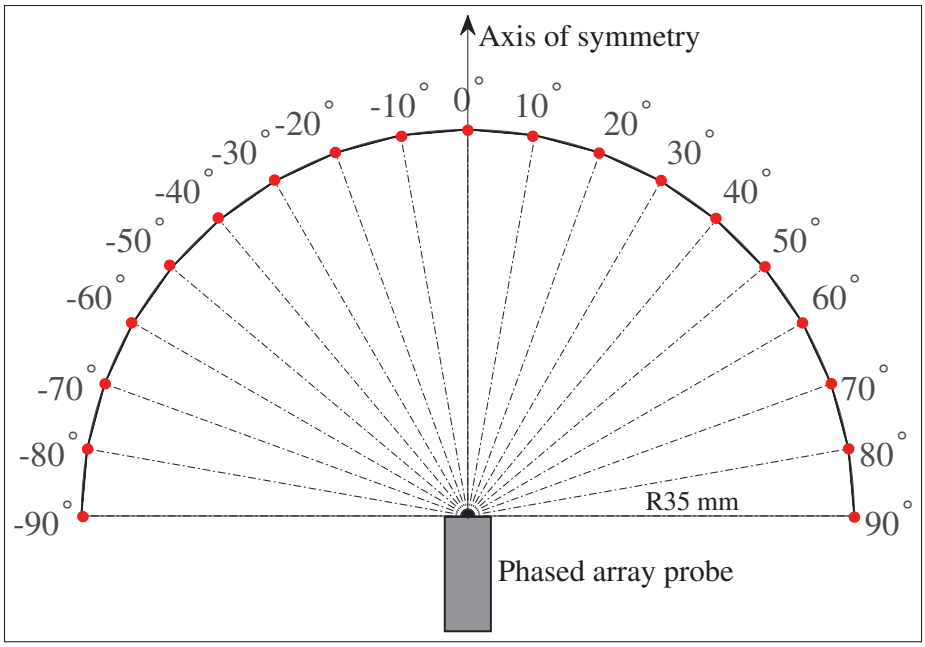

Figure 2.5 Schematic showing the monitoring nodes chosen across a circumferential line with a 35 mm radius and step increment of 10° to capture the out-of-plane displacement amplitude of Rayleigh wave to quantify the beam directivity and divergence angle

2.4 Results and discussion

2.4.1 Evaluation of Rayleigh wave selectivity

The Rayleigh wave selectivity was assessed using both FE simulations and experiments. A 2.25 MHz conventional phased array probe was simulated with the required delay to model a Rayleigh wave propagation. Figure 2.6 presents a snapshot of the contour of the total displacement magnitude, obtained from FE simulations. It was observed that the incident waves propagate in only one direction along the surface with uniform fields. This evidences the unidirectional excitation capacity of the proposed excitation method. In addition, the field displacements captured at four different time instances, shown in Figure 2.6, demonstrate that the energy of the generated waves is concentrated within a small depth below the surface. The measured velocity of the generated waves was found similar to the Rayleigh wave velocity of the simulated stainless steel plate. These characteristics attest to the wave generated through the method

proposed in this paper being a Rayleigh wave. It can also be observed that excited Rayleigh waves propagate dominantly along the surface with no other wave modes, which is the case scenario for a Rayleigh wave-based NDT inspection.

A 2D FFT analysis was also carried out to evaluate the Rayleigh wave selectivity and identify the excited wave modes. Both FE simulations and experimental measurements were used. The experimental setup used is shown in Figure 2.4(a). The excitation was done using a 2.25 MHz phased array probe. The elementary pitch of the probe used was 1 mm. If the same probe were to be used in reception, the maximum wavelength captured by the probe would be double the pitch and the corresponding captured frequency range would be limited to a maximum 1.5 MHz. Therefore, to overcome this limitation, a laser Doppler vibrometer was used in reception. The signals were acquired at a series of 50 monitoring points located at equally spaced steps of 0.3 mm, as shown in Figure2.4(a).

Figure 2.7 shows a 2-D FFT plot of FE simulated and experimentally measured signals. The thin gray lines in Figure2.7(a) correspond to side lobes which were also observed in the experimental measurements, as can be seen in Figure2.7(b). However, their amplitude was low. The yellow lines correspond to the measured Rayleigh wave velocity and the diagonal cyan lines correspond to the maximum measurable wavelength when using a 0.3 mm pitch. A very good Rayleigh wave selectivity was observed both in FE simulations and in experiments. As expected, the experimental results shown in Figure 2.7(b) are noisier than the simulated results presented in 2.7(a). This is most likely because the response of each element is not identical due to the non-uniform coupling/fabrication of the piezoelectric elements, unlike in the simulations.

A comparative study of the proposed and existing Rayleigh wave excitation methods was quantitatively carried out using FE simulations and experiments. The study was first conducted by simulating the proposed and existing methods as described in Section 2.3.2 at 3.5 MHz. To ensure an accurate comparison, the aperture of the comb transducer was kept similar to that of the conventional 3.5 MHz phased array probe (see Table 2.1 for the probe parameters) used to simulate the proposed method and the wedge technique. Also, the monitoring nodes were

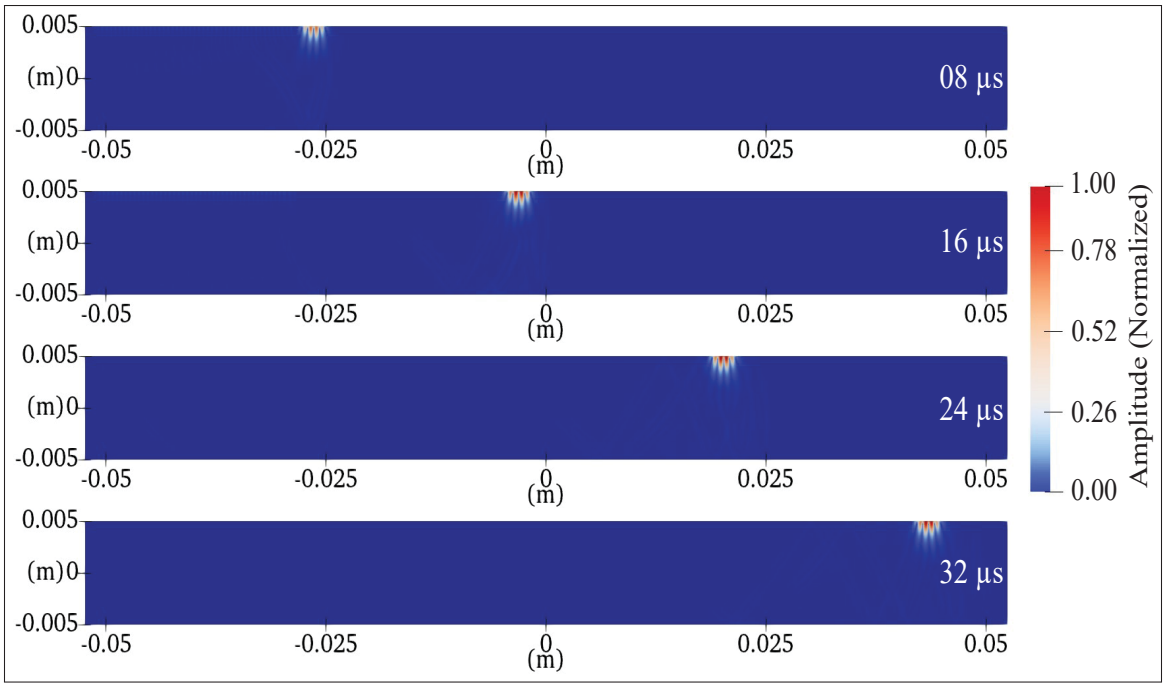

Figure 2.6 Snapshot of the contour of the total displacement magnitude captured at different time instances showing the Rayleigh wave propagation and selectivity

chosen similarly in all cases in order to record the out-of-plane displacement of the propagating waves. Monitoring node 1 was chosen below the transducer or wedge. However, monitoring nodes 2 and 3 were selected away from the probe and kept 30 mm apart from each other, as shown in Figure2.2.

Figure2.8 shows the normalized amplitude of the total field displacement and time traces of the out-of-plane displacement amplitude of Rayleigh waves excited using a comb transducer, the wedge technique, and a conventional phased array transducer, obtained from FE simulations. As expected, when the comb transducer was used, other ultrasonic wave modes such as longitudinal waves were seen along with the Rayleigh waves, especially when the transmission and reception were performed using the same transducer. As the comb transducer is equally sensitive in transmission and in reception of Rayleigh waves in both directions, there was no directional control. The Rayleigh wave can be seen propagating in both directions in Figure2.8(a).

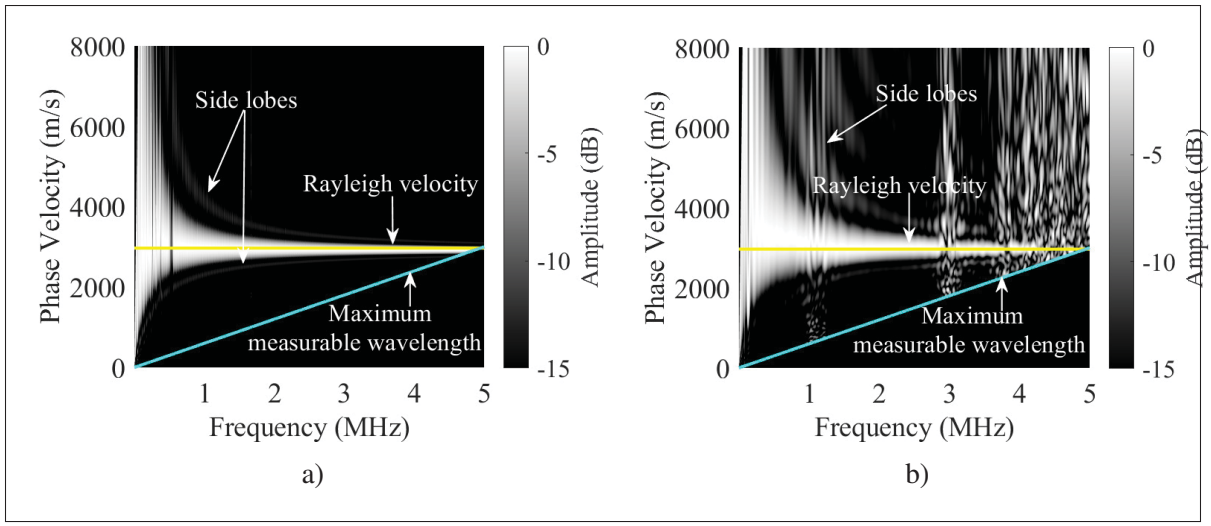

Figure 2.7 2-D Fourier transform of signals extracted on a 50 mm thick stainless steel block obtained from: (a) FE simulations and (b) Experiments. A 2.25 MHz phased array probe composed of an array of 64 elements with a 1 mm elementary pitch was used for the excitation and received using a laser vibrometer at the monitoring nodes selected along a line with an equally spaced step of 0.3 mm

The so-called Rayleigh wave excitation wedge technique has a significant advantage in terms of directional control over Rayleigh wave propagation. This can be verified in the field displacement shown in Figure2.8(b). The Rayleigh energy was seen propagating dominantly along the surface. However, along with Rayleigh waves, a small amount of energy unrelated to Rayleigh waves, such as surface skimming longitudinal waves (SSLW), shear waves, and head waves, were also seen. The SSLW and head waves attenuate faster than Rayleigh waves and are very small in amplitude when compared to the latter. They can hardly be observed whereas a small amount of shear waves can be noticed in the field displacement and time trace signal shown in Figure2.8(b). As the simulated plate thickness was 10 mm, due to the multiple reflections within the boundaries of the plate, the shear waves propagate along the plate. Although these shear wave components are very small in amplitude, they still appeared within the window chosen for calculating the RMS value of the noise, they increase the noise level in the estimation of SNR. It is important to note that in an infinitely thick part, the multiple reflections of shear waves would not be apparent.

The Rayleigh wave excitation method proposed in this paper to make it easy to obtain selective and unidirectional excitation capabilities equivalent to those obtained with the wedge technique. It can be observed from Figure2.8(c) that no other wave modes were generated along with Rayleigh waves, and that the propagation was only in one direction, right before the phased array transducer. It is interesting to note that despite having the same thickness no other wave modes were generated in the proposed method. As previously explained in Section 2.3.1, it is due to destructive interference that most of the other wave modes unrelated to Rayleigh waves get averaged.

Further, experimental validation was performed to verify the similar excitation capabilities noticed in Figure 2.8(b) and (c) obtained from the FE studies. Experiments were conducted using a 5 MHz phased array transducer on the stainless steel specimen shown in Figure 2.3. The experimental setup used is shown in Figure 2.4(b). In the case of the wedge technique, the probe was mounted on a commercial wedge (Olympus SA32-N55S-IHC). The propagating waves reflected from one edge of the test specimen were received using the same probe in a pulse-echo configuration in both measurements. To facilitate a better comparison, while doing the measurement using the proposed method the distance to be covered by the propagating waves was ensured to be approximately the same as it was in the case of the wedge technique. This was achieved by positioning the phased array transducer further away compared to the wedge from the edge of the test specimen. Also, the measuring parameters such as input voltage and gain were set the same for both measurements. The comparison of time traces of the out-of-plane displacement amplitude (raw output signal from the Verasonics) recorded at one of the elements of the phased array transducer obtained from experiments using the wedge technique and the proposed method is shown in Figure 2.9(a) and (b) respectively. The experimental results validate the similar excitation capabilities of the proposed method, to those obtained using the wedge technique. In addition, the proposed method provides a better signal amplitude even after positioning the transducer further away compared to the wedge from the edge of the test specimen, which can be noticed in Figure 2.9(b).

Table 2.2 Measured signal-to-noise ratio for different Rayleigh wave excitation methods

Excitation Methods	SNR (dB)	
	FE	Experiment
Comb Transducer	33	-
Wedge Technique	37	31
Phased array Transducer	56	41

Table 2.2 presents the measured SNR for a quantitative comparison between these Rayleigh wave excitation methods. The background noise was higher in amplitude with the comb transducer, which accounts for this transducer having the lowest SNR value. In the case of the wedge technique, a slightly higher SNR was obtained. However, the proposed method shows overall a better SNR than the two other methods presented in this paper. As expected, the proposed method provides a better SNR compared to the wedge technique mainly because by eliminating the wedge the attenuation loss due to the couplant used between the wedge and test specimen interface is eliminated. This helps to achieve a better signal amplitude and hence an enhanced SNR is obtained. The qualitative comparison presented in Figure2.8 and 2.9 and the quantitative comparison shown in Table 2.2 illustrate that the method proposed in this paper provides a better SNR as well as ensures an excellent Rayleigh wave selectivity along with a unidirectional propagation.

2.4.2 Influence of the elementary pitch of the transducer on excitability and selectivity

The proposed Rayleigh wave excitation method uses a conventional ultrasonic phased array transducer to achieve directional and selective excitation. Because Rayleigh waves are non-dispersive in nature, they are not affected by the frequency. Therefore, in the proposed excitation method, the selection of the elementary pitch of the transducer is not required to be much smaller than the Rayleigh wavelength. To validate this, our studies were further extended using FE simulations. 2-D FE models with four different pitches were used to understand the influence of the elementary pitch of the transducer on the Rayleigh wave's excitability and selectivity. A 5 MHz phased array probe was simulated. The pitch was selected in terms of Rayleigh

wavelength (λ_R) and ranged from λ_R to $3\lambda_R$. The width of each element was chosen according to a commercial 5MHz probe available in the laboratory. The simulated element width was 0.42 mm in all cases.

Figure2.10 presents the 2-D FFT plot corresponding to four different pitches used in the simulations. As expected, the elementary pitch has no appreciable effect on the excitation and selectivity of the Rayleigh wave. This is mainly because the Rayleigh wave propagates with a constant speed. Therefore, the Rayleigh wave component emitted from the excitation of each element gets superposed with the excitation of next element and becomes stronger. However, because of destructive interference, the other wave modes attenuate, and most of them get canceled out. This demonstrates that the Rayleigh wave can be excited using any conventional phased array transducer.

2.4.3 Excitability using probes of different frequency ranges

As observed in Section 2.4.1, the Rayleigh wave penetration depth is up to approximately one wavelength. The ability of Rayleigh wave to characterize surface cracks of different depths depends on the frequency of the phased array probe chosen for the excitation. Therefore, the present study was further extended to evaluate the flexibility of the proposed method in handling the Rayleigh wave excitation using a range of probe frequencies. Measurements were performed using two more phased array probes having centers frequency of 3.5 MHz and 5 MHz and an elementary pitch of 0.5 mm. The experimental setup used is shown in Figure2.4(b). The excitation and reception were done using the same phased array probe in a pulse-echo configuration. The amplitude of the out-of-plane displacement of the Rayleigh wave reflected from one edge of the stainless steel block used as a test specimen was captured by all the elements of the phased array probe. A 2-D FFT was performed on the extracted signals and results, corresponding to 3.5 MHz and 5 MHz, are shown in Figure2.11(a) and (b) respectively. As expected, a significant improvement in SNR was found when the reception was realized using a phased array probe instead of laser interferometry. As previously mentioned, the yellow lines correspond to the measured Rayleigh wave velocity, and the diagonal cyan lines, to the maximum

measurable wavelength. As the excitation and reception were performed using the same probe with a 0.5 mm elementary pitch, the Nyquist wavelength, equal to a space sampling of 0.5 mm, was 1 mm. Hence, the maximum frequency range captured was limited to 3 MHz. However, the probe used in the measurement had centers frequency of 3.5 MHz and 5 MHz. Figure2.11(a) shows that Rayleigh waves excited using a 3.5 MHz probe have a better selectivity in the 1.5 MHz to 3 MHz frequency range. However, at low frequencies (<1.5 MHz), the selectivity is not good, probably due to the small aperture of the 3.5 MHz transducer. However, in Figure2.11(b), an excellent Rayleigh wave selectivity was observed when the excitation was done using a 5 MHz transducer, as this transducer has a larger aperture than a 3.5 MHz transducer. Small spots of energy were observed on the right top corner of 2-D FFT plot, and were more pronounced when measurements were done using a 3.5 MHz phased array probe. This was most likely due to the cross-talk between the piezoelectric elements and the non-uniformity of the placement of the piezoelectric elements inside the probe. The results shown in Figure 2.11 confirm the possibility of exciting Rayleigh waves using a wide range of frequencies through the proposed excitation method. The frequency range of the phased array probe can thus also be chosen based on the sensitivity of surface cracks to be measured.

2.4.4 Excitability on different waveguide material

The main drawback of all existing Rayleigh wave excitation methods lies in their inability to excite Rayleigh waves on different waveguide materials Chakrapani & Bond (2018). Therefore, to validate the flexibility of the proposed Rayleigh wave excitation method, that this method could easily be adapted for different waveguide material, experimental measurements were conducted on a range of materials. Photographs of the test samples used are shown in Figure2.3. The velocity of the generated wave was calculated using the TOF information. Theoretically, for all real media (0<Poisson's ratio<0.5), the Rayleigh wave velocity varies from 87 to 96 % of the shear wave velocity Graff (1975). Therefore, the theoretical Rayleigh wave velocity for all the test samples was predicted to be 92 % of the measured shear wave velocity. The measured Rayleigh wave velocity was then compared with the theoretically estimated velocity, as shown in

Table 2.3 Comparison of experimentally measured and theoretically predicted Rayleigh wave velocities of different waveguide materials

Material	Rayleigh wave velocity (m/s)	
	Experimentally measured	Theoretically estimated (92% of Shear wave velocity)
Stainless steel	2969	2934
Aluminium	2941	2898
Low carbon steel	2988	2995
Plexiglass	1245	1288

Table 2.3. The comparison shows a striking agreement between the measured and theoretical Rayleigh wave velocity values. This indicates that the method proposed in this paper has the potential to excite Rayleigh waves on different materials using the same phased array probe.

2.4.5 Directivity and divergence of Rayleigh wave beam

The directivity of the transmitted Rayleigh wave beam was determined using a 3D FE model and verified by experimental measurements. The setup shown in Figure 2.4(a) was used for the experimental measurements. A polar plot comparing the beam directivity of the Rayleigh wave generated using the proposed Rayleigh wave excitation method, obtained from FE simulations and experimental measurements are shown in Figure2.12. The beam directivity of Rayleigh waves simulated using three phased array probes centered at 2.25 MHz, 3.5 MHz and 5 MHz, was estimated and validated with an experimentally measured beam directivity, using a 2.25 MHz phased array probe. It can be observed that the Rayleigh wave beam induced by the excitation has a clear directive. Most of the Rayleigh energy is propagating right before the phased array transducer. Indeed, the maximum displacement amplitude is centered at 0°. Another clear advantage of the proposed method is that with it, energy loss due to leakage represented by side lobes was minimal and almost negligible. Figure2.12 also shows that the diffraction angle of the Rayleigh wave beam at half maximum (-6dB) is approximately 20°. A narrow beam is targeted, particularly when dealing with an imaging application, as it helps improve the lateral resolution of the image. The beam width can further be reduced with an increased passive aperture of the

probe. The next section looks at how probe passive aperture affects the beam directivity and divergence.

2.4.6 Influence of probe passive aperture on beam directivity and divergence

3-D FE models were also used to predict the influence of probe passive aperture on beam directivity and divergence. A 2.25 MHz phased array transducer with a passive aperture of 7 mm was used for the experimental measurements. The experimental setup used is shown in Figure 2.4(a). The same probe was simulated to allow a better comparison. In addition, to understand the effect of probe passive aperture, FE models with two different passive apertures of 4 mm and 0.5 mm were used. Figure2.13 shows a polar plot representing a beam directivity and divergence comparison for three different passive apertures. It was observed that there was no significant variation in beam directivity with a reduced passive aperture. The maximum displacement amplitude is concentrated at 0° in all cases. The beam divergence remained unchanged up to a 4 mm passive aperture. The beam divergence increased slightly when the passive aperture fell to 0.5 mm. However, on a positive note, even with the least possible passive aperture, the diffraction angle at half maximum (-6 dB) is approximately 24°.

The proposed method works well for the test specimens with a flat surface. The excitation of Rayleigh waves on a curved surface through a conventional phased array transducer is limited when using the method proposed in this paper. If the surface of the test specimen is curved under the probe aperture, then poor coupling between the elements of the probe and the test specimen would result in poor transduction. However, we also believe that if a curved linear array transducer is excited with an appropriate delay, then this limitation can be overcome. Ultimately, one overall positive observation that can be drawn from this study is that, unlike existing methods, the one proposed herein is capable of exciting unidirectional and selective Rayleigh waves without using a wedge. The method allows the flexibility to generate Rayleigh waves on different waveguides using the same conventional phased array transducer.

2.5 Conclusion

This work presents an innovative method for the excitation of Rayleigh waves using an ultrasonic phased array probe. A linear time delay based on the elementary pitch and on the Rayleigh wave speed was implemented during the excitation of elements. The possibility of exciting Rayleigh waves using a conventional phased array probe was verified in simulations and experimentally. 2-D FE simulations were used to understand the characteristics of the generated waves and ensure that they were Rayleigh waves. A 2-D FFT analysis was also performed on the signals obtained from FE simulations and experiments in order to investigate the selectivity of the Rayleigh waves. A quantitative comparison in terms of SNR was done between the proposed and existing methods, using FE simulations and experiments. The SNR obtained for the proposed method from FE simulations and experiments was 56 dB and 41 dB respectively showed overall better performance than existing methods such as the wedge technique and comb transducer. Results showed excellent Rayleigh wave selectivity and demonstrated that the method is able to excite Rayleigh waves without using a wedge. 3D FE simulations were used to determine the beam directivity and divergence of generated Rayleigh waves and then verified experimentally. Furthermore, experiments were conducted to validate the flexibility of the method in exciting Rayleigh waves using different frequency ranges. The ability to handle excitation on different waveguides using the same phase array probe was also verified experimentally. The results obtained from these measurements show that the proposed method has the potential to excite unidirectional selective Rayleigh waves using any conventional phased array transducer and can easily be adapted to different waveguides. Therefore, the method can be considered as a suitable alternative to existing Rayleigh wave excitation methods. Furthermore, the new Rayleigh wave excitation method can be extended to develop a Rayleigh wave-based surface crack characterization method. The proposed method can also be used for various applications such as measuring the material properties (stiffness or Young's modulus), surface roughness estimation, and surface coating thickness measurement.

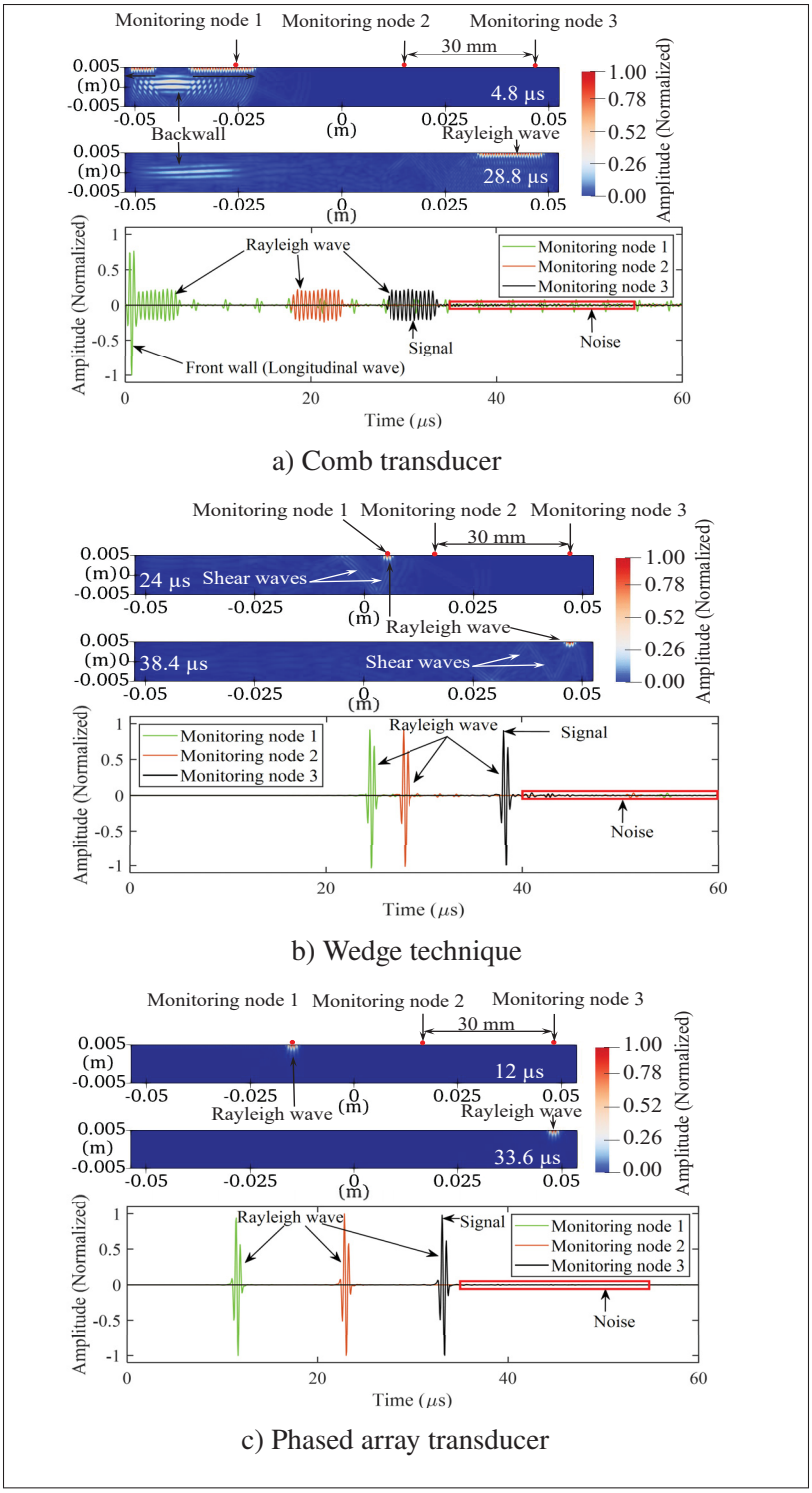

Figure 2.8 Snapshot of the total field displacement and time trace signal showing a qualitative comparison between the proposed and existing Rayleigh wave excitation methods

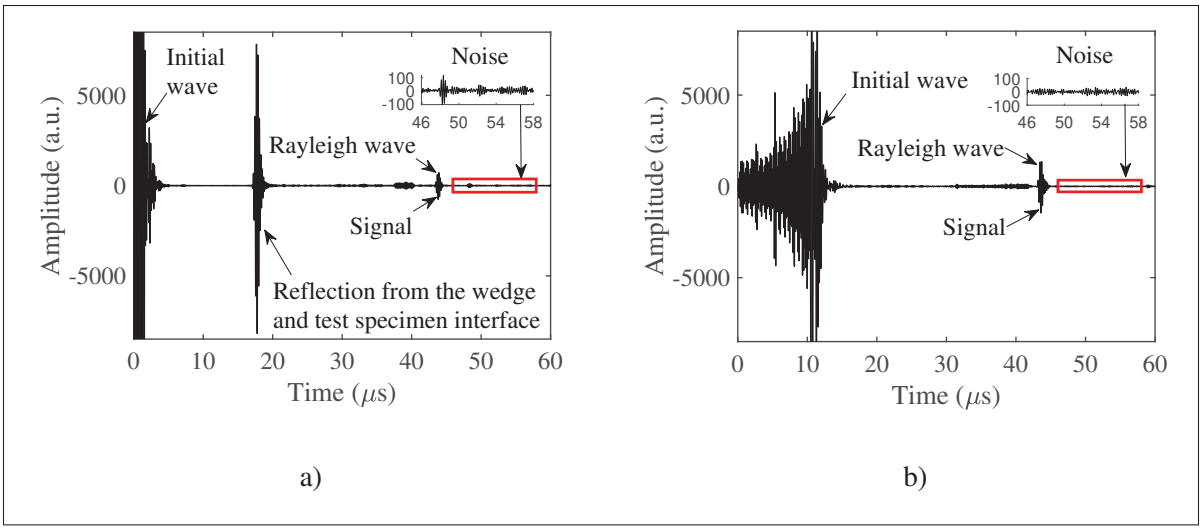

Figure 2.9 Comparison of the experimentally measured time traces of the out-of-plane displacement amplitude (raw output signal from the Verasonics) recorded at one of the elements of the phased array transducer using: (a) wedge technique and (b) phased array transducer

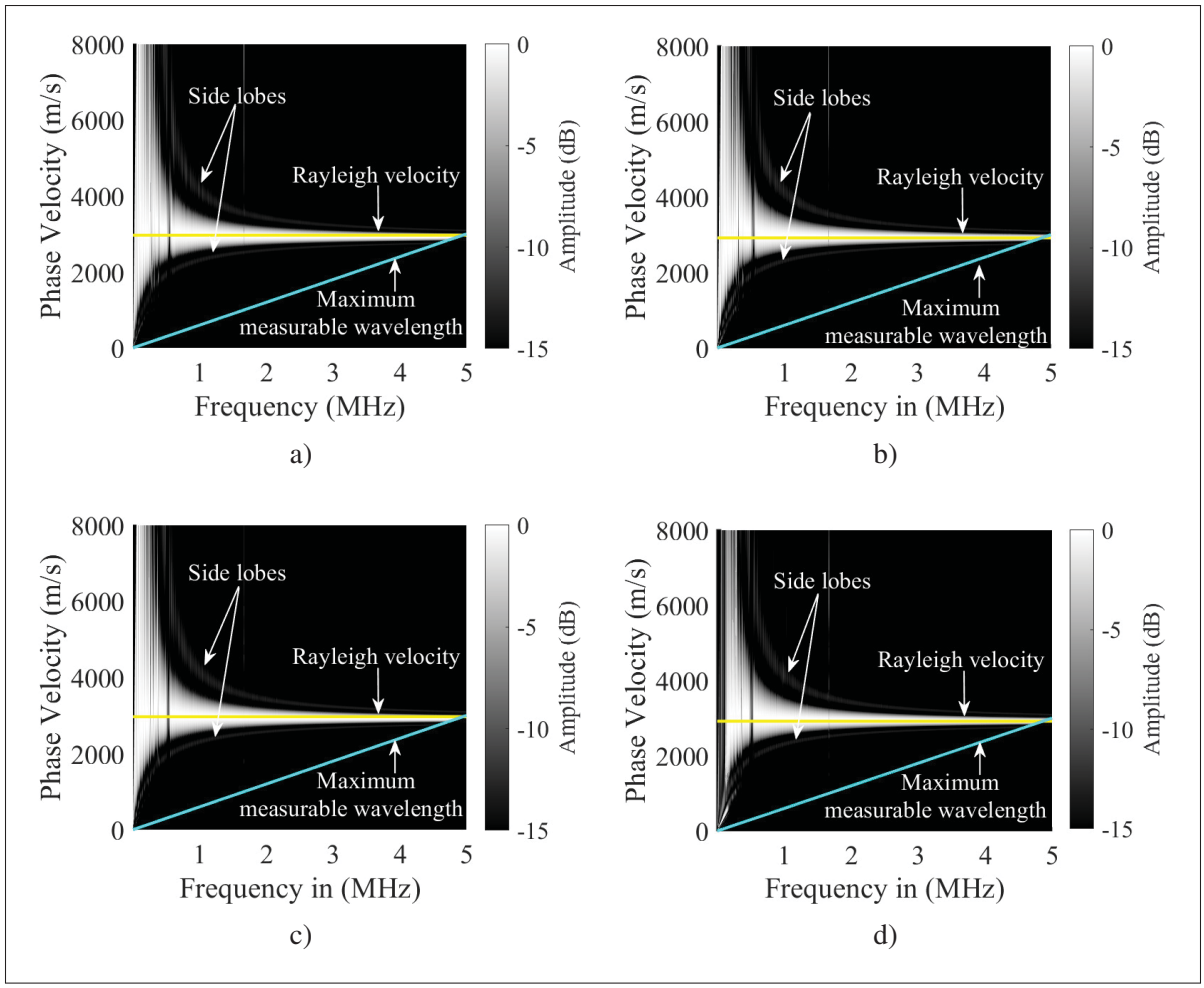

Figure 2.10 2-D Fourier transform of the signals extracted from the FE simulations representing the Rayleigh wave selectivity for various simulated pitches: (a) pitch=λ_R, (b) pitch=1.5λ_R (c) pitch=2λ_R and (d) pitch=3λ_R

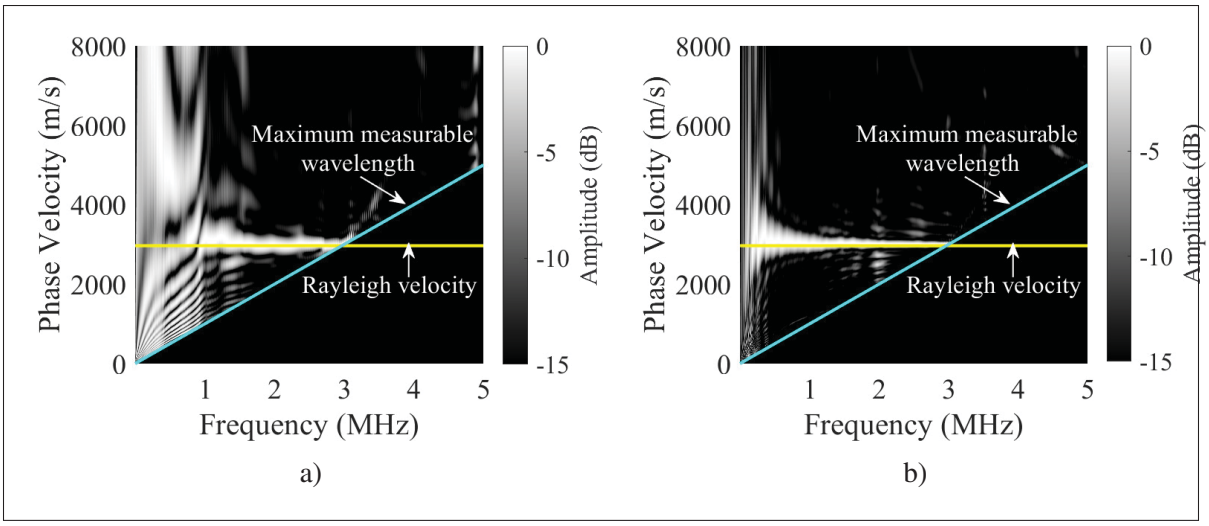

Figure 2.11 2-D Fourier transform of the signals extracted from the experimental measurements on a stainless steel block using a phased array probe centered at a frequency of: (a) 3.5 MHz and (b) 5 MHz

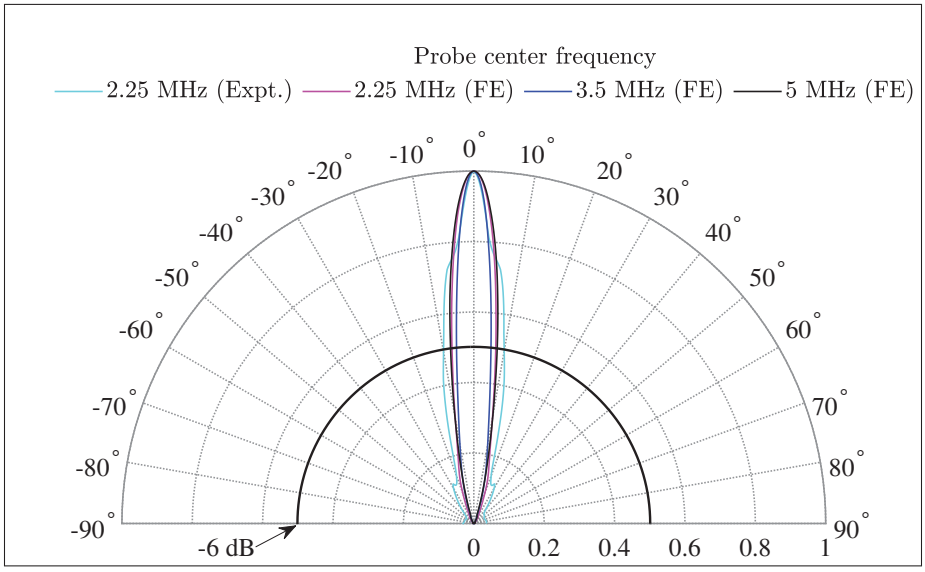

Figure 2.12 Polar plot shows the beam directivity and divergence angle of the generated Rayleigh waves obtained from an FE simulation for 2.25 MHz, 3.5 MHz, 5 MHz probe frequencies and experiments corresponding to 2.25 MHz probe

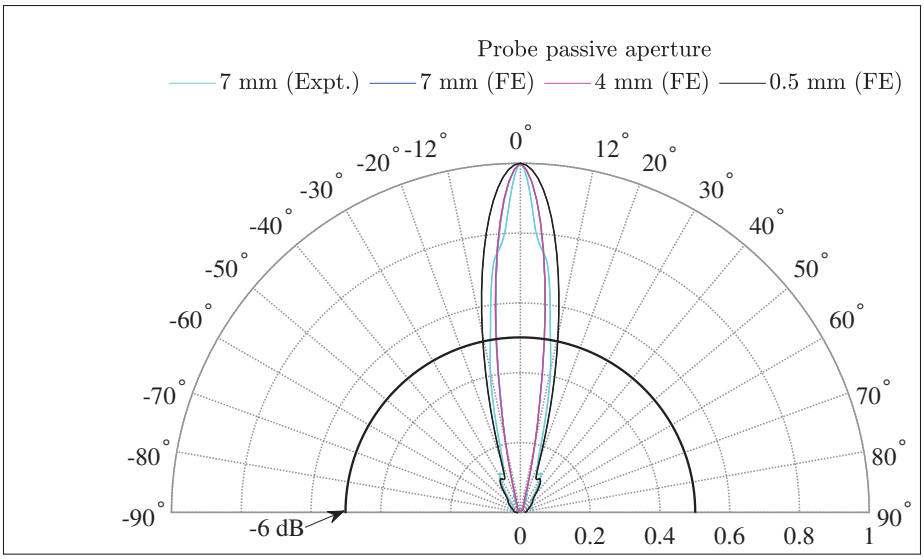

Figure 2.13 Polar plot shows the beam directivity and divergence angle of the generated Rayleigh waves obtained from FE simulation for 0.5 mm, 4 mm and 7 mm passive aperture and experiments corresponding to 7 mm passive aperture

CHAPTER 3

SURFACE BREAKING CRACK SIZING METHOD USING PULSE-ECHO RAYLEIGH WAVES

Bhupesh Verma[1] , Pierre Bélanger[1]

[1] Département de Génie Mécanique, École de Technologie Supérieure,
1100 Notre-Dame Ouest, Montréal, Québec, Canada H3C 1K3

Article published in the journal « Ultrasonics » in March 2024.

(DOI:https://doi.org/10.1016/j.ultras.2023.107232)

3.1 Abstract

Surface cracks are common in various industries. Eddy current testing (ECT) is commonly used for crack sizing but necessitates complex calibration standards and a highly trained inspector. Moreover, for large-area inspections, it requires additional scanning arrangements. In recent years the wedge technique-based Rayleigh wave crack sizing method has attracted significant research interest due to its unidirectional excitability. However, Rayleigh wave features generated at crack tips are often weak and masked under noise, and they mostly attenuate before reaching the receiving probe due to the couplant between the wedge-test specimen interface. Consequently, sizing the crack depth is difficult using a pulse-echo setup. This work presents a wedge-free pulse-echo Rayleigh wave method for surface crack sizing using a conventional phased array transducer. Eliminating the wedge removes a couplant layer leading to lower attenuation, enabling the transducer to capture crack tip features. This allows the sizing of surface cracks in pulse-echo using the time-of-flight (TOF) information. Furthermore, leveraging the phased array system, an averaging technique employed to the time trace signals captured by the transducer elements effectively averages out the other wave modes generated at crack geometries by the scattering of Rayleigh waves. This significantly minimizes sizing errors and enhances the signal-to-noise ratio (SNR). The performance of the proposed method is demonstrated through finite element simulations and experiments. Experiments with electric discharged machined (EDM) notches on test specimen surface at various angles and depths mimicking

surface-breaking cracks show accurate sizing within a 5% error. The proposed method offers flexibility in performing inspections using a wide frequency range and can be easily applied to different materials using any conventional phased array transducer. This enhances its adaptability for industrial applications in the characterization of surface cracks.

3.2 Introduction

Surface discontinuities that develop in engineering components due to extreme operational and environmental conditions affect the integrity and service life of structures. Nondestructive testing (NDT) methods play a crucial role in the inspection and assessment of the structural integrity and safety of such structures. Dye penetrant inspection, magnetic particle inspection (MPI), eddy current testing (ECT), thermography, and ultrasonic testing (UT) are NDT methods that allow to detect and characterize surface discontinuities. These methods were reviewed and summarized in Cawley (2001).

ECT is the most widely used technique among these methods as it is highly sensitive to surface and near-surface discontinuities. A considerable body work has been published on the inspection and sizing of surface cracks using ECT Helifa *et al.* (2006); Yamada, Hasegawa, Ishihara, Kiwa & Tsukada (2008); Mohseni, Habibzadeh Boukani, Ramos França & Viens (2020) and eddy current array probe Huang, Sakurai, Takagi & Uchimoto (2003); Yusa *et al.* (2014); Xie *et al.* (2015). However, an accurate depth and length sizing of surface cracks using ECT is challenging as it requires a complex calibration Van Drunen & Cecco (1984); Fan *et al.* (2015) and a highly trained inspector. Moreover, the eddy current method has a limited penetration depth, and consequently, the detection depth range is limited using it. While EMAT arrays Isla & Cegla (2017) and ultrasonic arrays Felice *et al.* (2014); Peng *et al.* (2018); Saini *et al.* (2022) have a wide range of applications in the characterization of surface-breaking cracks (SBCs), they, however, focus mainly on the characterization of SBCs situated on inaccessible back surfaces of components. A study introduced the frequency-domain multiple signal classification (F-MUSIC) model Yang, Wang, Zhou, Xu & Su (2022), allowing the visualization of damage

using a guided wave array. Nevertheless, obtaining spatial phase information for beam focusing remains challenging due to the signals measured from the sparse array.

In the past few decades, research has surged in utilizing ultrasonic Rayleigh waves to characterize surface discontinuities due to their ability to propagate over extended distances, and hence, enable the scanning of relatively large areas with just a few probe locations. Consequently, many researchers have dedicated their efforts to the development of NDT methods that utilize Rayleigh waves for detecting and characterizing surface cracks. Most of these methods size surface cracks by correlating Rayleigh wave features, including amplitude Cook & Berthelot (2001a); Blackshire & Sathish (2002); Aldrin (2004); Arias & Achenbach (2004); Edwards *et al.* (2006); Zeng *et al.* (2019); Zhang *et al.* (2020), reflection and transmission coefficients Hassan & Veronesi (2003); Vu & Kinra (1985); Vu (1986); Scala (2003); Zhou *et al.* (2015); Deng *et al.* (2019); Li *et al.* (2020), and TOF information concerning transmitted and mode-converted waves Cooper *et al.* (1986); Jeong (2005); Matsuda *et al.* (2006); Jian *et al.* (2006); Masserey & Mazza (2007); Yan *et al.* (2018); Xiao *et al.* (2022); Li *et al.* (2023), with crack geometry. However, it is worth noting that recent advancements have introduced diverse Rayleigh wave based techniques for evaluating surface-breaking cracks, as presented in Li, Ma, Fu & Krishnaswamy (2018); Xu *et al.* (2022); He, Liu, Cheng, Yang & Li (2023).

Jian *et al.* (2007) used the finite element method (FEM) to investigate the in-plane and out-of-plane displacements of scattered waves at surface cracks, explaining how these waves contribute to enhancing the amplitude of Rayleigh waves in the near field. However, amplitude-based sizing is inconsistent because the defect signal's amplitude from real flaws may not always behave like reference flaws in calibration standards. Moreover, surface roughness or surface coatings may lead to frequency dependent attenuation leading to difficult interpretation of the results. TOF sizing methods are typically more reliable in nondestructive evaluation (NDE). Matsuda *et al.* (2006) proposed a method to measure surface crack depth, utilizing the arrival time of Rayleigh waves from the crack tip. The necessity of placing the excitation laser and receiver in close proximity to the crack restricts the widespread application of this method. Similarly, other researchers Jian *et al.* (2006); Masserey & Mazza (2007); Xiao *et al.* (2022) have employed

the arrival time of transmitted Rayleigh waves across the surface cracks for depth assessment. However, this requires the help of an additional probe or laser interferometry system in a pitch-catch mode to perform the inspection. This complicates the experimental configuration and performing the inspection using a pitch-catch configuration is not ideal, especially for one-sided applications. Dutton *et al.* (2011) explored how laser generated Rayleigh waves interact with angled surface defects, aiming to understand Rayleigh wave behavior after interacting with such defects and size them using wave arrival times. Building on this research, Hernandez-Valle *et al.* (2014) adopted a similar approach for sizing branched surface-breaking defects using laser ultrasound. However, the bulk wave modes generated along with the Rayleigh waves make the signal processing complex. Authors in Cooper *et al.* (1986); Jeong (2005); Li *et al.* (2023) have highlighted the potential of mode-converted Rayleigh waves from the crack tip for crack depth measurement. However, they observed decreasing mode-converted Rayleigh wave amplitude as crack depth increased. These studies utilized laser ultrasound, which offers benefits like not requiring a couplant and, hence, enabling the possibility of capturing mode-converted Rayleigh waves. However, cost, difficulty of implementation in an industrial setting, and safety concerns limit applications of laser-based methods. This restricts the broad application of the mode-converted Rayleigh wave based sizing approach for inspections. A recently developed EMAT array based technique for generating Rayleigh waves provides flexibility through phase delay control between channels, allowing ultrasound wavelength adjustment without changing the physical separation of coils Xiang *et al.* (2020). Although this method has been effective in detecting and characterizing surface defects, the results are once again presented by analyzing the peak-to-peak amplitude of transmitted Rayleigh waves. This approach can be affected by interference with other wave modes scattered at surface cracks, resulting in amplitude variations. Additionally, it requires a pitch-catch setup for inspections, making the experimental setup more complex. While the wedge technique is known for its efficient Rayleigh wave generation and reception Rose (1999), it presents challenges due to the couplant layer between the wedge and the test specimen interface. This couplant layer hinders the reception of mode-converted Rayleigh wave features, especially those generated at crack tips, which are often weak and tend to attenuate before reaching the receiving probe. Therefore, the aim of this work is to develop

an easy-to-implement method for detecting and sizing surface cracks that can overcome the limitations observed in prior research that relies on the mode-converted Rayleigh wave from the crack tip and is solely based on TOF.

This paper presents a conventional phased array transducer based pulse-echo Rayleigh wave method for precise sizing of surface-breaking cracks. It utilizes a specific mode-converted Rayleigh wave originating from the crack tip that had been previously overlooked in earlier research due to its delayed arrival. The approach introduced in this paper leverages this wave's TOF information to size surface cracks accurately. Additionally, employing an averaging approach in reception using time trace signals captured by transducer elements helps mitigate interference from other wave modes generated at crack geometries. This process leads to significant enhancements in the SNR and effectively minimizes errors in sizing.

The paper is organized as follows: Section 3.3 presents the materials and methods, including an overview of the method used for the Rayleigh wave transduction. This is followed by the experimental details and the method used for FE simulations to demonstrate the proposed sizing method. Next, a presentation of the proposed sizing method is given. In Section 3.4, the results obtained from the FE simulations and experimental studies are presented, compared, and discussed. Finally, in Section 3.5 conclusions are drawn.

3.3 Materials and methods

3.3.1 Rayleigh wave transduction

The available Rayleigh wave excitation and detection methods using piezoelectric transducers, EMAT, lasers, and air-coupled ultrasonic transducers were reviewed and summarized in Chakrapani & Bond (2018). A piezoelectric transducer mounted on an angled wedge is considered to represent an efficient and most accepted approach due to its selective and unidirectional excitation capabilities. However, the requirement of fabricating a new wedge for a specific material makes this approach limited. To overcome the limitations of the

existing Rayleigh wave excitation methods, recently a method using a conventional phased array transducer was developed Verma & Bélanger (2023). In this method, a linear time delay law based on the elementary pitch of the transducer and on the Rayleigh wave speed of the test specimen was designed and implemented, to achieve selective and unidirectional excitation of Rayleigh waves without using a wedge. This delay law is easily adaptable to conventional phased array transducers of various frequencies and flexible for generating Rayleigh waves on different materials using the same transducer. Moreover, this excitation method offers better signal amplitudes for low-voltage inputs. Therefore, the Rayleigh wave excitation method given in Verma & Bélanger (2023) is adapted in this paper for the proposed surface crack sizing method and is briefly described here.

The amplitude A of a transmitted Rayleigh or Lamb mode using a transducer array can be expressed by the general equation:

$$A(x) = X \cdot F(\omega) \cdot C_n(x) \cdot H(\omega) \tag{3.1}$$

where X represents the particle displacement, $F(\omega)$ denotes the frequency response of the elements, $C_n(x)$ signifies the coupling coefficient between the waveguide surface traction and the targeted wave mode, and $H(\omega)$ is the only parameter on which the amplitude A depends and can further be modified to control the excited wave mode by adding an appropriate time delay t_0 to the array elements (without altering the element spacing), expressed as:

$$H(\omega) = \sum_{i=1}^{N} e^{j[\omega(t-t_i)\pm k_x(x-x_i)]} = \frac{sin[N\pi\left(\frac{p}{\lambda} \pm \frac{t_0}{T}\right)]}{sin[\pi\left(\frac{p}{\lambda} \pm \frac{t_0}{T}\right)]} e^{j\left[\omega\left(t-\frac{N-1}{2}t_0\right)\pm k_x(x-x_c)\right]} \tag{3.2}$$

In Equation 3.2, the symbol ± represents the direction of propagation along the x-axis, " − " sign corresponds to $+x$ direction and " + " sign corresponds to the $-x$ direction, p is the pitch (element spacing) of the transducer, λ is the wavelength, T is the period and equals to $1/f$, ω is the angular frequency, k_x is the wavenumber along the propagation direction x, N is the number of elements of the array, and x_c is the center location of the array transducer.

To maximize the amplitude A, the norm of $H(\omega)$ needs to be maximized. $|H(\omega)|$ reaches its maximum value when $\frac{p}{\lambda} \pm \frac{t_0}{T} = n$, where n is an arbitrary integer. Thus, the wavelength of the targeted mode can be written as $\lambda = \frac{p}{n \pm (t_0/T)}$, allowing for the amplification of specific modes by selecting a particular t_0. However, in the case of a phased comb transducer with a fixed elementary pitch equal to the wavelength of the targeted wave mode, the excitation zone in the phase velocity vs frequency diagram is influenced by the input signal frequency. This results in the activation of various nearby values of arbitrary integer n. Consequently, various zones in the phase velocity vs frequency diagram are amplified, and achieving the excitation of a specific mode becomes challenging. It is possible to amplify a specific zone corresponding to a particular phase velocity by selecting a significantly smaller elementary pitch (p) of the transducer compared to the wavelength (λ) of the targeted mode. In this case, the value of the arbitrary integer n becomes very small as the ratio $p/\lambda \ll 1$. With the nearest possible value of n being 0, the excitation becomes independent of the frequency, and the relationship $\lambda \cdot f = C_{ph} = \frac{p}{t_0}$ holds. Where f represents the frequency and C_{ph} is the targeted phase velocity. Thus, by adding a time delay t_0 to each element, it becomes possible to specifically target a desired phase velocity provided the value of p is much smaller than λ. Particularly, when it comes to exciting Rayleigh waves, the criterion of $p \ll \lambda$ is no longer necessary as the Rayleigh wave velocity is independent of the frequency. As a result, it becomes feasible to excite and receive Rayleigh waves using any conventional phased array transducer. This can be achieved by providing a time delay t_0 between the emission of each element, which is calculated based on the elementary pitch p of the transducer and Rayleigh wave speed C_R in the waveguide, as follows:

$$t_0 = \frac{p}{C_R} \tag{3.3}$$

In general, the linear time delay law for estimating the required delay of each element to generate Rayleigh waves can be expressed as:

$$t_i = \frac{p * (i-1)}{C_R} \tag{3.4}$$

where t_i is the time delay corresponding to the i^{th} element of the phased array transducer and i ranges from 1 to N (total number of elements of the array) p is the elementary pitch and C_R is the Rayleigh wave velocity in the test specimen to be inspected.

3.3.2 Experimental details

Two sets of test specimens with surface breaking notches were used in this work. They are shown schematically in Figure 3.1. The notches were produced by electrical discharge machining (EDM) on the surface of both specimens using a 0.3 mm diameter wire. In the first specimen, an EDM notch oriented normal to the surface of the test specimen (referred to as a 0° notch hereafter) and varying in depth from 1 mm to 5 mm across the width of a 20 mm thick aluminum plate was machined as shown schematically in Figure 3.1(a). In order to evaluate the performance of the proposed sizing method, the measurement was conducted at four different locations, having different depths D_1, D_2, D_3 and D_4 as depicted in Figure3.1(a). Further, to evaluate the flexibility of the proposed method, the second specimen used in the measurement comprised four EDM notches with different angles in a 19 mm thick steel plate. All the notches in the second specimen were of a constant 5 mm depth and inclined at 0°, 10°, 20° and 30° with respect to the surface normal, as shown schematically in Fig3.1(b).

The configuration of the experimental measurements used in the present work is shown in Figure3.1(c). The pulse-echo Rayleigh wave excitation and reception technique used in the proposed sizing method is flexible and easily adaptable to phased array transducers of various frequencies. Therefore, a conventional 3.5 MHz phased array transducer was used for all measurements. The signal generation and emission of each element of the phased array was controlled using a Verasonics Vantage 64 LE controller. A Hann windowed toneburst centered at 3.5 MHz was sent to each element with the required delay estimated using Equation 3.4. The back-propagation of the incident waves after interacting with the notch geometries was captured by the same phased array transducer used for the excitation. The experimental data was imported to the MATLAB environment to estimate the notch size using the method proposed in this paper.

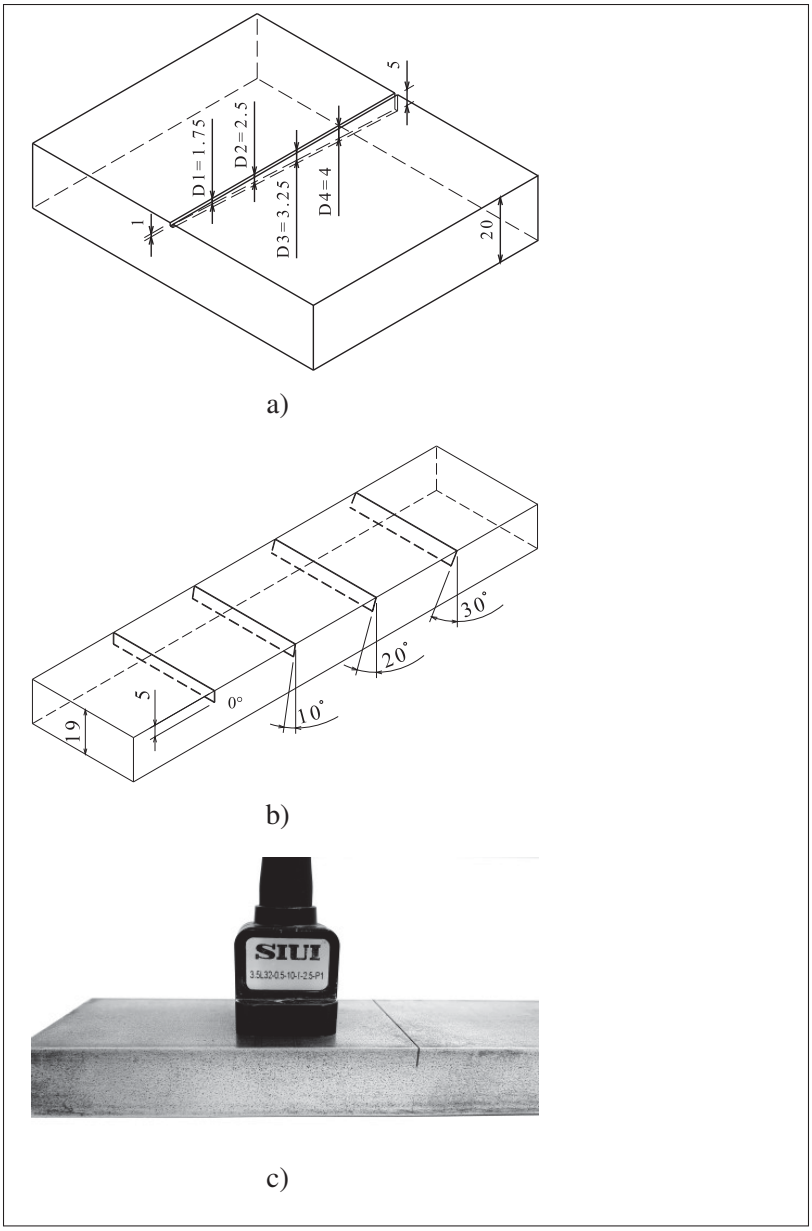

Figure 3.1 (a) Schematic of an aluminum plate sample with a surface breaking notch with a varying depth profile across the width of the plate (dimensions are in mm); (b) schematic of a steel plate sample with notches inclined at various angles (dimensions are in mm), and (c) configuration for experimental measurements

In order to ensure the repeatability of the results, the measurements were conducted 5 times with different probe positions located 20 mm 30 mm 40 mm 50 mm and 60 mm from the notch.

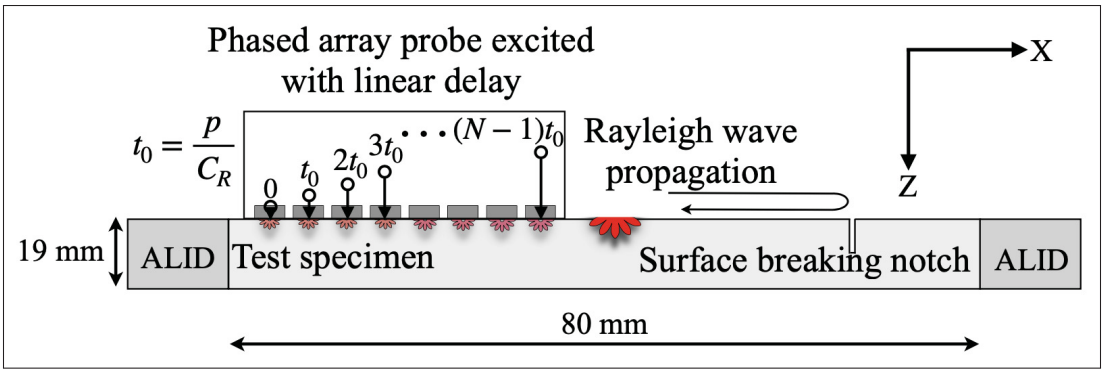

Figure 3.2 Schematic of finite element model used to simulate the propagation of Rayleigh waves and their interactions with an EDM notch-like defect

3.3.3 Finite Element simulations

Numerical simulations are often used to predict the expected experimental results and physical insight of a complex problem. In the present work, FE simulations were conducted to simulate the propagation of Rayleigh waves and their interactions with an EDM notch-like defect. All the simulations presented here were performed using a graphics processing unit (GPU)-based accelerated FE code provided by Pogo Huthwaite (2014). A schematic of the two-dimensional FE model used is shown in Figure 3.2. A 19 mm thick steel plate (Young's modulus 200 GPa, density 7800 kg/m^3, Poisson's ratio 0.3) was discretized using two-dimensional plane strain elements. 20 elements per the shortest wavelength were considered to ensure a converged solution for the elastic wave propagation problem. The step time (δt) was chosen to satisfy the time marching simulation stability criterion as $\delta t \leq 0.8\Delta x/C_{max}$ Drozdz *et al.* (2006), where Δx is the smallest element size in the finite element mesh and C_{max} is the fastest mode velocity. The absorbing layers with increased damping (ALID) method was used to design and create the absorbing boundary layers at both ends of the plate to reduce reflections Drozdz *et al.* (2006); Rajagopal *et al.* (2012). An EDM notch-like defect similar to those in the test specimens was created to facilitate experimental comparisons. A conventional phased array transducer was simulated. The nodes on the top surface of the plate were selected and excited using a 3-cycle Hann windowed toneburst centered at 3.5 MHz. These nodes correspond to a 32-element phased array with a 0.5 mm elementary pitch and a 0.08 mm element interspace. The selected nodes

were excited with the required delay for generating Rayleigh waves, obtained using Equation 3.4. The reflections of the wave propagating along the surface from the notch geometries were received at the same nodes chosen for the excitation.

3.3.4 Proposed method for the sizing of surface breaking EDM notches

A thorough understanding of the Rayleigh wave scattering sequences at the EDM notch is needed to extract the features of Rayleigh waves generated by the notch geometries. So that, these Rayleigh wave features can be used in the characterization of surface cracks. The Rayleigh waves scattering process at a surface crack is described in Verma & Bélanger (2023); Masserey (2006) using numerical simulations. These scattering patterns are visually illustrated in a schematic shown in Figure 3.3 for reference. The incident Rayleigh waves propagate along the surface, and upon the first interaction with the notch edge, they are reflected, transmitted and diffracted into the bulk waves (longitudinal and shear waves). These reflected Rayleigh waves (referred to as R_r) can be used to locate the surface cracks. The transmitted Rayleigh waves follow the notch face and reach the notch tip, where they scatter once again. Most of the energy from the transmitted Rayleigh wave is again diffracted into longitudinal and shear waves and a very small amount of the energy is reflected and transmitted on the notch faces. Interestingly, the shear wave mode generated at the notch tip propagates in the bulk of the test specimen, and reflects back towards the notch tip after hitting the backwall. Upon encountering the notch tip, a new Rayleigh wave mode is generated. This newly generated Rayleigh wave propagates on both notch faces, and after scattering at the left and right notch edges the remaining Rayleigh energy propagates along the surface. The energy is then captured by the same phased array transducer used for the excitation. This new Rayleigh wave mode is referred to as R_n hereafter. The sizing method proposed herein is mainly based on the arrival time of the signal R_n.

The features of the Rayleigh wave generated at the end of the scattering sequences by the notch geometry sometimes interfere with or are masked under the wave modes unrelated to Rayleigh waves generated at the notch edge and tip. This makes the identification and separation of the signal R_n from other wave modes difficult. Therefore, an averaging approach consistent with

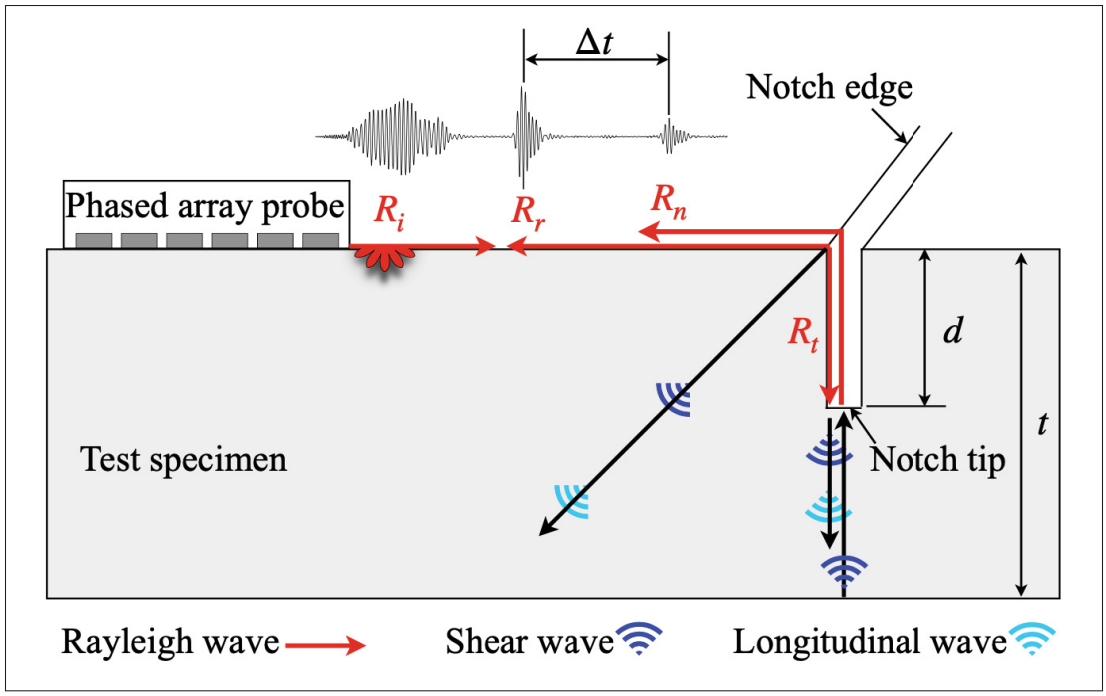

Figure 3.3 Schematic illustrating Rayleigh wave interactions with an EDM notch and the Rayleigh wave path used for precise sizing using the proposed method. R_i represents the incident Rayleigh wave, R_r is the Rayleigh wave reflected from the notch edge, R_t signifies the Rayleigh waves that propagate along the notch face, and R_n is the newly generated Rayleigh wave mode resulting from the reflection of the shear wave mode (generated at the notch tip) from the back wall, encountering the notch tip

the delay-line systems Manes, Atzeni & Susini (1983) commonly used in ultrasound phased array imaging techniques was employed to mitigate the influence of wave modes unrelated to Rayleigh waves. In this approach, the time traces of out-of-plane displacement recorded by the transducer elements were temporally shifted using a specific time delay to ensure Rayleigh waves arrived at all elements at the same time. The specific time delay was determined considering the elementary pitch (p) of the phased array transducer and the experimentally measured Rayleigh wave velocity (C_R) in the test specimen, as outlined in Equation 3.5.

$$(t_0)_k = (k-1) \cdot \frac{p}{C_R} \tag{3.5}$$

This adjustment ensured the phase synchronization of Rayleigh wave components across all elements. Subsequently, the time series resulting from this process was summed, leading to constructive interference. Consequently, the output signal predominantly contained Rayleigh wave features generated by the notch geometries, while the majority of other unrelated wave modes were effectively averaged out due to destructive interference. The amplitude $A(t)$ of the time series after this averaging procedure can be expressed as:

$$A(t) = \frac{1}{N} \sum_{k=1}^{N} A_{(k)} \left(t + (t_0)_k\right) \tag{3.6}$$

where N is the total number of elements of the probe used in averaging, p is the elementary pitch of the transducer, C_R is the Rayleigh velocity in the waveguide, and $A_{(k)}$ is the time series corresponding to the $(N)^{th}$ element. The resulting time series thus carries the information related to the Rayleigh wave and can be used in the reconstruction of the notch depth in the case of a 0° notch, or of the notch face length, in the case of an inclined notch.

Figure 3.3 shows a schematic illustration of the proposed sizing method and the Rayleigh wave path used for precise sizing through this approach. Here, the TOF information between the signal R_r and R_n is used. As observed, the new Rayleigh wave mode R_n is generated when the shear wave mode (generated at the notch tip) reflects from the back wall and encounters the notch tip. Thus, the TOF (Δt) between the signal R_r and R_n can be expressed as:

$$\frac{d}{C_R} + \frac{t - d}{C_S} = \frac{\Delta t}{2} \tag{3.7}$$

where d is the notch depth or notch face length, t is the thickness of the test specimen, C_R is the Rayleigh wave velocity and C_S is the shear wave velocity of the waveguide. Further, after simplification, Equation 3.7 can be rewritten to estimate the notch depth in the case of 0° notch, or the notch face length, in the case of the inclined notch, as:

$$d = \frac{C_R \cdot \left(\frac{\Delta t}{2}\right) - t \cdot R_{R/S}}{1 - R_{R/S}} \tag{3.8}$$

where $R_{R/S}$ is the ratio of Rayleigh wave to shear wave velocity of the waveguide material.

3.3.5 Rayleigh wave velocity calibration

In order to have an accurate sizing of the notch, the Rayleigh wave velocity of the test specimen is required. Therefore, the Rayleigh wave velocity in both the test specimens was measured before the measurements were conducted. The reflections of the incident Rayleigh waves, from the two edges across the thickness of the test specimen, named edge *A* and edge *B* in the schematic shown in Figure 3.4(a), were received using the same probe. Figure 3.4(b) presents the typical time traces of the out-of-plane displacement amplitude corresponding to one of the elements of the phased array probe for the steel test specimen. The reflections from edges *A* and *B* can clearly be seen in Figure 3.4(b). The frequency spectrum corresponding to the reflected signals from edges *A* and *B* is shown in Figure 3.4(c). The velocity was calculated using the TOF between the wave packets corresponding to the reflections from edges *A* and *B* of the test specimen. The measured Rayleigh wave velocity was 2988 m/s and 2941 m/s for the steel and aluminum test specimens, respectively.

3.4 Results and discussion

3.4.1 0° notch depth sizing

The interaction and scattering sequences of Rayleigh waves with a 0° notch, as well as the eventual generation of a new Rayleigh wave mode at the notch tip, were first verified using FE simulations. The Rayleigh wave excitation was achieved using a conventional 3.5 MHz phased array probe. Figure 3.5 shows the snapshots of the contour of the total field displacement amplitude of Rayleigh waves when they interact with a 5 mm deep simulated surface breaking notch with a 0.3 mm width. The incident Rayleigh wave R_i propagates along the surface, as

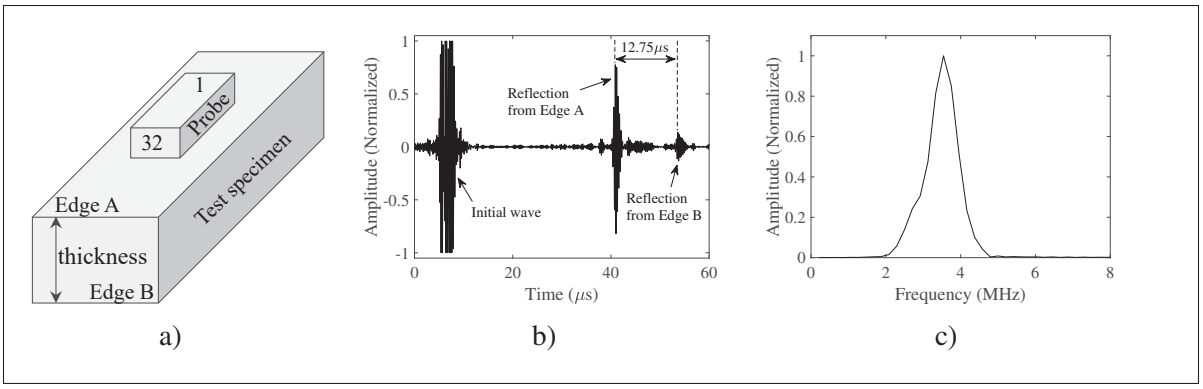

Figure 3.4 Experimental excitation and reception of Rayleigh wave on test sample using a 3.5 MHz conventional phased array probe: (a) schematic of test specimen configuration during measurements; (b) typical time traces of the amplitude of the out-of-plane displacement corresponding to one of the elements of the phased array probe on the steel plate sample, having a thickness of 19 mm, and (c) corresponding frequency spectrum

shown in Figure 3.5 (a). Upon reaching the opening of the notch (referred to as the notch edge hereafter), Rayleigh waves scattered and generated a reflected Rayleigh wave R_r, transmitted Rayleigh wave R_t, and bulk wave modes (longitudinal (L_1) and shear (S_1) wave) can be seen in Figure 3.5(b). The transmitted Rayleigh wave R_t follows the notch face and when it reaches the notch tip, it scatters once again and diffracts into a longitudinal (L_2) and a shear (S_2) waves, as can be seen in Figure 3.5(c). In addition, a small amount of the energy from R_t is reflected and transmitted on the notch faces, and upon reaching the notch edge, they further scatter. The signals carrying the remaining reflected and transmitted Rayleigh energy from the notch tip are mostly very weak and masked under the noise, and hence difficult to visualize.

Furthermore, the shear wave mode S_2 propagates into the bulk of the material and reflects after hitting the backwall, as shown in Figure 3.5(d). The reflected S_2 signal encounters the notch tip and generates a new Rayleigh wave mode, which propagates on the notch faces, as can be seen in Figure 3.5(e). Upon reaching the notch edge, this newly generated Rayleigh wave is scattered again in a similar fashion and the remaining energy propagates along the surface, as shown as R_n in Figure 3.5(f).

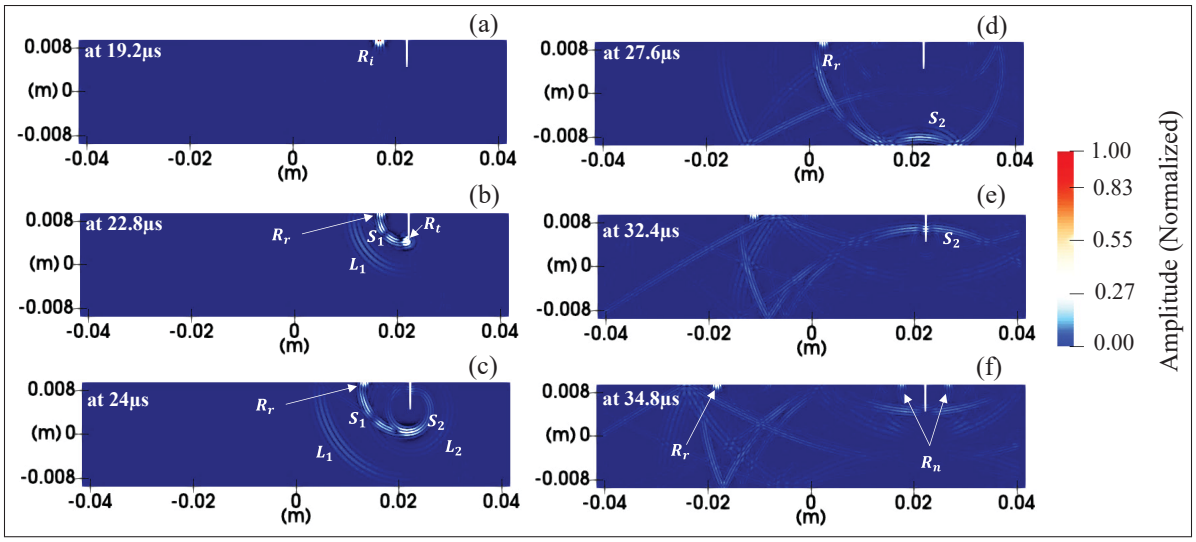

Figure 3.5 Snapshots of the contour of total displacement magnitude by the scattering of Rayleigh wave at a 0° EDM notch, recorded at different time instances: (a) incident Rayleigh waves (R_i); (b) scattering of the incident Rayleigh waves at the left opening of the notch (notch edge); (c) scattering of the transmitted Rayleigh waves at the tip of the notch; (d) propagation of the shear wave mode (S_2) towards the notch tip after hitting the backwall; (e) interaction of reflected shear wave mode (S_2) with the notch tip and generation of the new Rayleigh wave mode (R_n), and (f) propagation of the new Rayleigh wave mode (R_n) along the surface

The corresponding time traces of the out-of-plane displacement amplitude recorded at one of the elements of the array transducer, obtained from the FE simulation and experiments, are shown in Figure 3.6(a) and (b), respectively. The Rayleigh wave signals reflected from the notch edge R_r and the newly generated Rayleigh wave R_n can clearly be seen. Also, along with these signals, other wave modes unrelated to the Rayleigh waves generated by the scattering of incident Rayleigh waves at the notch edge and tip can be seen in between signals R_r and R_n. However, the signals related to Rayleigh waves shown in Figure 3.6 are well separated. Nevertheless, depending on the test specimen thickness and notch depth, the other wave modes may sometimes overlap with the signal R_n and become a possible source of error when estimating the notch size using the method proposed in this paper. Therefore, to attenuate these other wave modes, the averaging approach described in Section 3.3.4 was used in reception. A comparison of the resulting time series after averaging of experimentally measured signals obtained using Equation

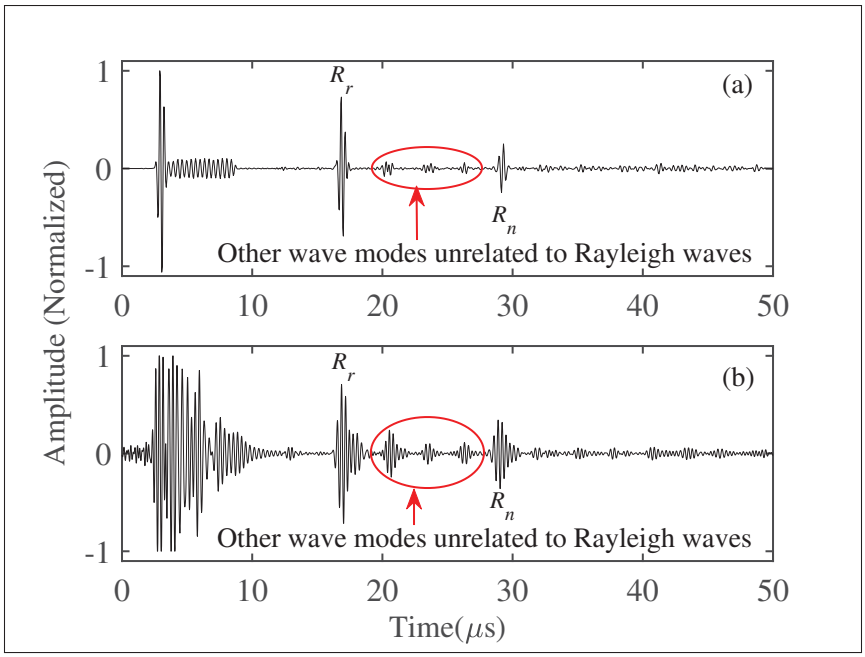

Figure 3.6 Time traces of the out-of-plane displacement amplitude of Rayleigh wave scattered by a 5 mm deep 0° notch, obtained from: (a) FE simulation and (b) experimental measurements

3.6, and before averaging, is shown in Figure 3.7. It can be noted in Figure 3.7(b) that most of the wave modes unrelated to Rayleigh waves are averaged, and the signal information is mostly related to the Rayleigh wave features generated at the notch geometries remain as expected. This is a clear advantage of using the phased array based averaging approach in reception, as it provides a configuration equivalent to what is present when using the wedge technique while preserving the information intact relevant to the crack tip.

From Figure 3.7(b), it was also noted that along with the signal R_r and R_n, another small peak appeared at around 40μs. This peak corresponds to second new Rayleigh wave modes generated at the notch tip by the scattering of multiple backwall reflections of S_2. The generation of multiple new Rayleigh wave modes depends on the distance between the notch tip and the backwall. If the distance between is short, then there is a possibility of having multiple peaks corresponding to the new Rayleigh wave mode. The signal R_r can be used to locate surface

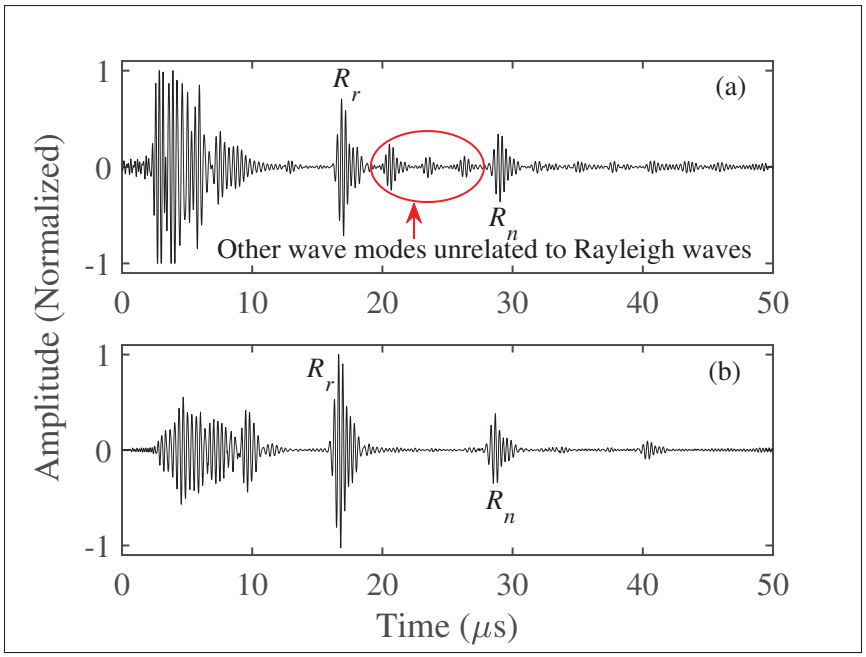

Figure 3.7 Experimentally measured time traces of the out-of-plane displacement amplitude of Rayleigh wave for a 5 mm deep 0° notch obtained: (a) before averaging and (b) enhanced amplitude after averaging

discontinuities. The TOF (Δt) between the signal R_r and R_n is used to estimate the notch depth in the case of a 0° notch, and the notch face length, in the case of the inclined notch.

First, the measurements were conducted on the test specimen with a 0° notch varying in depth across the width, as shown in Figure 3.1(a). The bar chart shown in Figure 3.8 represents a comparison between the actual and experimentally measured value of the notch depth corresponding to four different depths across the width of the test specimen also shown schematically (cross-sectional view) in Figure 3.8. The measured value shown here is the average of 5 measurements conducted in all cases. The vertical bar represents the maximum and minimum values of the measured depth among the 5 measurements conducted to ensure repeatability of the results. The estimated percentage error in the notch depth measurement is given in Table 3.1. All the measured depths are in the vicinity of the known actual depths. From Table 3.1, it can be noted that the maximum error recorded was under 5% for all the

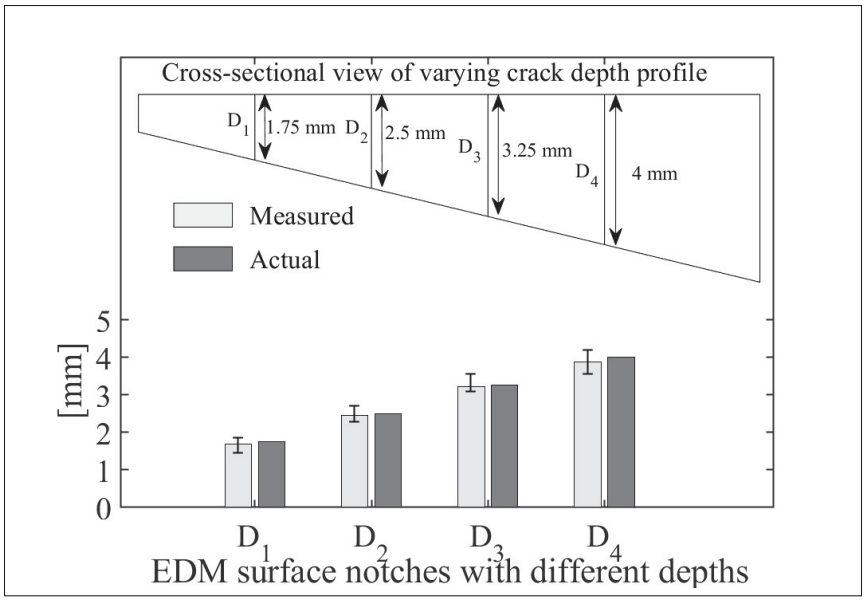

Figure 3.8 Comparison of the actual and experimentally measured notch depth for a 0° notch with varying depth profile

measurements. A good repeatability of the results was observed, with maximum deviations within 10%.

As the method proposed herein is mainly based on the new Rayleigh wave mode (R_n) generated at the notch tip, it is important to understand the influence of the notch depth on the generation of the new Rayleigh wave mode (R_n). Therefore, the present study was further extended using both FE simulations and experiments. FE models were used to simulate a 0° notch with various notch depths and the corresponding amplitude of the Rayleigh wave mode generated at the notch geometries by the scattering of incident Rayleigh waves was examined. In this case, the Rayleigh wave wavelength is a very important parameter as the Rayleigh energy is confined within a few Rayleigh wave wavelengths below the surface of the test specimen. Therefore, the simulated depth of the notch was chosen in terms of Rayleigh wave wavelength (λ_R) ranging from $0.5\lambda_R$ to $6.25\lambda_R$.

Figure 3.9 shows how the amplitude of the reflected (R_r) and the newly generated Rayleigh wave mode (R_n) behave with increasing notch depths. The amplitude of the signals R_r and R_n

Table 3.1 Percentage measurement error for a 0° notch with varying depth

Notch depth	D_1	D_2	D_3	D_4
Actual depth (mm)	1.75	2.50	3.25	4.00
Measured depth (mm)	1.69	2.45	3.21	3.88
% Error in measurement	3.42	2.00	1.23	3.00

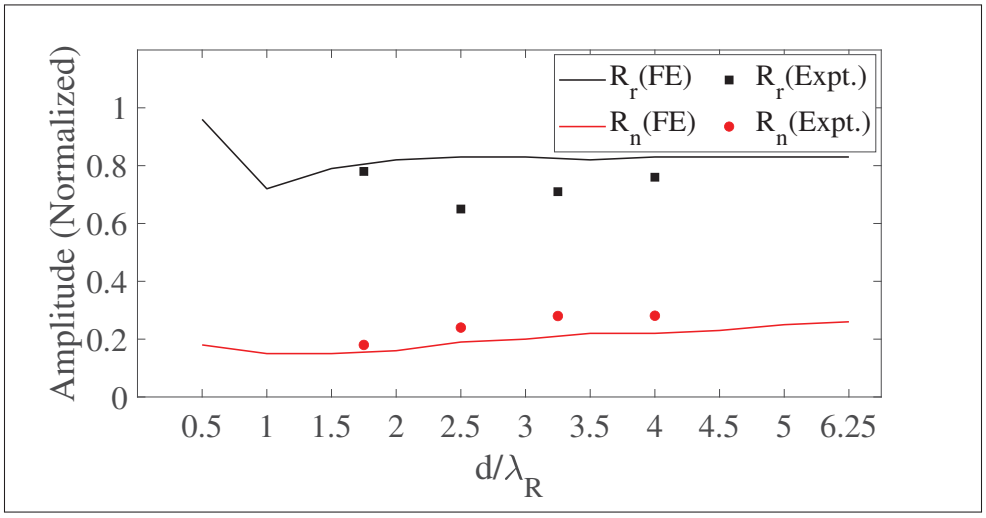

Figure 3.9 Plot of the normalized amplitude of the reflected and newly generated Rayleigh waves versus notch depths normalized with Rayleigh wavelength. The displayed amplitudes are extracted from time trace signals associated with a single element of the phased array transducer

were normalized with the maximum amplitude of the incident waves, while the notch depths were normalized with the Rayleigh wave wavelength. It can be noted that the generation of the new Rayleigh wave mode was found common, regardless of the size of the notch depths. This demonstrates that the proposed method works well for a 0° notch and can accurately size surface features with a minimum depth approximately equal to sub-wavelength. Furthermore, it is important to note, that the proposed sizing method is flexible to perform the inspection using a wide range of frequencies. This allows for the selection of a suitable center frequency of the phased array probe based on the sensitivity of surface cracks to be measured. Consequently, the proposed method enables the accurate sizing of crack depths ranging from shallow to deep.

From Figure 3.9, we note that the amplitude of signal R_n increases slightly with an increase in the depth of the notch. This is most likely because, with the increased notch depth, the distance between the notch tip and the backwall reduces. Consequently, the S_2 mode attenuates less, leading to the observed increase in the amplitude of the new Rayleigh wave mode with the increased notch depth. It was also observed that for notch depths beyond 1.5 times the Rayleigh wave wavelength, the amplitudes of the reflected Rayleigh waves remain unchanged. However, within the notch depth range where d/λ_R is less than 1.5, the reflected Rayleigh wave amplitudes were observed to oscillate. This phenomenon is likely due to the fact that the Rayleigh waves have a penetration depth of approximately a few Rayleigh wave wavelengths below the surface, and the notch depth in this range is approximately equal to or less than the Rayleigh wave penetration. Consequently, the scattering of incident Rayleigh waves at both the notch edge and tip becomes indistinct, leading to interference between Rayleigh wave features generated at these locations and resulting in the observed amplitude variation. However, since the proposed sizing method relies on the TOF information between signals R_r and R_n, variations in amplitude do not affect the accuracy of the proposed method. This demonstrates the potential of the proposed sizing method for sizing a 0° notch.

Previous research, as noted in references Cooper *et al.* (1986); Li *et al.* (2023), employed an additional mode-converted Rayleigh wave originating from the crack tip to assess crack depth. This mode is generated through shear wave reflection from the crack tip directly to the surface, subsequently transforming into Rayleigh waves and propagating along the surface. These studies used laser ultrasound techniques. Laser ultrasound techniques have an advantage in that no couplant is needed. This characteristic enables the detection of this specific mode-converted Rayleigh wave. However, in our proposed sizing method, which uses a couplant layer between the probe and the test specimen, this feature was not as pronounced. Its absence offers an advantage as it helps prevent potential confusion and sizing inaccuracies that might arise from the inclusion of this feature.

3.4.2 Inclined notch face length sizing

Experiments were further extended to evaluate the flexibility of the proposed method in sizing a notch inclined at an angle with respect to the surface normal. The test specimen used for the measurements is shown schematically in Figure 3.1(b). All the notches have a constant depth of 5 mm. As Rayleigh waves propagate along the notch face, the measured value obtained using Equation 3.8 delivers the notch face length rather than the depth, in this case. Figure 3.10 shows a bar chart comparing the actual and experimentally measured values of the notch face length, along with a schematic representation of the measured inclined notches. The notch face lengths shown here (S_1, S_2, S_3 and S_4) respectively correspond to a $0°$, $10°$, $20°$ and $-10°$ notch. The measurement corresponding to a $-10°$ notch shown here was done just to ensure that the proposed method works well from the other side of the notch as well. The measured notch face length is the average out of 5 measurements taken during experiments. The vertical bar represents the maximum and minimum measured values of the notch face length from 5 measurements. The percentage error calculated in the notch face length measurement is given in Table 3.2.

From Figure 3.10 and Table 3.2, it is clear that the proposed method has the potential to reconstruct the notch face length accurately within a 5% error range. The maximum deviations in the repetition of the results are under 10%, which is typically expected in any practical measurements. However, this method cannot measure the notch face length for notches inclined beyond $20°$. In order to understand the cause of this limitation of the proposed sizing method, our studies were further extended using FE simulations. A 5 mm deep notch inclined at an angle of

$30°$ with the surface normal was simulated. The snapshots of the contour of the total field displacement amplitude of the Rayleigh wave interaction with the simulated $30°$ inclined notch is shown in Figure 3.11. The incident Rayleigh waves propagate along the surface, as can be seen in Figure 3.11(a), and are scattered at the notch edge and at the notch tip, as shown in Figure 3.11(b). We noted that the scattering sequences of incident Rayleigh waves at the

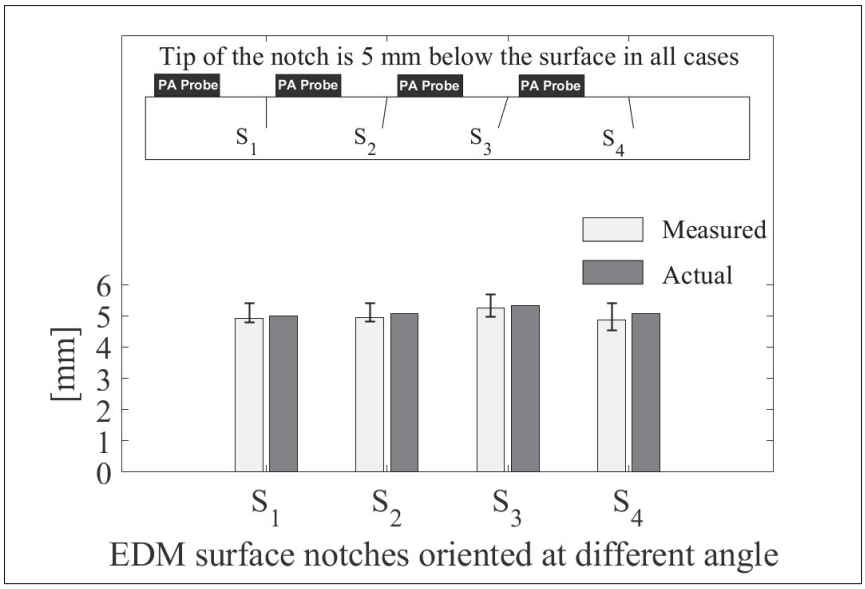

Figure 3.10 Bar chart showing the actual and experimentally measured face lengths of EDM notches inclined at various angles, with a constant depth of 5 mm

Table 3.2 Percentage error in face length measurement of notches inclined at different angles, with a constant 5 mm depth

Notch angles (°)	S_1 (0°)	S_2 (10°)	S_3 (20°)	S_4 (−10°)
Actual length (mm)	5.00	5.08	5.32	5.08
Measured length (mm)	4.92	4.95	5.24	4.86
% Error in measurement	1.60	2.55	1.50	4.33

notch geometries occur similarly to what was previously explained in section 3.4.1 for a 0° notch, except for the generation of a new Rayleigh wave mode at the notch tip. In the case of an inclined notch, the shear wave mode (S_2) generated at the notch tip propagates in the bulk of the material and impinges the backwall at an angle that is equal to the notch inclination angle with the surface normal. For this reason, most of the energy is reflected away from the notch tip, and the total energy reaching back to the notch tip is lower, as can be seen in Figure 3.11(c). Consequently, the new Rayleigh wave mode (R_n) generated at the notch tip is very weak, and is indeed almost negligible (see Figure 3.11(d)). Typical time traces of the out-of-plane

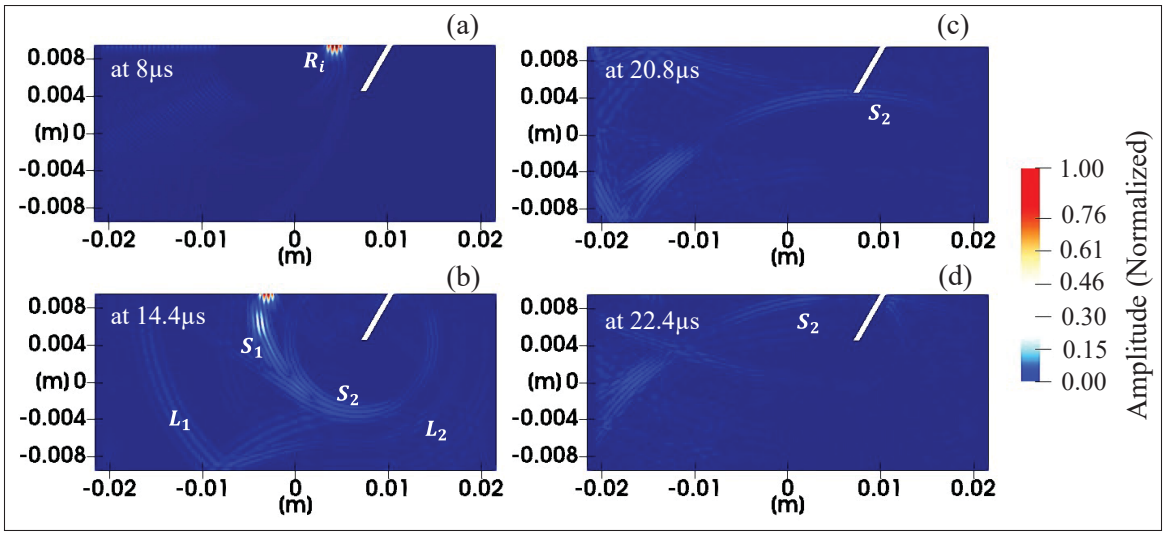

Figure 3.11 Snapshots of the contour of total displacement magnitude by the scattering of Rayleigh wave at an EDM notch inclined 30° from the surface normal, recorded at different time instances: (a) incident Rayleigh waves; (b) scattering of the incident Rayleigh waves at the left opening of the notch as well as scattering of transmitted Rayleigh waves at the notch tip; (c) interaction of reflected shear wave mode S_2 with the notch tip, and (d) the new Rayleigh wave mode (R_n) generation (almost negligible and difficult to visualize)

displacement corresponding to one element of the phased array, obtained from FE simulation and experiments, are shown in Figure 3.12(a) and (b), respectively. It was noted that the signal R_n is very weak and masked under background noise. Following implementation of the averaging in reception on the experimentally measured signal, the resulting time series was presented in Figure 3.12(c). Even after averaging, there is no appreciable enhancement, and it is difficult to visualize the signal R_n.

Due to the almost negligible signal strength of R_n observed in the case of the 30° inclined notch, it becomes crucial to examine the behavior of signal R_n amplitude as the notch angles increase. To gain insights into the impact of the notch angle on signal R_n amplitude, FE simulations were conducted. These simulations involved a 5 mm deep notch inclined at various angles with the surface normal. The amplitude variation of signal R_n with increasing notch angles is depicted in Figure 3.13. The decrease in amplitude of signal R_n is evident with increasing notch angles, eventually after 25° the amplitude approaches towards zero. Additionally, beyond a certain point,

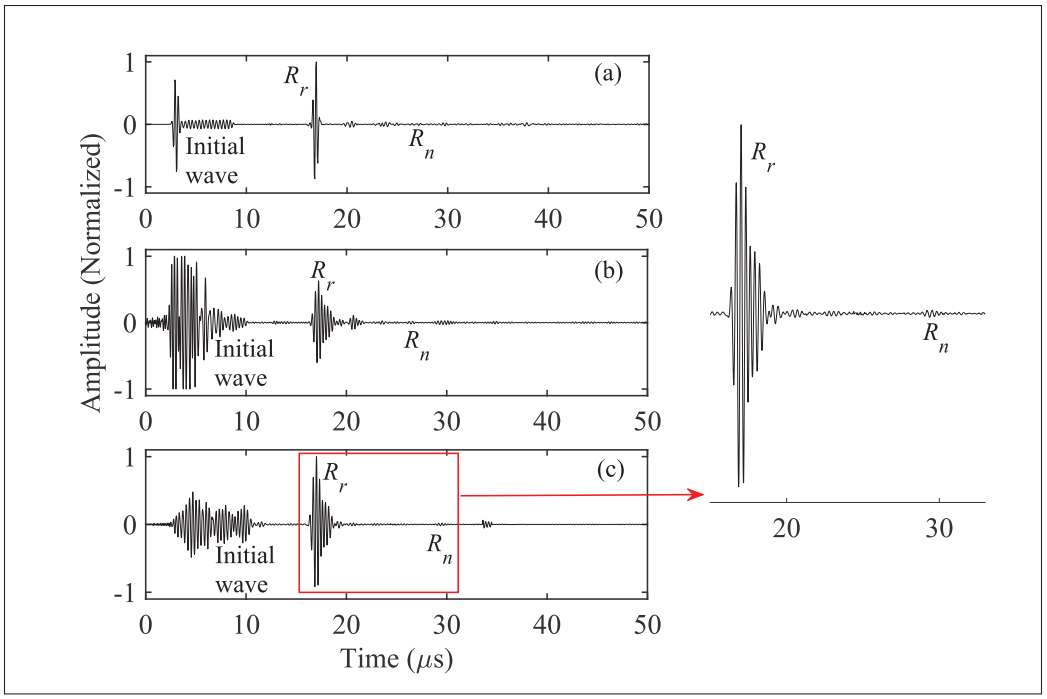

Figure 3.12 Time traces of the out-of-plane displacement amplitude of Rayleigh wave for a 5 mm deep and 30° inclined notch obtained: (a) from FE simulation; (b) experimentally before averaging, and (c) experimentally after averaging

the generation of the new Rayleigh wave mode ceases to occur. As a result, the applicability of the proposed sizing method is limited for notches inclined beyond 20°. Moreover, in the case of inclined notches, the proposed method measures the notch face length instead of the notch depth. Therefore, the depth of inclined notch becomes slightly overestimated when using this method.

3.4.3 Sizing of notch with a finite length of different orientation

In this study, the test samples used in the experimental measurements consisted of EDM notches with infinite notch lengths oriented perpendicularly to the Rayleigh wave propagation direction. The proposed sizing method works effectively for this type of notch. However, its applicability is not limited solely to this scenario. It is believed that the same principles apply to realistic cracks, which often involve surface cracks with finite lengths. However, to investigate the effectiveness of the proposed method in sizing finite-length EDM notches with different orientations relative

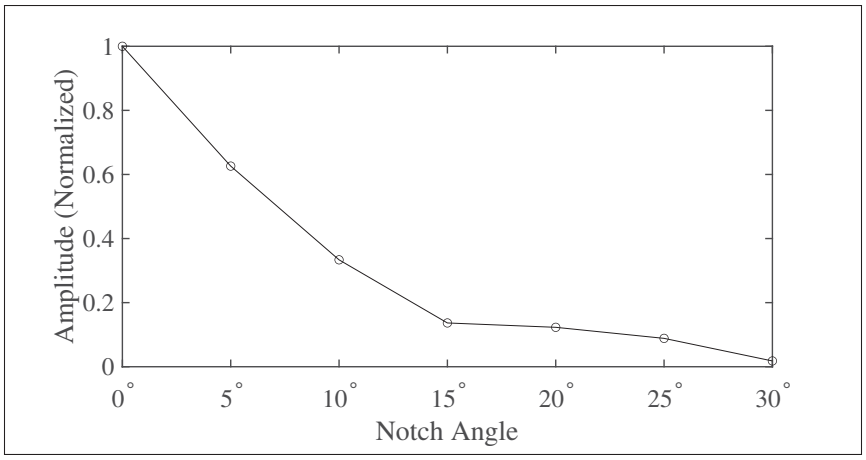

Figure 3.13 Plot showing the simulated amplitude (normalized) of the signal R_n at different notch angles

to the focal axis, our studies were further extended using finite element simulations. The initial 2-D FE model was extended to a 3-D model with the mesh consisting of 8-node cubic brick elements. These EDM notches had a constant depth of 5 mm and finite lengths measuring 4 mm and oriented at angles 90°, 80°, 70°, and 60° with respect to the focal axis. These notches were located 10 mm from the probe position. It is important to mention here that the notch length of 4 mm was chosen in each case to place them within the ultrasonic Rayleigh wave beam's divergent region, which extends approximately 20° at half maximum (-6dB) for a probe passive aperture measuring 10 mm Verma & Bélanger (2023). All the nodes corresponding to the passive aperture and the element width of the same 3.5 MHz phased array probe used for other experimental measurements were chosen for the excitation. The reflections of the wave propagating along the surface from the notch geometries were received at the same nodes selected for the excitation. The time trace signals recorded at monitoring nodes were used to implement averaging in reception. The resulting amplitudes of the Rayleigh wave mode generated at the notch geometries by the scattering of incident Rayleigh waves are presented in Figure 3.14. Typical time traces of the out-of-plane displacement of Rayleigh wave amplitude (normalized) corresponding to 90°, 80°, 70°, and 60° orientations relative to the focal axis are shown in Figure 3.14 (a), (b), (c), and (d) respectively. As expected, the present method works efficiently for a finite-length notch oriented at 90° relative to the focal axis, as evident in Figure

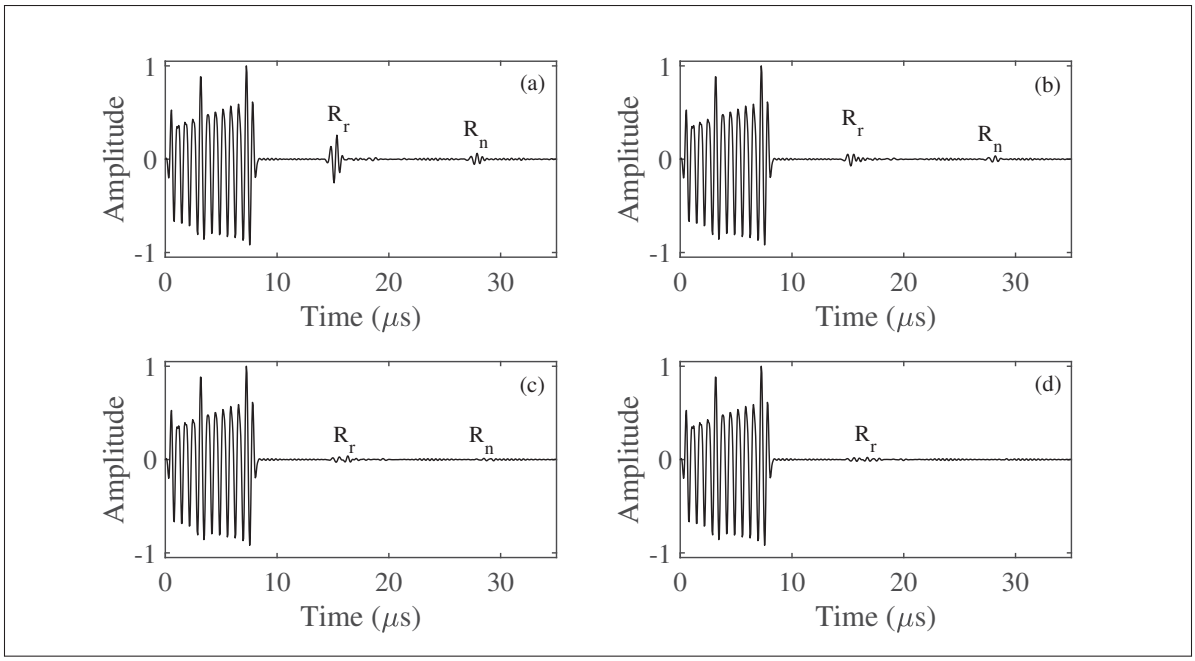

Figure 3.14 Simulated time traces of normalized out-of-plane displacement amplitude of Rayleigh waves interacting with notches of 5 mm constant depth and 4 mm finite length, oriented at various angles with respect to the focal axis: (a) 90°, (b) 80°, (c) 70°, and (d) 60°

3.14 (a). It can also be noted from Figure 3.14 (b) and (c), that the proposed method is capable of sizing notches oriented between 90° to 70° with respect to the focal axis. However, beyond this range, the signals R_r and R_n were not detected. This is likely due to the fact that the Rayleigh energy reflects from the notch at an angle matching its orientation. Consequently, as the angle of the notch's orientation changes from 90° to 0° relative to the focal axis, progressively less Rayleigh energy from the notch geometries reaches back to the probe. Beyond a certain point, particularly after 70° as it approaches the focal axis, it no longer returns to the probe. Hence, the proposed sizing method is applicable for notch lengths oriented between 90° to 70° from the focal axis. Therefore, during the inspection workflow, the inspector would need to rotate the probe around the defect to ensure detection and sizing.

It is important to note that in-service parts containing realistic surface cracks often have rough and nonplanar rear faces (backwalls). In this study, the backwalls of the samples were parallel

but not as smooth as polished surfaces, nor as rough as in-service parts. It is believed that as long as the backwall is not curved, this method should be effective. Additionally, having an extremely smooth backwall like a polished one is not a necessity when using the R_n mode for sizing. An increase in roughness may lead to scattered reflections, potentially reducing the amplitude of the signal R_n. Nonetheless, it is still believed that the new Rayleigh wave mode can be consistently generated, enabling the sizing of surface-breaking cracks even with rough backwalls. However, further research is required to determine the specific level of roughness at which this method remains effective.

In summary, the positive observation our studies yield regarding the proposed method is that it enables estimation of the crack depth in pulse-echo measurements using the Rayleigh wave features generated at the crack tip by the scattering of incident Rayleigh waves, unlike existing Rayleigh wave methods. Additionally, this method facilitates precise sizing of surface cracks inclined between 0° to 20° from the surface normal, and surface cracks oriented between 90° to 70° relative to the focal axis, with an error range below 5%.

3.5 Conclusion

This work introduced a pulse-echo Rayleigh wave method for accurately sizing surface-breaking notch-like defects. It utilized a conventional ultrasonic phased array transducer to selectively generate and receive Rayleigh waves. An averaging approach during reception significantly improved the SNR by reducing unrelated Rayleigh wave modes. The method's performance was validated through simulations and experiments, demonstrating precise sizing of the notch depth for 0° notches and the notch face length for notches inclined from the surface normal within a 5% error margin. The results revealed its potential to accurately size surface cracks inclined between 0° to 20° from the surface normal, and surface cracks oriented between 90° to 70° relative to the focal axis. Notably, the method exhibited the ability to size surface features with depths approximately equal to the sub-wavelength. Moreover, its capability to inspect across a broad range of frequencies enables the precise sizing of crack depths, spanning from shallow

to deep. Overall, the findings of this study present a promising technique for accurate surface defect sizing using pulse-echo Rayleigh waves.

CHAPTER 4

MATRIX PHASED ARRAY-BASED RAYLEIGH WAVE IMAGING FOR COMPLETE CHARACTERIZATION OF SURFACE BREAKING CRACKS

Bhupesh Verma[1] , Pierre Bélanger[1]

[1] Département de Génie Mécanique, École de Technologie Supérieure,
1100 Notre-Dame Ouest, Montréal, Québec, Canada H3C 1K3

Article submitted to the journal « NDT&E International » in November 2023.
(Under Review)

4.1 Abstract

This paper presents a novel approach for acquiring Rayleigh wave full matrix capture (FMC) using a conventional matrix phased array transducer, without involving a wedge. In this approach, the rows of the matrix phased array are used to selectively excite and detect Rayleigh waves. This is achieved by implementing a specific linear time delay and averaging in the post-processing of bulk wave FMC data from the matrix array transducer. This advancement enhances flexibility by eliminating the need for material-specific wedges and eliminates transmission loss associated with wedges. Notably, the absence of a wedge allows the reception of Rayleigh wave features related to the crack tip used for crack depth sizing. Furthermore, utilizing Rayleigh wave FMC data, surface crack imaging through the total focusing method (TFM) enables complete characterization, including both crack length and depth estimation in a single measurement, unlike the existing methods. Experiments and finite element simulation results using electric discharged machined (EDM) notch resembling surface cracks on the test specimen surface demonstrate accurate sizing of the crack length and depth within a 5% error.

4.2 Introduction

Cracks on the surface of solid structures, resulting from challenging operational conditions and environmental factors, pose significant risks to structural integrity and overall lifespan, impacting diverse industries such as aerospace, railway, petrochemical, and power. Ultrasonic

waves hold the potential for assessing such cracks. Specifically, ultrasonic arrays with bulk waves have been utilized by many researchers Felice *et al.* (2014); Peng *et al.* (2018); Haupert, Ohara, Carcreff & Renaud (2019); Saini *et al.* (2022) to characterize surface-breaking cracks (SBCs). However, their primary focus was on evaluating SBCs located on inaccessible back surfaces of components.

Over the years, ultrasonic Rayleigh waves have emerged as a valuable tool for in-service nondestructive testing (NDT) inspections and characterization of surface cracks. These waves propagate along the surface, with their energy concentrated to a few wavelengths below the surface, enhancing their sensitivity to the surface and near-surface cracks on the same side Rose (1999). Significant research literature has been dedicated to the detection and sizing of surface cracks through Rayleigh wave-based NDT methods Cook & Berthelot (2001a); Hassan & Veronesi (2003); Arias & Achenbach (2004); Jian *et al.* (2006); Edwards *et al.* (2006); Masserey & Mazza (2007); Dutton *et al.* (2011); Rosli, Edwards & Fan (2012); Zhou *et al.* (2015); Thring, Fan & Edwards (2016); Li *et al.* (2018); Deng *et al.* (2019); Zeng *et al.* (2019); Li *et al.* (2020); Zhang *et al.* (2020); Xiang *et al.* (2020); Xu *et al.* (2022); Xiao *et al.* (2022); Wang & Tang (2022); Li *et al.* (2023); He *et al.* (2023); Xiao & Cui (2023); Wu, Jiang, Fang & Ng (2023). However, these techniques are limited to measuring the depth of surface cracks exclusively. Conversely, accurate length measurement of surface cracks is equally crucial. To address this challenge, researchers have shifted their focus to imaging surface cracks using Rayleigh waves Ouchi *et al.* (2015) and leaky Rayleigh waves Shen *et al.* (2021) involving immersion testing configuration. However, these approaches face limitations inherent in immersion testing. For instance, the amplitude of the leaky Rayleigh wave is significantly influenced by both the water path length and focal length. The Rayleigh wave amplitude depends on the distance it propagates during the conversion from incident longitudinal to Rayleigh waves. Notably, Rayleigh waves experience high attenuation in an immersion testing setup, restricting the region of interest (ROI) to just a few millimeters from the source. Moreover, implementing water immersion testing directly on large structures is challenging in industrial environments. The use of linear phased arrays, mounted on a wedge that coupled to the surface of the test

specimen, has been explored for surface crack imaging, using both linear Ohara *et al.* (2017, 2022) and non-linear surface acoustic waves Ohara *et al.* (2019). Results show that these methods are suitable only when the ROI to be inspected is directly beneath the wedge, limiting their applicability in industrial settings. Recently proposed surface crack imaging method employing the total focusing method (TFM) with full matrix capture (FMC) data acquired using the wedge technique Hoyle *et al.* (2019); Ducousso & Reverdy (2020), has shown promising results, capable of expanding the ROI outside the wedge. However, drawbacks include transmission loss at the wedge-test specimen interface and the need to fabricate new wedges for specific materials and applications. A potential solution lies in a laser ultrasound-based FMC-TFM approach Qian *et al.* (2021) for surface crack imaging, although safety concerns and associated costs with the laser setup limit its widespread use.

To overcome the aforementioned limitations, this study introduces a novel approach for obtaining Rayleigh wave FMC using a conventional matrix phased array transducer. This approach increases flexibility by removing the necessity for a customized wedge for each material. Additionally, the absence of a wedge eliminates transmission loss at the wedge-test specimen interface, allowing for the reception of Rayleigh wave features from the crack tip, and contributing to precise crack depth measurements. Ultimately, the Rayleigh wave FMC data is utilized for surface crack imaging using TFM, providing a comprehensive characterization that includes both crack length and depth estimation in a single measurement—a capability lacking in existing methods.

The rest of the paper is organized as follows: Section 4.3 provides details on materials and methods, including a basic overview of the adapted method for Rayleigh wave generation and detection and its expansion to achieve the proposed Rayleigh wave FMC acquisition approach. The subsequent presentation introduces the TFM imaging algorithm. This is followed by the experimental details and the model used for finite element simulations. This section ends with a presentation of the methods used for sizing surface features. In Section 4.4, the results are presented, and compared and they are then discussed. Finally, Section 4.5 draws conclusions from this study.

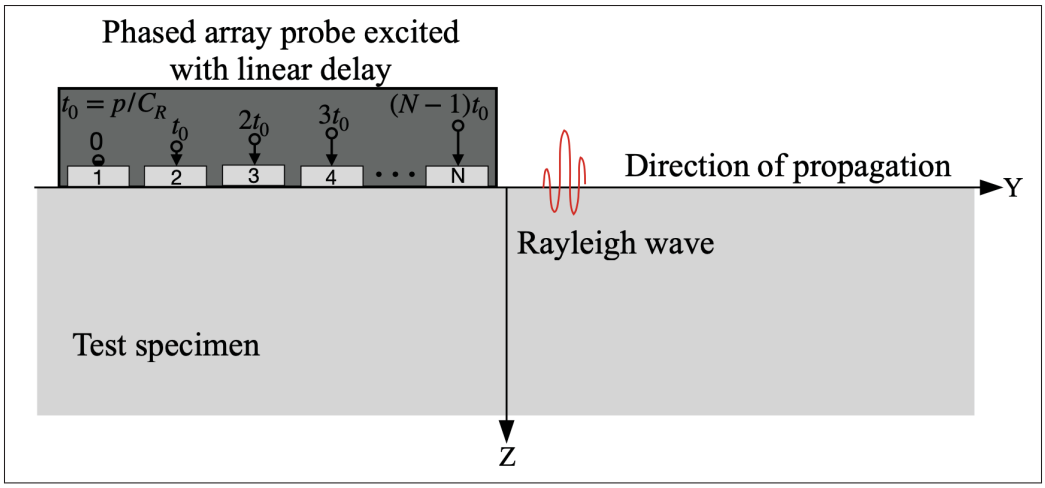

Figure 4.1 Illustration of the Rayleigh wave excitation method using a linear ultrasonic phased array transducer

4.3 Materials and methods

4.3.1 Rayleigh wave generation and detection

The various methods available for the generation and detection of Rayleigh waves were reviewed and their advantages and disadvantages were presented in Chakrapani & Bond (2018). A promising and viable solution to the limitations of existing techniques with unidirectional and selective excitability is offered by a recently developed Rayleigh wave excitation method Verma & Bélanger (2023), where Rayleigh waves were generated by emitting with each element of a phased array transducer with a specific time delay as shown in Figure 4.1. This specific time delay applicable to conventional phased array transducers was chosen based on the elementary pitch (p) of the transducer and the waveguide Rayleigh wave velocity (C_R) as $t_0 = p/C_R$. The required delay for each element can be described as:

$$(t_0)_i = \frac{p * (i-1)}{C_R} \tag{4.1}$$

where $(t_0)_i$ represents the time delay corresponding to the i^{th} element of the phased array transducer and i ranges from 1 to the total number of elements in the array N. The implementation

of these time delays to transducer elements and their emissions were controlled using the Verasonics Vantage system. The Rayleigh wave excitation method presented in reference Verma & Bélanger (2023) has shown significant advancements. However, the cost implications of array scanners that offer programmable control are prohibitive and might hinder the accessibility of this method. Therefore, in the present work, a cost-efficient alternative approach is used. In contrast to implementing time delays during the emission of transducer elements, as done in Verma & Bélanger (2023), they were applied in the post-processing data contained in the FMC. This allows achieving the same Rayleigh wave excitation capabilities as obtained in Verma & Bélanger (2023). Moreover, the advent of portable array scanners, along with recent price reductions, has made FMC acquisition more attainable, thereby enhancing the method's accessibility.

In the FMC acquisition approach, each element i within the array transducer is sequentially excited, followed by the reception at all elements j. Consequently, a N-element array generates a matrix $\mathbf{S}_{ij}(t)$ containing a total of $N \times N$ time trace signals $s_{ij}(t)$, where each signal corresponds to a possible transmitter-receiver combination. The FMC matrix $\mathbf{S}_{ij}(t)$ has dimensions of $l \times N \times N$, with l representing the length of the time trace signal. Following the completion of the acquisition of FMC, MATLAB is used to post-process the FMC. The signals from each transmission i and corresponding reception are shifted in time using the same time delay derived from Equation 4.1 and summed, as expressed in Equation 4.2.

$$\mathbf{S}_j(t) = \sum_{i=1}^{N} s_{ij}\left(t + (t_0)_i\right) \tag{4.2}$$

where $(t_0)_i$ is the time delay associated with the i^{th} element transmission and i ranges from 1 to N, which is the total number of elements in the array. As a result, the FMC matrix $\mathbf{S}_{ij}(t)$ transformed into a $l \times N$ matrix $\mathbf{S}_j(t)$ containing a total N time trace signals $s_j(t)$. When the FMC acquisition was conducted with the transducer positioned before surface cracks, these signals correspond to the back-propagated Rayleigh waves after interacting with the surface cracks, captured by the same transducer elements. These signals also carry other wave modes

unrelated to Rayleigh waves generated by the scattering of incident Rayleigh waves at surface cracks. The presence of other wave modes can potentially disrupt the intended Rayleigh waves. To effectively average out wave modes unrelated to the Rayleigh waves, these signals $s_j(t)$ are temporally shifted using the same time delay from Equation 4.1. This synchronizes the phase of the Rayleigh wave components across all elements. The resulting signals are then averaged according to the expression given in Equation 4.3.

$$A(t) = \frac{1}{N} \sum_{j=1}^{N} s_j \left(t + (t_0)_j\right) \tag{4.3}$$

where $(t_0)_j$ is the time delay corresponding to the j^{th} received element and j ranges from 1 to total number of array elements N. This averaging process creates constructive interference, which enhances the Rayleigh wave amplitude, while simultaneously causing destructive interference that attenuates other wave modes. Consequently, Equation 4.3 yields a single time trace signal $A(t)$, corresponding to the N^{th} element of the transducer. This signal primarily contains information related to the Rayleigh wave features that are generated at the surface crack geometries.

4.3.2 Rayleigh wave FMC acquisition

Rayleigh wave FMC acquisition typically involves a linear phased array transducer mounted on a wedge, coupled to the test specimen surface using a couplant. However, limitations arise due to the requirement of fabricating a new wedge for each material and application. Moreover, the wedge technique suffers from transmission losses at wedge interfaces during both transmission and reception, which limits the reception of features related to the crack tip. To overcome this, a novel approach is proposed for Rayleigh wave FMC acquisition, offering increased flexibility by eliminating the need for custom wedges. In this approach, a conventional $n \times n$ matrix phased array transducer is used. The Rayleigh wave transduction method using a linear phased array FMC, described in Section 4.3.1, is expanded to encompass matrix phased array FMC to achieve Rayleigh wave FMC. In this setup, each row along the Y-axis (refer to Figure 4.2(a)) of the matrix phased array can be considered as a linear array and employ them sequentially

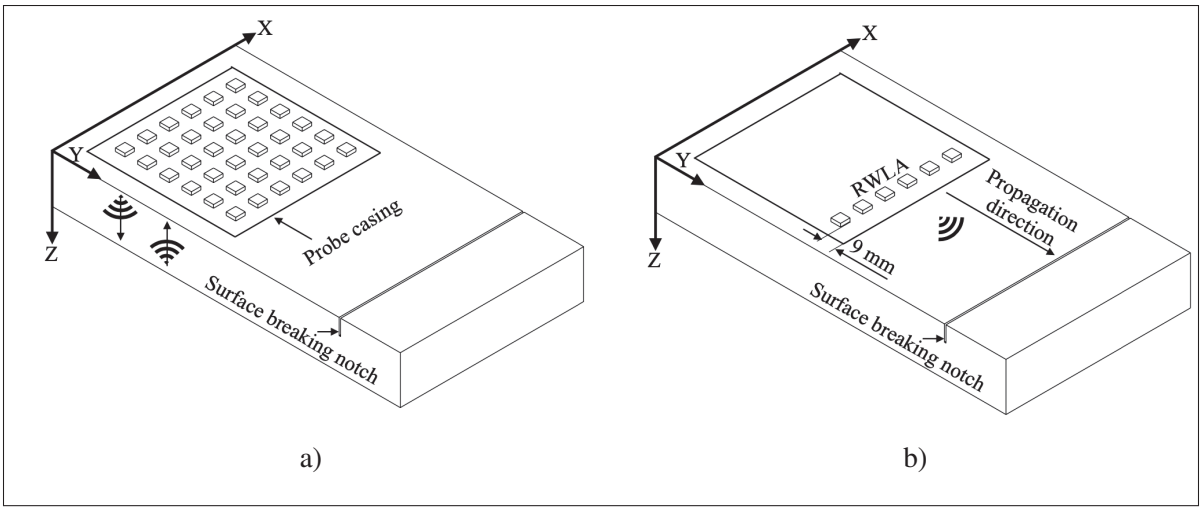

Figure 4.2 (a) Schematic depicting wave propagation within the material bulk before applying the time delay. (b) Schematic illustrating the redirection of bulk waves onto the surface and their propagation as Rayleigh waves after implementing the linear time delay

to transmit Rayleigh waves while receiving at all rows within the matrix array. For doing this, an identical linear time delay is calculated using Equation 4.1 for each of these rows. The variable i in Equation 4.1 spans from 1 to the number of elements n present in each row of the matrix array. These time delays are subsequently implemented to the matrix FMC data, and the averaging process, as described in Section 4.3.1, is applied individually to each row within the matrix array. Consequently, the original size of the FMC matrix, initially $l \times M \times M$ (where $M = n * n$), transforms into a new matrix with dimensions $l \times n \times n$, with l representing the length of the time trace signal and n is the number of elements present in each row of the matrix array. This transformed matrix represents the Rayleigh wave FMC and corresponds to a linear array composed of the end elements from each individual row as shown in Figure 4.2(b) and referred to as Rayleigh wave linear array (RWLA).

4.3.3 Reconstruction of surface cracks using total focusing method (TFM)

The total focusing method (TFM) is an advanced post-processing algorithm used to create images of a specific ROI within the test specimen using the FMC. In this study, the Rayleigh wave FMC

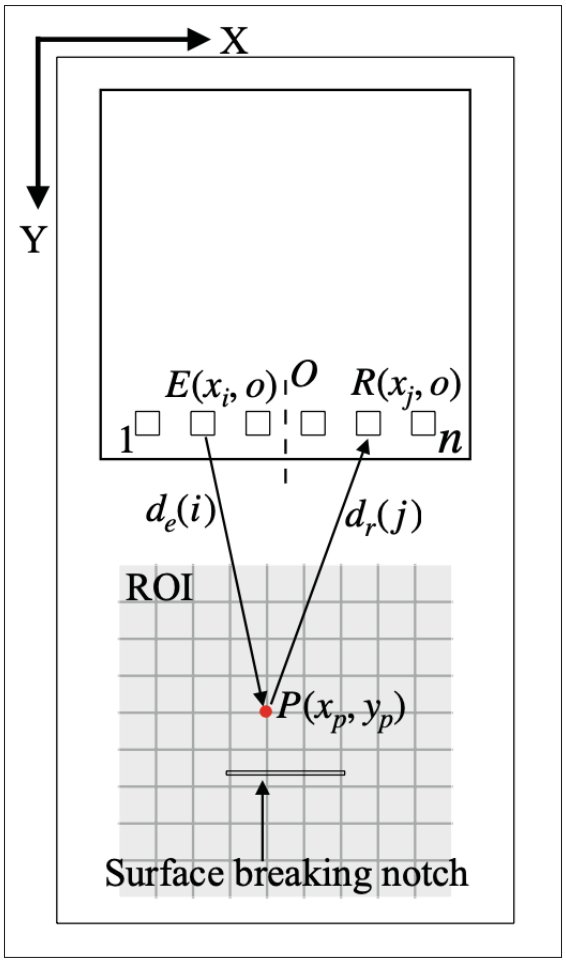

Figure 4.3 Schematic illustrating the principle of Rayleigh wave FMC-TFM imaging

is used to image surface cracks through the TFM imaging algorithm, as illustrated schematically in Figure 4.3. This begins with dividing the ROI into a grid of pixels. Subsequently, a coherent summation of signals from all possible transmitter-receiver pairs takes place to synthesize focal points at each pixel location, producing a fully focused image. The intensity of the image at each pixel point P, denoted as $I(x, y)$, can be expressed by:

$$I(x, y) = \left| \sum_{i=1}^{n} \sum_{i=1}^{n} H\left(s_{ij}(t_{ij})\right) \right| \tag{4.4}$$

In this equation, H denotes the Hilbert transform, s_{ij} represents the time trace signals from all possible transmitter-receiver pairs, and t_{ij} signifies the arrival time of Rayleigh waves traveling from the emitter (i) to the pixel P, and subsequently back to the receiver (j). Assuming that Rayleigh waves propagate along the path that minimizes travel time, following Fermat's principle, this arrival time can be estimated using the following equation:

$$t_{ij} = d_e(i) + d_r(j) = \frac{\sqrt{(x_p - x_i)^2 + y_p^2} + \sqrt{(x_p - x_j)^2 + y_p^2}}{C_R} \tag{4.5}$$

In this equation, x_i and x_j represent the spatial positions of i^{th} emitter and j^{th} receiver, respectively, in the x-direction with respect to the origin O, assuming it is at the center of the array. (x_p, y_p) denotes the coordinates of pixels within the ROI, and C_R is the Rayleigh wave velocity of the waveguide.

4.3.4 Experimental setup and FEM model

Figure 4.4(a). presents the experimental configuration used in this study. A 3 MHz conventional 11×11 matrix phased array probe comprising 121 elements, with an elementary pitch of 1 mm in both directions was used. The probe was placed in contact with a steel test specimen that was 19 mm thick and featured a surface-breaking notch measuring 5 mm deep. The notch on the test specimen surface was generated using electric discharge machining (EDM) with a 0.3 mm diameter wire. A very thin layer of oil was used in between the probe-test specimen interface to ensure effective coupling. The transducer was connected to a Verasonics Vantage 64 LE controller for conducting the FMC acquisition, operating at a sampling rate of 62.5 MHz. A 3-cycle Hann windowed toneburst was sent to each element. As the Vantage 64 LE system can control the transmission of 64 elements and the probe used in this study has 121 elements, the acquisition was carried out in two steps.

The Rayleigh wave wavelength at 3 MHz closely matches the probe's elementary pitch of 1 mm. However, to synthesize a wave field without unwanted grating lobes, the elementary pitch must be less than half a wavelength Schmerr (2015). Unfortunately, the only 3 MHz matrix phased

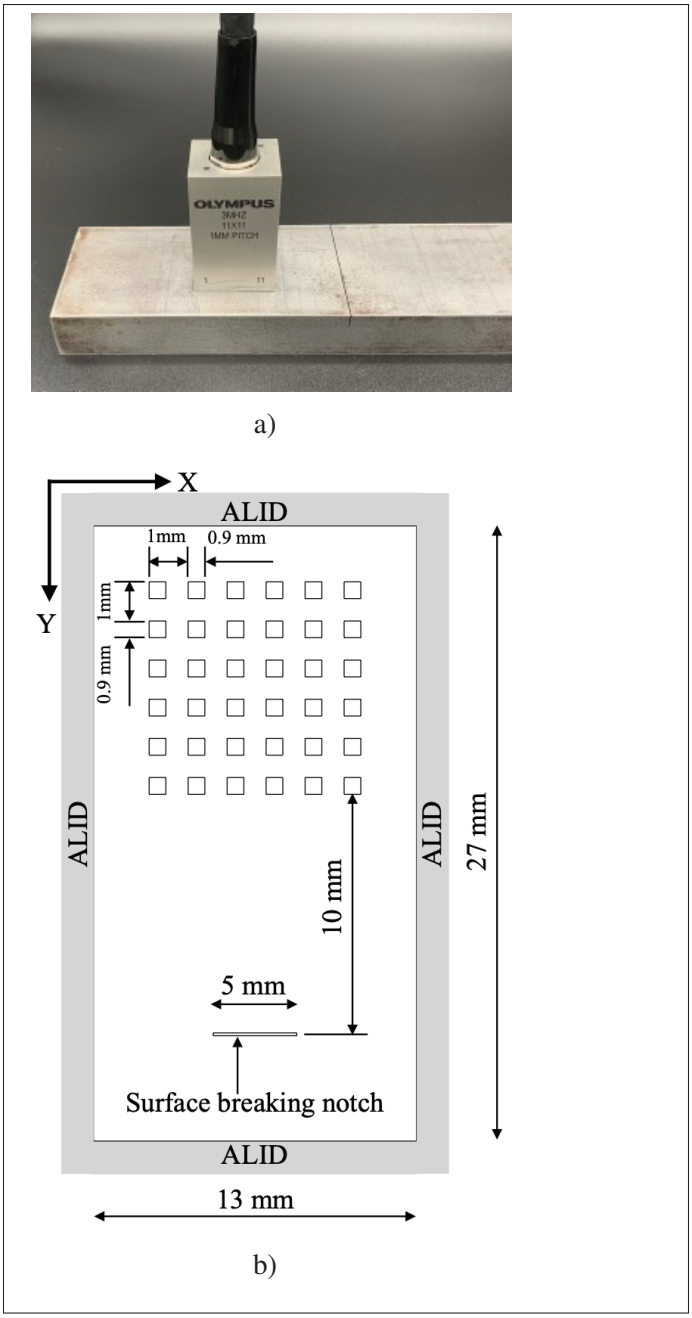

Figure 4.4 (a) Configuration for experimental measurements and (b) Schematic of the FEM model for a 19 mm thick steel plate (top view)

array probe available in our laboratory had an elementary pitch closely matching the Rayleigh wave wavelength. Obtaining a matrix phased array probe with a smaller pitch compared to

the Rayleigh wave wavelength was not feasible. Nevertheless, this limitation was overcome by utilizing the probe's frequency bandwidth and leveraging the flexibility of the Verasonics Vantage system to control the center frequency of the emitted toneburst. Therefore, to increase the Rayleigh wave wavelength relative to the available 1 mm elementary pitch, a reduced center frequency of 2 MHz was chosen. It is important to note that even though a 3 MHz matrix array probe with a 1 mm elementary pitch was involved, a 3-cycle Hann windowed toneburst centered at 2 MHz was employed throughout this study.

FEM simulations were performed using the Pogo finite element package Huthwaite (2014), which is an explicit time-domain finite element solver for linear elastodynamic problems. A three-dimensional steel plate (Young's modulus 200 GPa, density 7800 kg/m^3, Poisson's ratio 0.3) was modeled with a mesh consisting of 8 node cubic brick elements. A schematic of the FE model is shown in Figure 4.4(b). The element size was set to accommodate 15 elements per shortest wavelength, aiming to achieve a converged solution for the elastic wave propagation problem. The time step was chosen to prevent the fastest ultrasonic wave packet from skipping an element within a single time increment Drozdz *et al.* (2006). All surfaces except the top and bottom were assigned absorbing boundaries using absorbing layers with increased damping (ALID) method Drozdz *et al.* (2006); Rajagopal *et al.* (2012) to avoid reflections. A conventional matrix phased array transducer was simulated. The nodes located on the top surface of the plate were selected to create an array comprising 121 elements in an 11×11 configuration, each with a 1 mm $\times$ 1 mm elemental pitch. The designated nodes were excited with a 3-cycle Hann windowed toneburst centered at 2 MHz to record the FMC. Subsequently, both experimental and simulated raw FMC datasets were imported into MATLAB for the implementation of the procedure described in Section 4.3.2, transforming raw FMC data into Rayleigh wave FMC. Followed by the generation of TFM surface crack images.

4.3.5 Surface-breaking notch depth and length estimation

In this study, the depth estimation of EDM notches was accomplished using a sizing method introduced in the authors' prior research Verma & Bélanger (2023). This depth-sizing approach

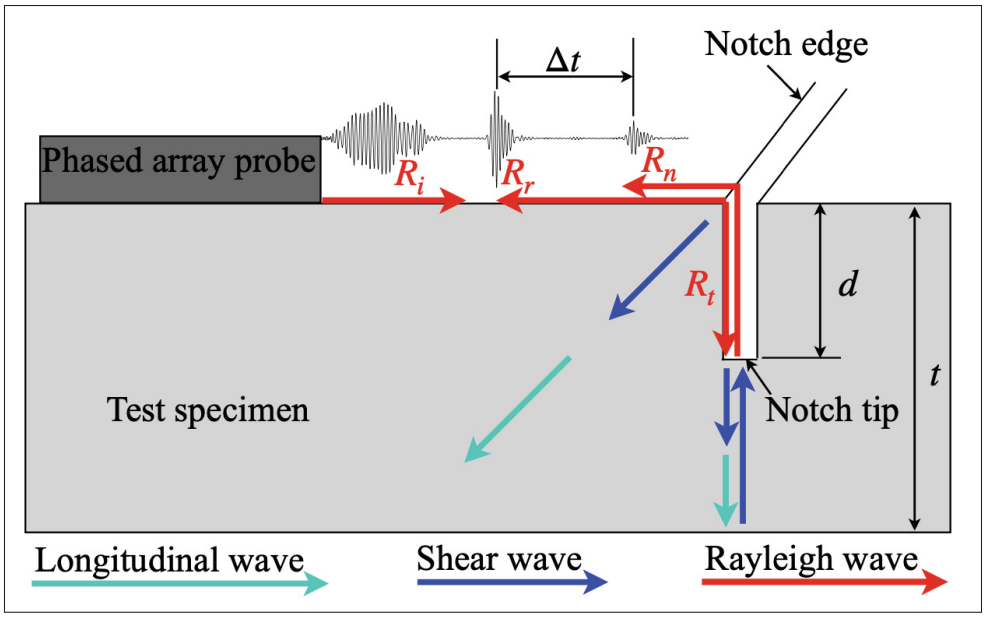

Figure 4.5 Schematic of the resulting time trace signal from the interaction of Rayleigh waves with an EDM notch and a visual representation of the Rayleigh wave's path employed for accurate depth sizing. R_i denotes the incident Rayleigh wave, R_r represents the Rayleigh wave reflected from the notch edge, R_t indicates the Rayleigh waves propagating along the notch face, and R_n denotes the newly generated Rayleigh wave mode that results from the backwall reflection of the shear wave mode (generated at the notch tip) as it encounters the notch tip

relies on the measurement of the time-of-flight (ToF) between the initial reflection of incident Rayleigh waves from the notch's edge and a specific mode-converted Rayleigh wave, generated at the notch tip and resulting from the reflection of the shear wave mode (which is generated by the scattering of Rayleigh waves at the notch tip) from the back wall, encounters the notch tip.

As previously described in Section 4.3.2, the approach used in this study for Rayleigh wave generation and detection results in a time trace signal that primarily contains information related to Rayleigh wave features developed at the notch. A visual representation of the Rayleigh wave's path used for precise depth sizing and a schematic of the resulting time trace signal are presented in Figure 4.5.

The required ToF (Δt) can be calculated using the following expression:

$$\frac{d}{C_R} + \frac{t-d}{C_S} = \frac{\Delta t}{2} \tag{4.6}$$

where d represents the notch depth, t signifies the thickness of the test specimen, and C_R and C_S stand for the velocities of the Rayleigh wave and shear wave in the waveguide, respectively. Following further simplifications Equation 4.6 can be rearranged to estimate the notch depth as:

$$d = \frac{\Delta X - t \cdot R_{R/S}}{1 - R_{R/S}} \tag{4.7}$$

where $\Delta X = C_R \cdot (\Delta t/2)$ is the distance between the intended signals employed for depth estimation and $R_{R/S}$ is the ratio of Rayleigh wave to shear wave velocity of the waveguide material.

Hence, determining the value of ΔX allows for the accurate sizing of notch depth using Equation 4.7. Considering the notch's edge and tip act as ideal reflectors, the desired Rayleigh wave features originating from these points correspond to the maximum intensity pixels in the images. Consequently, the maximum intensity pixels aligned with the ultrasonic beam direction are utilized to identify the positions of signals R_r and R_n, and subsequently, to determine the value of ΔX and the depth of the notch. Whereas, for estimating the notch length, the maximum intensity pixels in the image perpendicular to the ultrasonic beam direction, employing the 6 dB drop method, are used.

4.4 Results and discussion

In order to validate the FMC-based method and ensure that the SNR was equivalent to the method described in Verma & Bélanger (2023), a 3.5 MHz linear 32-element phased array probe with a 0.5 mm elementary pitch, connected to the Verasonics Vantage system was used. The probe was positioned 30 mm from the EDM notch, in direct contact with the test specimen. A thin layer of oil was used to ensure a proper coupling. To achieve Rayleigh wave transmission, the necessary linear time delays during the emission of transducer elements, as derived from Equation 4.1, were implemented. The back-propagated waves, after interaction with the notch

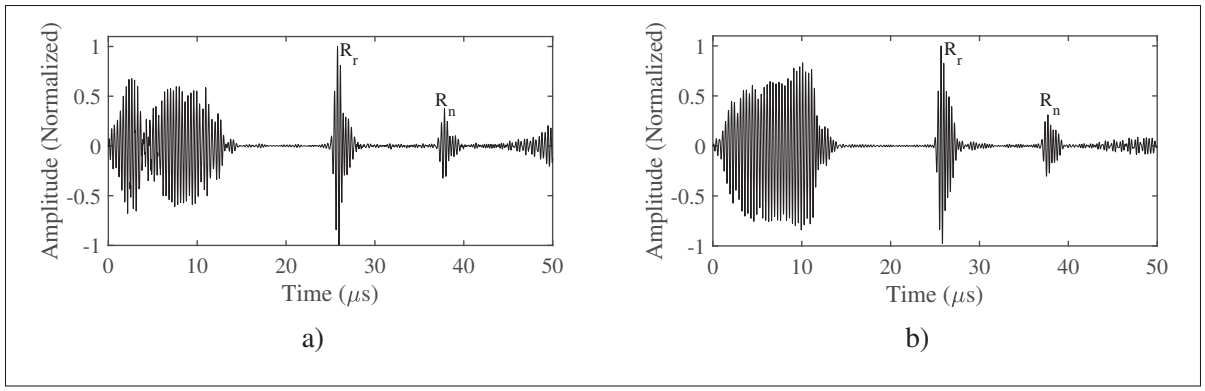

Figure 4.6 Experimentally measured time traces of the out-of-plane displacement amplitude of Rayleigh wave features generated at a 5 mm deep notch, obtained: (a) by implementing the linear time delay between the phased array transducer elements during emission and averaging in reception, and (b) by implementing the same linear time delay for transmission and reception during the post-processing of FMC data

geometries, were captured by the same phased array probe in a pulse-echo configuration. The signals received by the transducer elements were employed for averaging in reception, utilizing Equation 4.3. The resulting signal from this procedure was compared to the outcome of the Rayleigh wave generation and detection approach used in this study. For this purpose, the same 3.5 MHz probe in an identical pulse-echo configuration, positioned at the same distance from the notch, was employed and the FMC acquisition was conducted. The acquired FMC data was then post-processed as detailed in Section 4.3.2. Figure 4.6 illustrates the comparison of the resulting time trace signals from these two measurements. As observed in Figure 4.6(a) and (b), it is evident that the approach employed in this study offers equivalent excitation and reception capabilities as demonstrated in reference Verma & Bélanger (2023).

Experiments were conducted using the measuring configuration shown in Figure 4.4 (a). The measurements were carried out for four distinct probe positions to ensure the repeatability of results: 5 mm, 10 mm, 15 mm, and 20 mm intervals between the EDM notch and the probe casing face, aligned parallel to the EDM notch. It is important to note that there exists an approximate 9 mm gap between the RWLA elements (refer to Figure4.2(b)) and the probe casing face. Consequently, the actual distances between the notch edge and RWLA elements

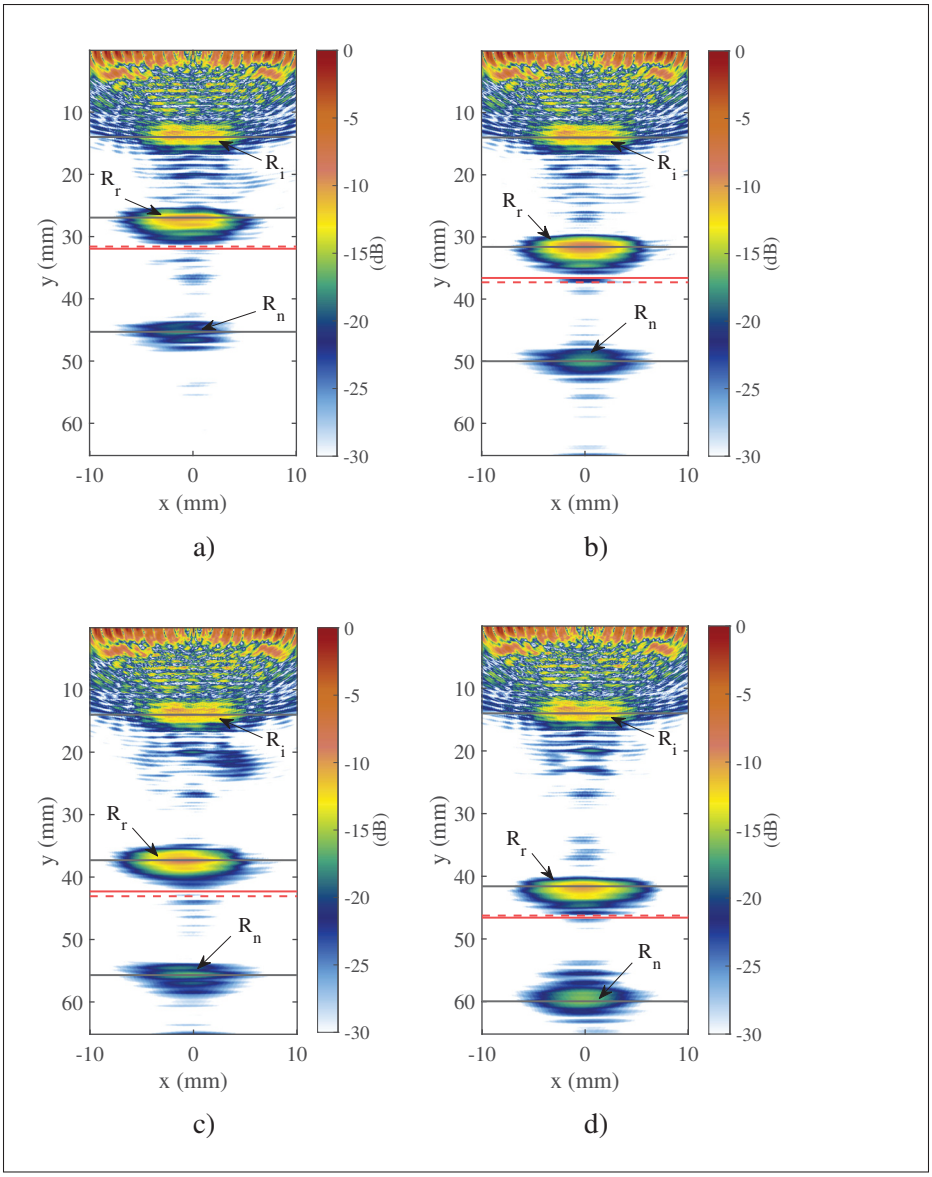

Figure 4.7 Rayleigh wave FMC-TFM image obtained from the experimental measurements at four distinct probe positions relative to the notch: (a) 5 mm, (b) 10 mm, (c) 15 mm, and (d) 20 mm

corresponding to these measurement positions are 14 mm, 19 mm, 24 mm, and 29 mm. The FMC-TFM images obtained from these experimental measurements are presented in Fig 4.7 (a), (b), (c), and (d). The Rayleigh wave features, including the incident Rayleigh wave (R_i), reflection from the notch edge (R_r), and the mode-converted Rayleigh wave mode (R_n) originating at the notch tip, necessary for locating and sizing the surface-breaking defects, can be noticed in

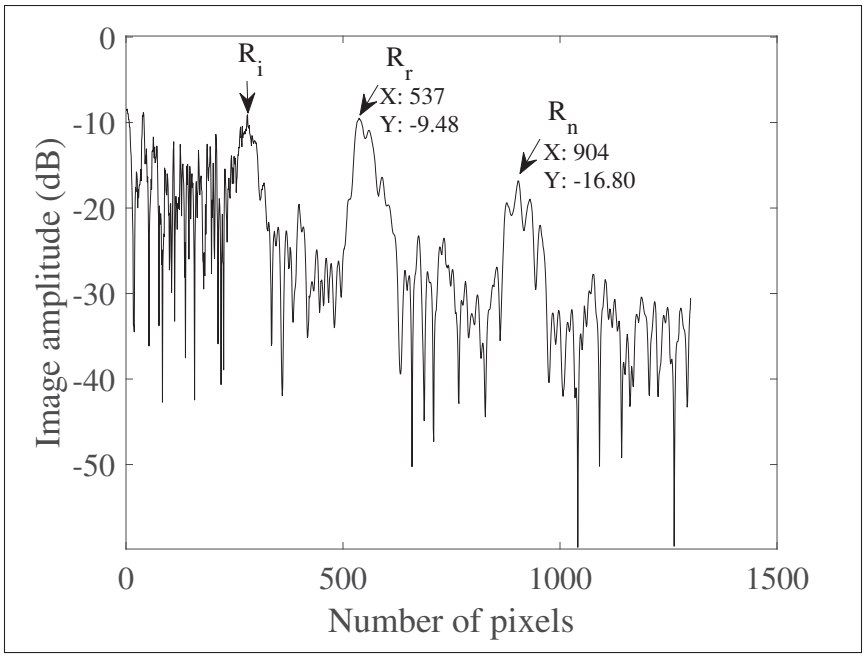

Figure 4.8 Intensity distribution of the FMC-TMF image of the EDM notch in the direction parallel to the ultrasonic beam obtained from experiments, revealing pixel positions of the intended Rayleigh wave signals utilized for notch depth sizing

these images. Ideally, the signal R_i should be positioned at 11 mm, aligning with the 11 mm probe aperture. However, there is a slight offset from the original position. This discrepancy is generated because, in the Verasonics Vantage system, the time trace signal commences from the start of the toneburst pulse, causing the signal R_i to shift from its expected actual position, as observed in all images. The position of the signal R_i serves as a reference to locate the EDM notch. As expected, the signal R_r appears at approximately the actual locations from the reference in all images. One can also notice that, due to the constant depth of the notch, the signal R_n originating at the tip consistently appears at the same distance from the signal R_r in all four measurements.

The distance ΔX between the signals R_r and R_n is determined by analyzing the maximum intensity pixels at the notch, which align with the direction of the ultrasonic beam. The FMC-TFM image intensity distribution parallel to the ultrasonic beam for the case where the probe is positioned 5 mm from the notch edge is shown in Figure 4.8. The pixel interval is

0.05 mm. The three highest peaks observed in Figure 4.8 correspond to the position of the intended signals R_i, R_r, and R_n. Similarly, for other cases, the intended signal positions were also obtained and are highlighted in Figure 4.7 with black solid lines. Utilizing the position of signals R_r and R_n, the value of ΔX can be measured and applied in the expression provided in Equation 4.7 to estimate the notch depth. The known actual depth is represented by a solid red line, while the estimated notch depth is illustrated by a dashed red line in Figure 4.7. The estimated notch depth for four different probe positions showed the repeatability of the results. These measured depths are averaged and then compared with the known actual value of the EDM notch, revealing a discrepancy of -4.4% for the 5 mm deep notch.

The 6 dB drop method employed in this study for determining the notch length is effective when the length is less than the probe aperture. However, the test specimen utilized in this investigation features an EDM notch with a length spanning the specimen's width, and the probe used has an 11 mm aperture. Consequently, we refrained from attempting to measure the notch length directly from the experimentally obtained data. Nevertheless, the effectiveness of the proposed method in sizing the notch length was evaluated through 3-D finite element simulations. A notch with a finite length measuring 5 mm and 8 mm deep was simulated. This notch was located 10 mm from the probe position. The nodes were selected on the top surface of the plate corresponding to a matrix probe consisting of 121 elements in an 11 × 11 configuration, each with a 1 mm × 1 mm elemental pitch. These nodes were excited with a 3-cycle toneburst centered at 2 MHz.

The FMC-TFM image obtained from finite element simulation is presented in Figure 4.9. Signals necessary for sizing the notch depth and length are visible in Figure 4.9. These signal's positions, identified by analyzing the maximum intensity pixels parallel to the ultrasonic beam at the simulated EDM notch, as illustrated in Figure 4.10 (a), are marked with a black solid line in Figure 4.9. These signals are observed in the TFM image at their expected locations. By utilizing the pixel positions of the signals R_r and R_n, the value of ΔX required for estimating the notch depth using Equation 4.7 was determined. The simulated notch depth is indicated by a solid red line, while the estimated notch depth is represented by a dashed red line in Figure

4.9. The estimated notch depth closely approximated the simulated notch depth, with a 1.1% error in the depth measurement. The notch length was determined using the maximum intensity pixels perpendicular to the ultrasonic beam at the simulated EDM notch. Figure 4.10(b) shows the transverse distribution of the EDM notch in the FMC-TFM image, with a pixel interval of 0.05 mm. Utilizing the 6 dB drop method, the estimated notch length exhibits a −5% error in measuring the simulated notch length of 5 mm.

The proposed method proves effective when utilized on test samples featuring EDM notches with consistent depth along their length. However, its applicability transcends this particular case. There is a belief that the underlying principles could be extended to notches with varying depths along their length. However, experimental validation of this hypothesis faced challenges due to the unavailability of appropriate test specimens. Additionally, conducting extensive numerical simulations was impeded by computational expenses, thus limiting the depth of discussion on this matter. Nonetheless, exploring the characterization of notches with non-uniform depth profiles remains a promising avenue for future research in this field.

4.5 Conclusion

A novel approach for Rayleigh wave FMC acquisition using a conventional matrix phased array probe is presented. The new approach comes with enhanced flexibility as the need for fabricating a new wedge for different materials and applications is no longer required. Moreover, it enables the reception of features related to the crack tip, by reducing transmission loss at the wedge-test specimen interface, aiding in depth sizing. The effectiveness of this approach is confirmed through both finite element simulations and experimental validations. The acquired FMC data is then utilized to reconstruct TFM images of surface-breaking defects, allowing for the combined estimation of length and depth in a single measurement, within a 5% error range. Therefore, the method outlined in this paper holds the potential for extension to industrial applications, ensuring accurate characterization of surface-breaking defects.

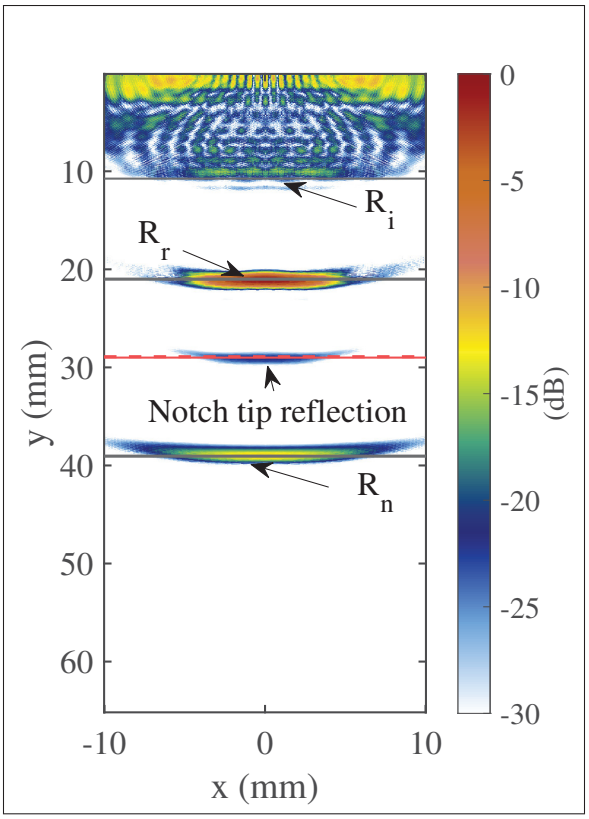

Figure 4.9 Rayleigh wave FMC-TFM image of a simulated EDM notch measuring 5 mm in length and 8 mm deep

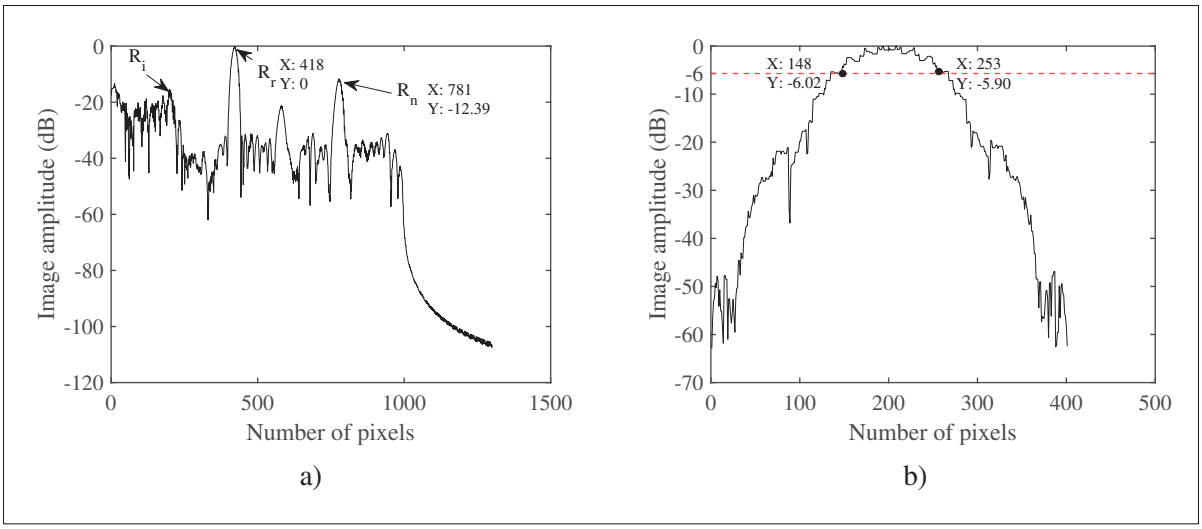

Figure 4.10 Intensity distribution of the FMC-TMF image of the EDM notch obtained from finite element simulations: (a) in the direction parallel to the ultrasonic beam, revealing pixel positions of the Rayleigh wave signals utilized in notch depth estimation, and (b) in the direction perpendicular to the ultrasonic beam, showing the application of the 6 dB drop method for sizing the EDM notch length

CONCLUSION AND RECOMMENDATIONS

In conclusion, this thesis has contributed to the field of NDT by introducing an innovative and easy-to-implement method for comprehensively characterizing surface-breaking cracks, presenting a valuable alternative to existing approaches. The widely employed NDT methods, such as ECT and PT, despite their prevalence, present notable limitations. ECT faces challenges in conducting large area inspections due to the requirement for additional scanning arrangements and achieving accurate depth and length sizing is challenging, demanding complex calibration. Signal losses, particularly in tightly closed cracks like fatigue cracks, further hinder measurement accuracy. Moreover, ECT is constrained by its limited penetration depth, restricting its detection range. Similarly, PT encounters setbacks related to surface preparation requirements, risking result misinterpretation. Moreover, PT is considered a polluting technique, and its environmental impact along with the need for post-inspection pollutant removal and subsequent sedimentation concerns, have attracted regulatory scrutiny, prompting a search for viable alternatives.

To address these limitations, the proposed innovative NDT method, which is based on ultrasonics Rayleigh waves, emerges as a credible alternative for inspecting surface defects across diverse industries. The decision to utilize ultrasonic Rayleigh waves stems from their concentrated energy within a few wavelengths beneath the surface, rendering them highly sensitive to surface and near-surface defects. Furthermore, their capability for long-distance propagation facilitates efficient inspections of large areas with minimal probe locations. While the generation and detection of Rayleigh waves can be accomplished through various methods, the wedge technique is considered the most efficient and widely accepted. However, limitations arise due to transmission losses at wedge interfaces during both transmission and reception. The wedge technique necessitates a new wedge for each specific material, as the required wedge angle for Rayleigh wave generation depends on the Rayleigh wave's wavelength. An innovative method that overcame these limitations associated with the wedge technique was developed and presented in Chapter 2. A conventional phased array transducer was used for generating Rayleigh waves by

implementing a linear time delay, designed based on the elementary pitch and on the Rayleigh wave speed, during the excitation of elements. Evaluation through finite element simulations and experimental measurements demonstrated the method's efficacy. Quantitative comparisons, particularly in terms of SNR, revealed superior performance compared to existing methods such as the wedge technique and comb transducer. The results indicate that the proposed method has the potential to selectively excite unidirectional Rayleigh waves using a conventional phased array transducer without the need for a wedge. Moreover, it can be easily adapted to different waveguides and excited across a wide range of frequencies. Therefore, this method evolves as a suitable alternative to existing Rayleigh wave excitation methods, offering remarkable flexibility. The findings of this study were published in the Journal of Ultrasonics in July 2023.

The new Rayleigh wave excitation method introduced in Chapter 2 was extended to develop a pulse-echo Rayleigh wave method for sizing surface cracks. Utilizing a conventional phased array transducer facilitated both the excitation and detection of Rayleigh waves. This study identified a specific mode-converted Rayleigh wave originating from the crack tip, previously overlooked in earlier research due to its delayed arrival. This wave was used to accurately size surface cracks, leveraging its TOF information. Implementing an averaging approach during reception, using time trace signals captured by transducer elements, effectively mitigated interference from other wave modes generated at crack geometries. This refinement significantly improved the SNR and minimized errors in sizing. Experimental trials involving EDM notches on test specimen surfaces, positioned at various angles and depths resembling surface-breaking cracks, demonstrated precise sizing of notch depths for 0° notches and notch face lengths for inclined notches within a 5% error margin. The results showcased the method's accuracy in sizing surface cracks inclined from 0° to 20° relative to the surface normal and those oriented between 90° to 70° relative to the focal axis. Notably, the method exhibited the capability to size surface features with depths approximately equal to the sub-wavelength. Its versatility across a broad frequency range enabled precise sizing of crack depths, ranging from shallow

to deep. This study reveals a promising method for accurately sizing surface defects using pulse-echo Rayleigh waves, providing a robust solution applicable to defect characterization across diverse industries. The results have been integrated into a manuscript submitted to the Journal of Ultrasonics in August 2023, currently undergoing its final revision process.

The method presented for exciting Rayleigh waves in Chapter 2 was further expanded to implement the FMC-TFM method for imaging surface cracks. This advanced approach enables comprehensive characterization by providing simultaneous length and depth estimation of surface cracks in a single measurement. A novel technique for Rayleigh wave FMC acquisition was developed in this study, utilizing a conventional matrix phased array probe. This innovative approach enhances flexibility by eliminating the need for fabricating a new wedge for different materials and applications, as traditionally required in Rayleigh wave FMC acquisition. The effectiveness of this approach was validated through both finite element simulations and experimental validations. The acquired FMC data was subsequently employed to reconstruct TFM images of surface-breaking cracks, facilitating the combined estimation of length and depth within a 5% error range in a single measurement. Consequently, the outlined method in this study exhibits the potential for extension to industrial applications, ensuring accurate and comprehensive characterization of surface-breaking defects. The results obtained from this study have been incorporated into a manuscript recently submitted to the Journal of NDT & E International for publication.

In summary, the proposed Rayleigh wave excitation method, coupled with a novel Rayleigh wave FMC acquisition approach and subsequent TFM imaging of surface cracks, demonstrates the capability to simultaneously determine the length and depth of surface cracks in a single measurement. To our knowledge, none of the established methods currently provide these combined features. Therefore, the results of this research contribute significantly to the

progression of non-destructive testing (NDT) methodologies and offer a valuable tool for inspecting surface defects across diverse industries.

As a suggestion for future work, it is recommended to explore the following domain:

- Considering the results presented in this thesis, the Rayleigh wave excitation method demonstrates effectiveness on test specimens with flat surfaces. However, its applicability is limited when dealing with curved surfaces, as the proposed method encounters challenges in achieving sufficient coupling between the phased array transducer elements and the curved specimen. A potential solution lies in the exploration of a curved array transducer design, coupled with an appropriate time delay law. This recommendation for future work aims to overcome the limitations and expand the applicability of the new Rayleigh wave excitation method, particularly for inspecting curved surfaces such as pipes and shafts.
- The use of thermal barrier coatings (TBC) on components such as high-pressure turbine (HPT) blades is commonplace to protect against oxidation and hot corrosion caused by hot gases. However, severe thermal stresses may lead to surface cracks in the substrate, often obscured beneath TBC layers. Detecting and inspecting such defects pose challenges for conventional NDT techniques. Considering the surface crack characterization method presented in this thesis, a future avenue of research involves exploring its potential for identifying and characterizing defects masked by TBC layers.
- Additionally, the novel approach proposed for surface crack characterization, validated through Electrical Discharge Machining (EDM) notches in the test sample, should be extended to assess stress corrosion cracks and fatigue cracks—common issues in the aerospace industry, thereby broadening the methodology's applicability and effectiveness. Such an expansion would enhance the versatility and practicality of the proposed technique in addressing a wider array of real-world scenarios.

APPENDIX I

SURFACE CRACK SIZING METHOD USING RAYLEIGH WAVES GENERATED BY ULTRASONIC PHASED ARRAY

Bhupesh Verma[1] , Pierre Bélanger[1]

[1] Département de Génie Mécanique, École de Technologie Supérieure,
1100 Notre-Dame Ouest, Montréal, Québec, Canada H3C 1K3

Manuscript published in the Proceeding of the ASME 2022 49th Annual Review of Progress in Quantitative Nondestructive Evaluation, San Diego, California, US, in July 2022.

(DOI:https://doi.org/10.1115/QNDE2022-98309) .

1. Abstract

Presence of surface breaking cracks on engineering structures such as rails, pressure vessels, turbine blades or pipelines affect the service life. Moreover, if the depth of such cracks is not known, then these parts are typically subjected to direct rejection. Economically this is highly expensive as it can cause the complete disruption of the service. Having an accurate knowledge of crack depth can be used in fracture mechanics analysis to estimate the remaining life of the structure. Among the available nondestructive testing (NDT) techniques, eddy current testing (ECT) is the most widely used method for the detection and sizing of such cracks due to their high sensitivity to surface and near surface defects. However, the size of surface cracks in length and depth requires a complex calibration. Moreover, the depth range is limited by the penetration depth of eddy current. Ultrasonic Rayleigh waves are recently attracting interest for the detection and characterization of surface cracks. The advantages include length and depth sizing as well as the possibility to scan a relatively large area from a limited number of probe positions. The generation of Rayleigh waves can be achieved using piezoelectric transducer, electromagnetic acoustic transducers, air-coupled transducer or laser ultrasound. A considerable research interest on the detection and sizing of surface crack using laser generated Rayleigh waves, has been observed. However, this technique requires extra safety from the users, may require surface preparation and the cost of the equipment is prohibitive. This work presents a method to measure

the depth of surface breaking electrical discharged machined (EDM) notches using Rayleigh waves excited and received through conventional ultrasonic phased array probes. Here, the generation of Rayleigh waves is achieved through appropriate delay between the emission of each piezoelectric element of the phased array probe. The time-of-flight (TOF) information of Rayleigh waves and their interaction with the geometry of the notches can be used to size its depth. A two-dimensional finite element (FE) model was used to demonstrate the proposed sizing method. Results obtained from FE simulations show excellent agreement between the measured and simulated true notch depth.

Keywords: Phased array, Rayleigh waves, excitation method, surface cracks, depth sizing.

2. Introduction

Development of surface discontinuities on engineering components subjected to critical thermal and mechanical stresses are common. Over a period of time this may lead to a stable crack growth, which limits the service life of the components or may sometimes result in a catastrophic failure. The impact of any such failure may have severe consequences on the environment and economy. In order to avoid any such failure and ensure the safety and reliability of the structure, routine inspection is necessary. There is a range of NDT techniques, reported in Cawley (2001), that offers the possibility to inspect and size the surface discontinuities. Among the available NDT techniques, eddy current testing (ECT) is the most widely used method for surface crack characterization Helifa *et al.* (2006), due to their high sensitivity to surface and near surface defects. However, the complete characterization requires a complex calibration. Moreover, the depth range is limited by the penetration depth of eddy current. Recently, a considerable research interest has been observed in the area of surface crack detection and sizing using ultrasonic Rayleigh waves Masserey & Mazza (2007); Xiao *et al.* (2022). The possible techniques for the generation and detection of Rayleigh waves are well summarized in Chakrapani & Bond (2018). The most efficient method for the excitation of Rayleigh wave is the wedge technique. However, Rayleigh waves undergoes transmission losses at the interfaces of wedge. Also, the ability to

excite on different waveguide material using the wedge technique is limited as a new wedge is needed if the waveguide material is changed.

Therefore, the aim of this work is to develop a method for the sizing of surface cracks based on the Rayleigh wave excited using a conventional phased array transducer. A delay between the emission of each element of phased array probe is implemented to achieve the generation of Rayleigh waves. The proposed Rayleigh wave excitation method is verified experimentally. Further, numerical simulation is used to study the propagation and scattering characteristics of Rayleigh wave across the surface breaking defect. TOF information of Rayleigh wave features from the geometry of the notches is used to measure the depth of the simulated EDM notch like defect.

The outline of the paper is as follows. First, the theoretical background of the Rayleigh wave excitation technique used in the proposed surface crack sizing method is given. This section is followed by the experiments conducted to achieve the Rayleigh wave generation through a phased array probe. Next, the finite element simulation results demonstrating the proposed surface crack sizing method are presented. Finally conclusions are drawn.

3. Theoretical Background

The generation of Rayleigh waves is possible using piezoelectric transducers or non-contact techniques such as electromagnetic acoustic transducers (EMAT), air-coupled transducers and laser ultrasound Chakrapani & Bond (2018). Non-contact methods have an advantage that no couplant is needed. However, the maximum operating frequency or bandwidth required for crack sizing are difficult to reach.

A method based on comb transducer Penttinen & Luukkala (1974) and interdigital transducer (IDT) Moulzolf *et al.* (2013) can also be used for the generation of Rayleigh waves. In a comb transducer an array of piezoelectric elements are placed in such a way that the inter element space is exactly equal to one Rayleigh wavelength. These methods provides a better

generation efficiency. However, unlike the wedge technique, for each application a new design with corresponding Rayleigh wavelength of the test specimen, needs to be fabricated.

To overcome these limitations, here, the Rayleigh wave generation is achieved through an ultrasonic phased array transducer. An appropriate delay required for the generation of Rayleigh waves, based on the elementary pitch of the transducer and the Rayleigh velocity of the waveguide material is added between the emission of each element. The estimation of the required delay and its theoretical background is discussed in subsection 3.1.

3.1 Rayleigh wave excitation using a phased array probe

Rayleigh wave excitation technique used here is a specific case of the comb excitation method. In the comb excitation method the mode can be controlled based on the inter element space, which should be equal to or a multiple of the targeted wavelength. However, the wave generation using a comb transducer is not unidirectional which is often required in NDT inspection. A time-delay periodic linear array (TDPLA) design based on the use of interference principle is proposed to excite Lamb waves in only one direction in plates Zhu & Rose (1999). A better mode control and selectivity is achieved relative to the comb transducer. However, an additional multi-channel source/receiver equipment is needed to control this TDPLA. Therefore, to overcome this limitation a multi-channel time-delay system is developed Li & Rose (2001) and combined with a phased array transducer to improve the excitation and mode control capability further. A significant improvement has been observed. However, the major drawback of this method is that the areas of excitation in the dispersion curve depends on the frequency at the selected phase velocity. Hence, an individual higher-order guided wave mode excitation is difficult to achieve. Veit & Bélanger (2020) recently developed a phased velocity excitation method using a conventional phased array probe. The elementary pitch of the transducer was chosen much smaller than the wavelength of the targeted mode, so that the excitation no longer depends on the frequency. In addition, a phase velocity excitation zone in the dispersion curve could be selected. Hence, a linear time delay calculated using the elementary pitch and specific phase velocity to be excited is provided between the emission of each element. The

implementation of the delay creates an angled plane wavefront, similar to the angled wedge excitation configuration.

Following this specific phase velocity based guided wave excitation method Veit & Bélanger (2020), the current Rayleigh wave excitation method is proposed in this paper. Here, the time delay (t_d) between the emission of elements is estimated based on the fixed elementary pitch of the transducer and the Rayleigh wave velocity of the waveguide, as given:

$$t_d = \frac{p}{V_R} \tag{A I-1}$$

where p is the pitch of the transducer, V_R is the velocity of Rayleigh waves in the waveguide.

The delay required for each element can be estimated as:

$$t_i = \frac{p \cdot (i-1)}{V_R} \tag{A I-2}$$

where t_i is the delay corresponds to i^{th} element, p is the pitch of the transducer, V_R is the velocity of Rayleigh waves in the waveguide.

4. Experiments

Experiments were performed using a conventional phased array probe to verify the proposed Rayleigh wave excitation method. The schematic of the experimental setup is shown in Figure I-1(a). Experimental measurements were conducted on a 50 mm steel block shown in Figure I-1(b). An appropriate delay calculated using Equation (A I-2) was implemented between the emission of each element of the phased array probe. An Olympus linear ultrasonic phased array probe 2.25L64 was used. The probe parameters are shown in Table I-1.

The signal generation and emission of each element was controlled by a Verasonics Vantage 64 LE controller. A hann windowed toneburst centered at 2.25 MHz was sent to each element with the required delay for Rayleigh wave generation. The generated wave was received using a laser

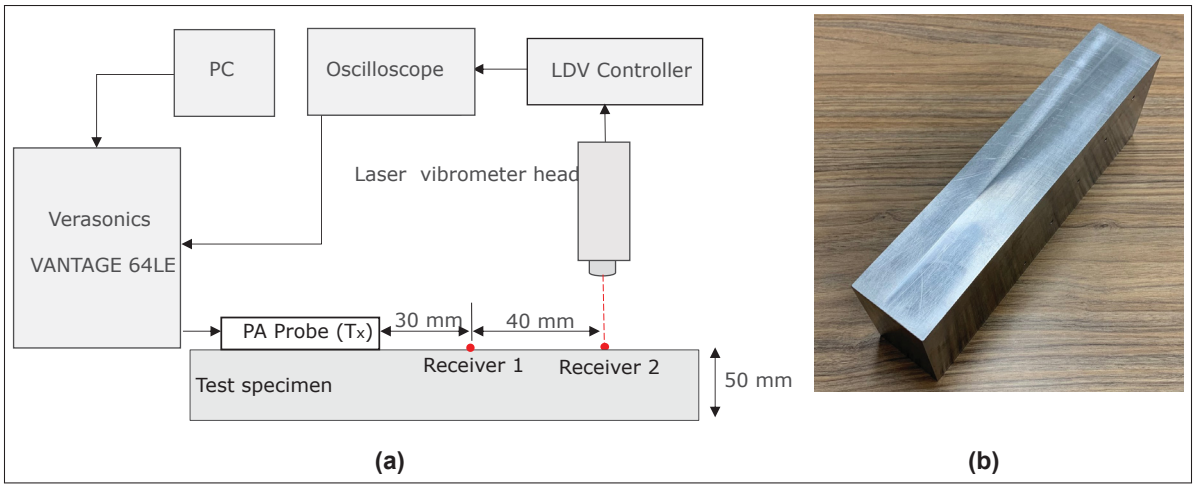

Figure-A I-1 (a) Schematic illustration of experimental setup and (b) Specimen of steel block

Table-A I-1 Parameters of phased array probe used in experiments

Transducer properties	
Frequency	2.25 MHz
Element count	64
Active aperture	64 mm
Passive aperture	7 mm
Pitch	1 mm

Doppler vibrometer (Polytec OFV-505, Polytec controller OFV-2570) and a high- definition 4-channel DSO9024H digital oscilloscope. To improve the signal-to-noise ratio a retro-reflective tape was also used. The wave propagating along the surface of the test specimen was captured at two different monitoring points. The first monitring point was 30 mm away from the probe and the propagation distance between two monitoring points are kept 40 mm as shown in Figure I-1(a).

Figure I-2 shows the typical time traces of the amplitude of the out-of-plane displacement of Rayleigh waves. The time-of-flight (TOF) of wave packets shown in Figure I-2 was used to measure the velocity of the excited waves. The measured velocity was 2962m/s and was found similar to the Rayleigh wave velocity of the test specimen. It can be observed that the wave

Table-A I-2 Material and FE parameters used in simulation

Material properties		FE Parameters	
Material	Steel	Element Size	$(\lambda/20)$
Young's Modulus (Gpa)	200	Element Type	CPE4R
Poisson's Ratio	7800	Frequency	2.25 MHz
Material Density (Kg/m^3)	0.3	Step Time	1 ns

generated through the excitation method proposed in this paper propagates with no other wave modes and ensure a satisfactory excitation of Rayleigh wave mode. Once the excited waves were verified as Rayleigh wave experimentally, further FE simulations were used to demonstrate the proposed depth sizing method using the same phased array probe in a pulse-echo configuration.

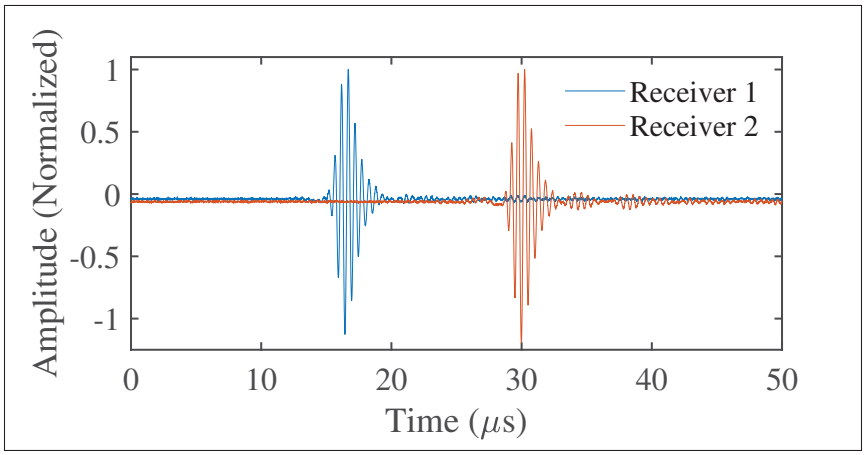

Figure-A I-2 Rayleigh wave amplitude of the out of plane displacement recorded experimentally at two monitoring position 40 mm apart to measure the Rayleigh wave velocity in a steel block

5. Finite Element Simulations

A two-dimensional finite element model was used to simulate the Rayleigh wave excitation using an ultrasonic phased array probe. An explicit time domain finite element solver for linear elastodynamics problem, provided by Pogo FEA Huthwaite (2014) a commercial software package was used for the modeling of the Rayleigh wave propagation. A detailed schematic of the studied configuration is shown in Figure I-3.

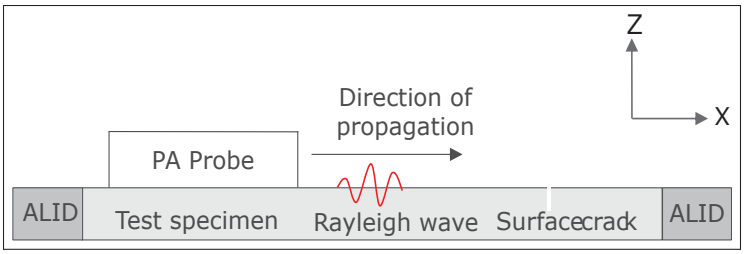

Figure-A I-3 Schematic of tow-dimensional finite element model used to simulate the Rayleigh wave propagation using ultrasonic phased arrays

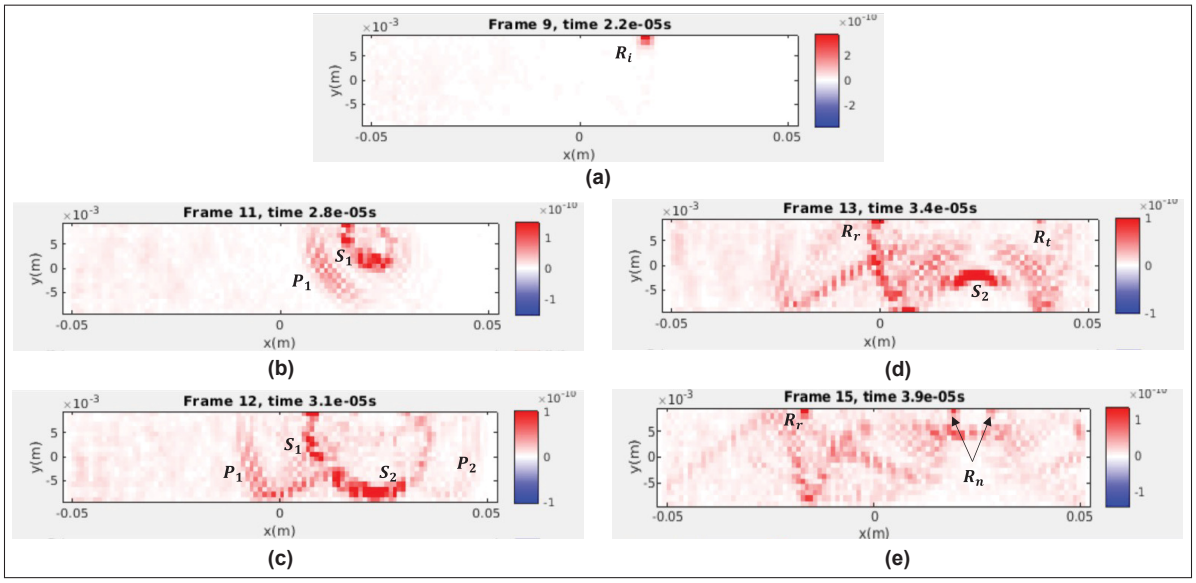

Figure-A I-4 Snapshots of the contour of total displacement magnitude by the scattering of Rayleigh wave at EDM notch-like defect, recorded at different time instances shows: (a) the incident Rayleigh waves, (b) scattering of the incident Rayleigh waves at the left opening of the notch, (c) scattering of the transmitted Rayleigh waves at the tip of the notch, (d) propagation of reflected and transmitted Rayleigh echoes from the notch tip along the surface and the interaction of reflected transversal S_2 mode with the notch tip and (e) propagation of the new Rayleigh wave mode (R_n) along the surface

A 20 mm thick steel block was modelled with the mesh consisted of two-dimensional 4 node plane strain elements. 20 elements per shortest wavelength were considered to ensure convergence of the solution. The step time chosen to satisfy the stability criteria of time marching simulation was one nanosecond. To avoid the reflections from the other ends, the absorbing boundary layers

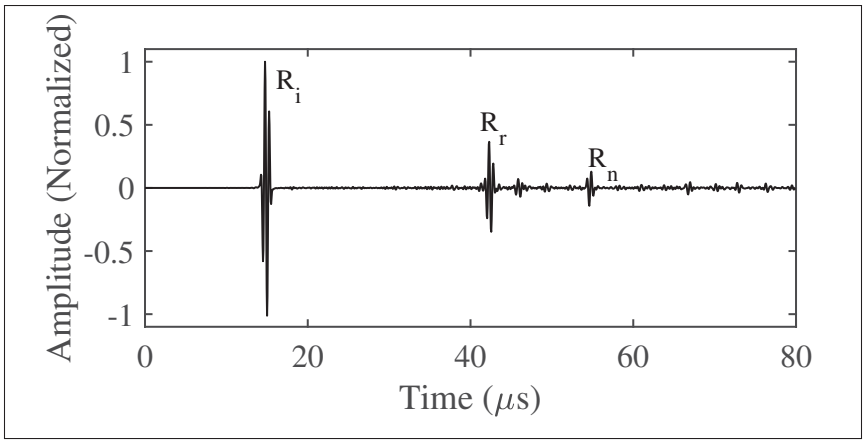

Figure-A I-5 Simulated time traces of Rayleigh wave interaction with a EDM notch like defect orientated normal to the surface, (R_r) is the Rayleigh echo reflected from the edge of surface slot and (R_n) is the new Rayleigh wave generated, when the reflection of shear wave S2 from the bottom of the plate encounter the tip of the notch

were created at both ends of the block Drozdz *et al.* (2006). A surface crack was created in this model by doing the mesh adjustment. In doing so, for the require crack depth, adjacent elements are disconnected and the elements in the direction relative to the decoupled nodes were allocated to the new nodes. The details of parameters used for simulating the Rayleigh wave propagation are listed in Table I-2.

The same phased array probe used in the experiments was simulated. The nodes corresponding to all the elements of the phased array probe were chosen on the top surface of the block for the excitation and detection. The elementary pitch was selected corresponds to the probe parameters given in Table I-1. A 3-cycle Hann windowed toneburst centered at 2.25 MHz was sent to each element with the time delay estimated using Equation A I-2. The reflection of Rayleigh waves from the notch geometries were examined by monitoring the out-of-plane displacement at the same nodes chosen for the excitation.

5.1 Rayleigh wave interaction with an EDM notch like defect

Table-A I-3 Percentage error in depth measurement of EDM notches with different depth

EDM surface notch depth	Simulated depth (mm)	Measured depth (mm)	% Error in measurement
Depth 1	5	4.83	3.4
Depth 2	4	3.8	5
Depth 3	3	2.79	7
Depth 4	2	1.9	5

FE simulations were carried out to further understand the scattering of Rayleigh waves when they interact with surface discontinuities. Figure I-4 shows the snapshots of the total displacement magnitude of Rayleigh wave interaction with an EDM notch-like defect.The Rayleigh wave packet excited using a phased array probe travels along the surface, referred here as the incident Rayleigh wave (R_i) and shown in Figure I-4(a). It can be clearly seen that the incident Rayleigh wave mode propagates dominantly with no other wave modes before reaching the opening of the notch (referred as the notch edge here onward). However, upon reaching the notch edge, the Rayleigh wave energy is either reflected, transmitted or converted to bulk wave modes as can be seen in Figure I-4(b). The Rayleigh wave reflected from the notch edge is referred as R_r. The reflected and transmitted waves carry a part of the total incident Rayleigh energy however, most of the energy is converted into longitudinal (P_1) and transversal wave (S_1) and propagates into the bulk of material as shown in Figure I-4(b). The transmitted Rayleigh waves follows the notch face and reaches the tip of the notch, where the same phenomenon is repeated. The transmitted Rayleigh energy is converted to longitudinal (P_2) and transversal wave (S_2) as shown in Figure I-4(c). Also, a small amount of transmitted Rayleigh energy is again reflected and transmitted across the tip and follow the notch faces. Upon reaching the notch edge (both left and right), they further scattered, and very small amount of the energy is seen propagating along the surface, depicted here as R_t in Figure I-4(d). Furthermore, the transversal mode (S_2) propagates into the bulk of material and reflects upon impingement of the backwall, as can be seen in Figure I-4(d). When this reflected S_2 mode encounter the notch tip, it generates a new Rayleigh waves mode which follow the notch faces and scattered again at the notch edge in a similar way as explained above. The remaining energy of the new Rayleigh wave modes propagates along the

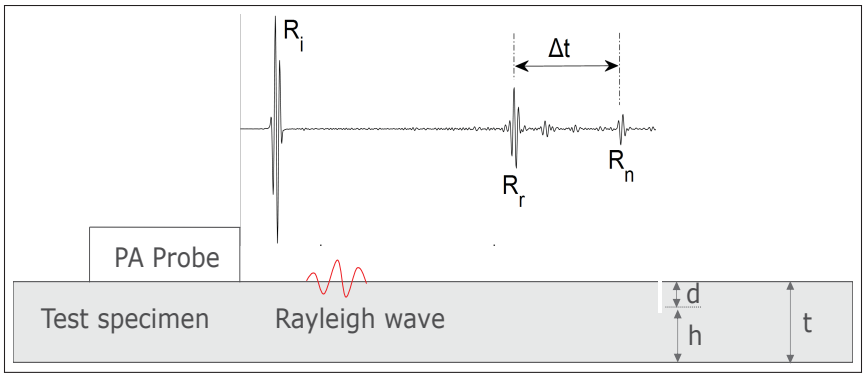

Figure-A I-6 Schematic illustration of the procedure followed in sizing of the notch depth

surface as shown in Figure I-4(e). This new Rayleigh wave mode will be referred as R_n hereafter and throughout in this paper. The generation of the Rayleigh wave R_n is in line previous work reported in the literature Masserey (2006).

Figure I-5 shows the typical signal of the simulated Rayleigh amplitude of the out-of-plane displacement obtained at one of the elements of the probe, generated after the scattering sequences of Rayleigh waves at the geometries of the notch. The echoes of Rayleigh waves from the notch edge R_r and the newly generated Rayleigh wave R_n can be clearly seen. Although, the other wave modes which are unrelated to the Rayleigh waves were also found between the R_r and R_n. However, they have a very low amplitude and has no influence on the proposed sizing method.

5.2 EDM notch depth sizing approach

The method proposed here for the sizing of the notch depth is based on the TOF information of the Rayleigh echoes R_r and R_n. The schematic illustration of the proposed notch depth sizing approach is shown in Figure I-6.

As observed from the discussion given in subsection 5.1 that the new Rayleigh wave mode R_n is generated when the reflected transversal mode (S_2) from the back wall encounter the tip of the

notch. Therefore, the travel time between R_r and R_n, represented as Δt in Figure I-6, can be written as,

$$\frac{d}{V_R} + \frac{t-d}{V_S} = \frac{\Delta t}{2} \tag{A I-3}$$

where, d is the notch depth, t is the thickness of the test specimen, V_R is the Rayleigh wave velocity and V_S is the shear wave velocity of the waveguide. On further simplification Equation A I-3 can be written to calculate the notch depth as,

$$d = \frac{V_R \cdot \left(\frac{\Delta t}{2}\right) - t \cdot C_r}{1 - C_r} \tag{A I-4}$$

where, C_r is the ratio of Rayleigh wave to shear wave velocity of the waveguide material.

The surface breaking EDM notches with different depth oriented normal to the surface were simulated. The simulated depths were then measured using Equation A I-4. The comparison of simulated true depth and measured depth using Equation A I-4 is shown in Table I-3. It has been observed that the proposed depth sizing method can measure the notch depth accurately within 7% error range.

6. Conclusion

This work presents a method for the sizing of surface breaking notch-like defect that uses time-domain Rayleigh wave signals excited through conventional ultrasonic phased array probes. First, the excitation of Rayleigh wave using a conventional phased array probe was verified experimentally. Experimental results showed excellent Rayleigh wave selectivity. Also, the measured velocity of the experimentally generated signals was found similar to the Rayleigh wave velocity of the waveguide. Further, the finite element time marching scheme was used to understand the Rayleigh wave scattering by an EDM notch-like defect and to demonstrate the proposed sizing method. The results obtained from FE simulations demonstrated that the

simulated notch depth can be measured accurately using the proposed sizing method with an error of less than 7%.

Further work is needed to understand the influence of crack orientation on the accuracy of the proposed sizing method.

LIST OF REFERENCES

Aldrin, J. C. (2004, 4). Models and Methodology for the Characterization of Surface-Breaking Cracks Using an Ultrasonic Near-Field Scattering Measurement. pp. 87-94. doi: 10.1063/1.1711610.

Alleyne, D. & Cawley, P. (1991). A two-dimensional Fourier transform method for the measurement of propagating multimode signals. *The Journal of the Acoustical Society of America*, 89(3), 1159-1168. doi: https://doi.org/10.1121/1.400530.

Arias, I. & Achenbach, J. D. (2004). A model for the ultrasonic detection of surface-breaking cracks by the scanning laser source technique. *Wave Motion*, 39, 61-75. doi: 10.1016/j.wavemoti.2003.06.001.

Auld, B. A. (1990). *Accoustic Fields And Waves In Solids Vol-1*. New York London Sydney Toronto: JOHN WILEY SONS.

Barnard, D. J. (2007). A variable pitch comb fixture for rayleigh wave generation and reception. *AIP Conference Proceedings*, 894(March), 1684–1690. doi: 10.1063/1.2718167.

Betta, G., Ferrigno, L. & Laracca, M. (2011). GMR-based ECT instrument for detection and characterization of crack on a planar specimen: A hand-held solution. *IEEE transactions on instrumentation and measurement*, 61(2), 505–512.

Blackshire, J. L. & Sathish, S. (2002). Near-field ultrasonic scattering from surface-breaking cracks. *Applied Physics Letters*, 80, 3442-3444. doi: 10.1063/1.1476722.

Blitz, J., Willsttäter, V., Oaten, S. & Hajian, N. (1987). Eddy-current surface-crack sizing in steel with high lift-off. *NDT international*, 20(2), 105–110.

Bowler, J. R. & Bowler, N. (2002). Evaluation of the magnetic field near a crack with application to magnetic particle inspection. *Journal of Physics D: Applied Physics*, 35(18), 2237.

Bray, D. E. & Stanley, R. K. (2018). *Nondestructive evaluation: a tool in design, manufacturing and service*. CRC press.

Cawley, P. (2001). Non-destructive testing—current capabilities and future directions. *Proceedings of the Institution of Mechanical Engineers, Part L: Journal of Materials: Design and Applications*, 215(4), 213-223. doi: 10.1177/146442070121500403.

Chakrapani, S. K. & Bond, L. J. (2018). Rayleigh Wave Nondestructive Evaluation for Defect Detection and Materials Characterization. *Nondestructive Evaluation of Materials*, 17, 266–282. doi: 10.31399/asm.hb.v17.a0006461.

Chakrapani, S. K., Dayal, V. & Barnard, D. (2013). Detection and characterization of waviness in unidirectional GFRP using rayleigh wave air coupled ultrasonic testing (RAC-UT). *Research in Nondestructive Evaluation*, 24(4), 191–201. doi: 10.1080/09349847.2013.786158.

Cheeke, J. (2012). *Fundamentals and Applications of Ultrasonic Waves*. CRC press. doi: https://doi.org/10.1201/b12260.

Cook, D. & Berthelot, Y. (2001a). Detection of small surface-breaking fatigue cracks in steel using scattering of Rayleigh waves. *NDT & E International*, 34(7), 483-492. doi: https://doi.org/10.1016/S0963-8695(00)00080-3.

Cook, D. & Berthelot, Y. (2001b). Detection of small surface-breaking fatigue cracks in steel using scattering of Rayleigh waves. *NDT E International*, 34(7), 483 - 492. doi: https://doi.org/10.1016/S0963-8695(00)00080-3.

Cooper, J., Dewhurst, R. & Palmer, S. (1986). Characterization of surface-breaking defects in metals with the use of laser-generated ultrasound. *Philosophical Transactions of the Royal Society of London. Series A, Mathematical and Physical Sciences*, 320(1554), 319–328. doi: https://doi.org/10.1098/rsta.1986.0121.

Date, K., Shimada, H. & Ikenaga, N. (1982). Crack height measurement — an evaluation of the accuracy of ultrasonic timing methods. *NDT International*, 15(6), 315 - 319. doi: https://doi.org/10.1016/0308-9126(82)90068-2.

Deng, P., He, C., Lyu, Y., Song, G., Jiao, J. & Wu, B. (2019). Detection of inner wall circumferential cracks in the special-shaped pipes using surface waves. *Journal of Nondestructive Evaluation*, 38(1), 1–12. doi: 10.1007/s10921-018-0554-5.

Doyle, P. & Scala, C. (1978). Crack depth measurement by ultrasonics: a review. *Ultrasonics*, 16(4), 164–170.

Drozdz, M., Moreau, L., Castaings, M., Lowe, M. J. S. & Cawley, P. (2006). Efficient Numerical Modelling of Absorbing Regions for Boundaries Of Guided Waves Problems. *AIP Conference Proceedings*, 820(1), 126-133. doi: 10.1063/1.2184520.

Ducousso, M. & Reverdy, F. (2020). Real-time imaging of microcracks on metallic surface using total focusing method and plane wave imaging with Rayleigh waves. *NDT & E International*, 116, 102311. doi: https://doi.org/10.1016/j.ndteint.2020.102311.

Dutton, B., Clough, A. R., Rosli, M. H. & Edwards, R. S. (2011). Non-contact ultrasonic detection of angled surface defects. *NDT and E International*, 44, 353-360. doi: 10.1016/j.ndteint.2011.02.001.

Eason, G. (1975). Wave motion in elastic solids 1975: K. F. Graff. Clarendon Press: Oxford University Press. 649 + xvii pp. ; price £15.00.

Edwards, R., Dixon, S. & Jian, X. (2006). Depth gauging of defects using low frequency wideband Rayleigh waves. *Ultrasonics*, 44(1), 93-98. doi: https://doi.org/10.1016/j.ultras.2005.08.005.

Eisenmann, D. J., Enyart, D., Lo, C. & Brasche, L. (2014). Review of progress in magnetic particle inspection. *AIP Conference Proceedings*, 1581(1), 1505–1510.

Fan, M., Cao, B., Yang, P., Li, W. & Tian, G. (2015). Elimination of liftoff effect using a model-based method for eddy current characterization of a plate. *NDT & E International*, 74, 66-71. doi: https://doi.org/10.1016/j.ndteint.2015.05.007.

Felice, M. V., Velichko, A. & Wilcox, P. D. (2014). Accurate depth measurement of small surface-breaking cracks using an ultrasonic array post-processing technique. *NDT & E International*, 68, 105-112. doi: https://doi.org/10.1016/j.ndteint.2014.08.004.

Ghosh, D., Beniwal, S., Ganguli, A. & Mukherjee, A. (2018). Reference free imaging of subsurface cracks in concrete using Rayleigh waves. *Structural Control and Health Monitoring*, 25(10), e2246. doi: https://doi.org/10.1002/stc.2246.

Graff, K. (1975). *Wave Motion in Elastic Solids*. Clarendon Press.

Hassan, W. & Veronesi, W. (2003). Finite element analysis of Rayleigh wave interaction with finite-size, surface-breaking cracks. *Ultrasonics*, 41(1), 41-52. doi: https://doi.org/10.1016/S0041-624X(02)00393-1.

Haupert, S., Ohara, Y., Carcreff, E. & Renaud, G. (2019). Fundamental wave amplitude difference imaging for detection and characterization of embedded cracks. *Ultrasonics*, 96, 132-139. doi: https://doi.org/10.1016/j.ultras.2019.02.003.

He, D. & Yoshizawa, M. (2002). Dual-frequency eddy-current NDE based on high-Tc rf SQUID. *Physica C: Superconductivity*, 383(3), 223–226.

He, D., Zhang, Y., Shiwa, M. & Moriya, S. (2013). Development of eddy current testing system for inspection of combustion chambers of liquid rocket engines. *Review of Scientific Instruments*, 84(1), 014701.

He, D., Wang, Z., Kusano, M., Kishimoto, S. & Watanabe, M. (2019). Evaluation of 3D-Printed titanium alloy using eddy current testing with high-sensitivity magnetic sensor. *NDT & E International*, 102, 90–95.

He, J., Liu, X., Cheng, Q., Yang, S. & Li, M. (2023). Quantitative detection of surface defect using laser-generated Rayleigh wave with broadband local wavenumber estimation. *Ultrasonics*, 132, 106983. doi: https://doi.org/10.1016/j.ultras.2023.106983.

Helifa, B., Oulhadj, A., Benbelghit, A., Lefkaier, I., Boubenider, F. & Boutassouna, D. (2006). Detection and measurement of surface cracks in ferromagnetic materials using eddy current testing. *NDT & E International*, 39(5), 384-390. doi: https://doi.org/10.1016/j.ndteint.2005.11.004.

Hernandez-Valle, F., Dutton, B. & Edwards, R. (2014). Laser ultrasonic characterisation of branched surface-breaking defects. *NDT & E International*, 68, 113-119. doi: https://doi.org/10.1016/j.ndteint.2014.08.009.

Holmes, C., Drinkwater, B. & Wilcox, P. (2005). Post-processing of the full matrix of ultrasonic transmit-receive array data for non-destructive evaluation. *NDT and E International*, 38(8), 701–711. doi: 10.1016/j.ndteint.2005.04.002. Publisher: Elsevier Other: in press.

Hoyle, C., Sutcliffe, M., Charlton, P. & Mosey, S. (2019). Large-area surface imaging methods using ultrasonic Rayleigh waves, phased array and full matrix capture for non-destructive testing. *Insight - Non-Destructive Testing and Condition Monitoring*, 61, 367-379. doi: 10.1784/insi.2019.61.7.367.

Huang, H., Sakurai, N., Takagi, T. & Uchimoto, T. (2003). Design of an eddy-current array probe for crack sizing in steam generator tubes. *Ndt & E International*, 36(7), 515–522. doi: https://doi.org/10.1016/S0963-8695(03)00050-1.

Hunter, A. J., Drinkwater, B. W. & Wilcox, P. D. (2008). The wavenumber algorithm for full-matrix imaging using an ultrasonic array. *IEEE transactions on ultrasonics, ferroelectrics, and frequency control*, 55(11), 2450–2462.

Hur, D. H., Choi, M. S., Lee, D. H., Kim, S. J. & Han, J. H. (2010). A case study on detection and sizing of defects in steam generator tubes using eddy current testing. *Nuclear engineering and design*, 240(1), 204–208.

Hurley, D. C. (1999). Nonlinear propagation of narrow-band Rayleigh waves excited by a comb transducer. *The Journal of the Acoustical Society of America*, 106(4), 1782–1788. doi: 10.1121/1.427927.

Huthwaite, P. (2014). Accelerated finite element elastodynamic simulations using the GPU. *Journal of Computational Physics*, 257, Part A(0), 687-707. doi: http://dx.doi.org/10.1016/j.jcp.2013.10.017.

Hévin, G., Abraham, O., Pedersen, H. & Campillo, M. (1998). Characterization of surface cracks with Rayleigh waves: a numerical model. *NDT E International*, 31(4), 289 - 297. doi: https://doi.org/10.1016/S0963-8695(98)80013-3. Non-destructive Testing in Civil Engineering.

Isla, J. & Cegla, F. (2017). EMAT phased array: A feasibility study of surface crack detection. *Ultrasonics*, 78, 1-9. doi: https://doi.org/10.1016/j.ultras.2017.02.009.

Jeong, H. (2005). Finite element analysis of laser-generated ultrasound for characterizing surface-breaking cracks. *Journal of mechanical science and technology*, 19, 1116–1122. doi: https://doi.org/10.1007/BF02984033.

Jian, X., Fan, Y., Edwards, R. S. & Dixon, S. (2006). Surface-breaking crack gauging with the use of laser-generated Rayleigh waves. *Journal of Applied Physics*, 100(6), 064907. doi: https://doi.org/10.1063/1.2353892.

Jian, X., Dixon, S., Guo, N. & Edwards, R. (2007). Rayleigh wave interaction with surface-breaking cracks. *Journal of Applied Physics*, 101(6), 064906. doi: https://doi.org/10.1063/1.2435803.

Lamb, H. (1917). On waves in an elastic plate. *Proceedings of the Royal Society of London. Series A, Containing papers of a mathematical and physical character*, 93(648), 114–128.

Le Jeune, L., Robert, S. & Prada, C. (2016). Plane wave imaging for ultrasonic inspection of irregular structures with high frame rates. *AIP Conference Proceedings*, 1706(1), 020010.

Lee, J., Lee, S., Jiles, D., Garton, M., Lopez, R. & Brasche, L. (2003). Sensitivity analysis of simulations for magnetic particle inspection using the finite-element method. *IEEE transactions on magnetics*, 39(6), 3604–3606.

Li, H., Pan, Q., Zhang, X. & An, Z. (2020). An approach to size sub-wavelength surface crack measurements using Rayleigh waves based on laser ultrasounds. *Sensors*, 20(18), 5077. doi: 10.3390/s20185077.

Li, J. & Rose, J. (2001). Implementing guided wave mode control by use of a phased transducer array. *IEEE Transactions on Ultrasonics, Ferroelectrics, and Frequency Control*, 48(3), 761-768. doi: 10.1109/58.920708.

Li, K., Ma, Z., Fu, P. & Krishnaswamy, S. (2018). Quantitative evaluation of surface crack depth with a scanning laser source based on particle swarm optimization-neural network. *NDT & E International*, 98, 208-214. doi: https://doi.org/10.1016/j.ndteint.2018.05.011.

Li, R., Liu, W., Li, Z., Liu, X., Li, H., Gu, S. & Song, Y. (2023). Depth evaluation for surface-breaking cracks with mode-converted Rayleigh waves generated by a point-focused laser. *Optics & Laser Technology*, 167, 109758. doi: https://doi.org/10.1016/j.optlastec.2023.109758.

Ma, T., Sun, Z., Zhang, W. & Chen, Q. (2016). A machine vision assisted system for fluorescent magnetic particle inspection of railway wheelsets. *AIP Conference Proceedings*, 1706(1), 150003.

Manes, G., Atzeni, C. & Susini, C. (1983). Design of a Simplified Delay System for Ultrasound Phased Array Imaging. *IEEE Transactions on Sonics and Ultrasonics*, 30(6), 350-354. doi: 10.1109/T-SU.1983.31439.

Masserey, B. (2006). *Ultrasonic surface crack characterization using Rayleigh waves*. (Ph.D. thesis, ETH Zurich, Zürich).

Masserey, B. & Fromme, P. (2008). On the reflection of coupled Rayleigh-like waves at surface defects in plates. *The Journal of the Acoustical Society of America*, 123(1), 88–98. doi: https://doi.org/10.1121/1.2805668.

Masserey, B. & Mazza, E. (2007). Ultrasonic sizing of short surface cracks. *Ultrasonics*, 46(3), 195-204. doi: https://doi.org/10.1016/j.ultras.2007.02.001.

Matsuda, Y., Nakano, H., Nagai, S. & Hiratsuka, H. (2006). Surface breaking crack evaluation with photorefractive quantum wells and laser-generated Rayleigh waves. *Applied Physics Letters*, 89(17), 171902. doi: https://doi.org/10.1063/1.2364579.

Mohseni, E., Habibzadeh Boukani, H., Ramos França, D. & Viens, M. (2020). A study of the automated eddy current detection of cracks in steel plates. *Journal of Nondestructive Evaluation*, 39(1), 1–12. doi: https://doi.org/10.1007/s10921-019-0647-9.

Moulzolf, S. C., Behanan, R., Pollard, T., Lad, R. & da Cunha, M. P. (2013). Capacitively coupled IDT for high temperature SAW devices. 255-258. doi: 10.1109/ULTSYM.2013.0066.

Na, J. K. & Blackshire, J. L. (2010). Interaction of Rayleigh surface waves with a tightly closed fatigue crack. *NDT & E International*, 43(5), 432-439. doi: https://doi.org/10.1016/j.ndteint.2010.04.003.

Ohara, Y., Oshiumi, T., Nakajima, H., Yamanaka, K., Wu, X., Uchimoto, T., Takagi, T., Tsuji, T. & Mihara, T. (2017). Ultrasonic phased array with surface acoustic wave for imaging cracks. *AIP Advances*, 7(6), 065214. doi: 10.1063/1.4989725.

Ohara, Y., Nakajima, H., Tsuji, T. & Mihara, T. (2019). Nonlinear surface-acoustic-wave phased array with fixed-voltage fundamental wave amplitude difference for imaging closed cracks. *NDT & E International*, 108, 102170. doi: https://doi.org/10.1016/j.ndteint.2019.102170.

Ohara, Y., Oshiumi, T., Wu, X., Uchimoto, T., Takagi, T., Tsuji, T. & Mihara, T. (2022). High-Selectivity imaging of the closed fatigue crack due to thermal environment using surface-acoustic-wave phased array (SAW PA). *Ultrasonics*, 119, 106629. doi: https://doi.org/10.1016/j.ultras.2021.106629.

Ouchi, A., Sugawara, A., Ohara, Y. & Yamanaka, K. (2015). Subharmonic phased array for crack evaluation using surface acoustic wave. *Japanese Journal of Applied Physics*, 54(7S1), 07HC05. doi: 10.7567/JJAP.54.07HC05.

Peng, C., Bai, L., Zhang, J. & Drinkwater, B. W. (2018). The sizing of small surface-breaking fatigue cracks using ultrasonic arrays. *NDT & E International*, 99, 64-71. doi: https://doi.org/10.1016/j.ndteint.2018.06.005.

Penttinen, A. & Luukkala, M. (1974). Surface wave generation by comb transducers. *Ultrasonics*, 12(6), 257–259. doi: 10.1016/0041-624X(74)90133-4.

Portzgen, N., Gisolf, D. & Blacquiere, G. (2006). Inverse wave field extrapolation: A different NDI approach to imaging defects. *IEEE transactions on ultrasonics, ferroelectrics, and frequency control*, 54(1), 118–127.

Qian, F., Xing, G., Yang, P., Hu, P., Zou, L. & Koukoulas, T. (2021). Laser-induced ultrasonic measurements for the detection and reconstruction of surface defects. 5, 38. doi: https://doi.org/10.1051/aacus/2021031.

Rajagopal, P., Drozdz, M., Skelton, E. A., Lowe, M. J. & Craster, R. V. (2012). On the use of absorbing layers to simulate the propagation of elastic waves in unbounded isotropic media using commercially available Finite Element packages. *NDT & E International*, 51, 30-40. doi: https://doi.org/10.1016/j.ndteint.2012.04.001.

Rayleigh, L. (1888). On the free vibrations of an infinite plate of homogeneous isotropic elastic matter. *Proceedings of the London Mathematical Society*, 1(1), 225–237.

Rose, J., Pelts, S. & Quarry, M. (1998). A comb transducer model for guided wave NDE. *Ultrasonics*, 36(1), 163-169. doi: https://doi.org/10.1016/S0041-624X(97)00042-5.

Rose, J. L. (1999). *Ultrasonic Guided Waves in Solid Media*. Cambridge University Press. doi: 10.1017/CBO9781107273610.

Rosli, M., Edwards, R. & Fan, Y. (2012). In-plane and out-of-plane measurements of Rayleigh waves using EMATs for characterising surface cracks. *NDT & E International*, 49, 1-9. doi: https://doi.org/10.1016/j.ndteint.2012.03.002.

Saini, A., Lane, C. J., Tu, J., Xue, H. & Fan, Z. (2022). 3D ultrasonic imaging of surface-breaking cracks using a linear array. *Ultrasonics*, 125, 106790. doi: https://doi.org/10.1016/j.ultras.2022.106790.

Scala, C. M. (2003, 2). Laser ultrasonics for surface-crack depth measurement using transmitted near-field Rayleigh waves. pp. 327-334. doi: 10.1063/1.1306068.

Schmerr, L. (2015). *Fundamentals of Ultrasonic Phased Arrays*. NY:Springer. doi: 10.1007/978-3-319-07272-2.

Seydel, J. (1982). Ultrasonic synthetic aperture focusing techniques in NDT. *Research techniques in nondestructive testing*, 6, 1–42.

Shen, X., Hu, H., Li, X. & Li, S. (2021). Study on PCA-SAFT imaging using leaky Rayleigh waves. *Measurement*, 170, 108708. doi: https://doi.org/10.1016/j.measurement.2020.108708.

Silk, M. (1976). The determination of crack penetration using ultrasonic surface waves. *NDT International*, 9(6), 290 - 297. doi: https://doi.org/10.1016/0308-9126(76)90071-7.

Sutcliffe, M., Weston, M., Dutton, B., Charlton, P. & Donne, K. (2012). Real-time full matrix capture for ultrasonic non-destructive testing with acceleration of post-processing through graphic hardware. *NDT E International*, 51, 16 - 23. doi: https://doi.org/10.1016/j.ndteint.2012.06.005.

Thring, C., Fan, Y. & Edwards, R. (2016). Focused Rayleigh wave EMAT for characterisation of surface-breaking defects. *NDT & E International*, 81, 20-27. doi: https://doi.org/10.1016/j.ndteint.2016.03.002.

Torello, D., Thiele, S., Matlack, K. H., Kim, J.-Y., Qu, J. & Jacobs, L. J. (2015). Diffraction, attenuation, and source corrections for nonlinear Rayleigh wave ultrasonic measurements. *Ultrasonics*, 56, 417-426. doi: https://doi.org/10.1016/j.ultras.2014.09.008.

Van Drunen, G. & Cecco, V. (1984). Recognizing limitations in eddy-current testing. *NDT International*, 17(1), 9-17. doi: https://doi.org/10.1016/0308-9126(84)90108-1.

Veit, G. & Bélanger, P. (2020). An ultrasonic guided wave excitation method at constant phase velocity using ultrasonic phased array probes. *Ultrasonics*, 102, 106039. doi: https://doi.org/10.1016/j.ultras.2019.106039.

Verma, B. & Bélanger, P. (2023). Surface Crack Sizing Method Using Rayleigh Waves Generated by Ultrasonic Phased Arrays. *49th Annual Review of Progress in Quantitative Nondestructive Evaluation*, 86595, V001T11A001.

Verma, B. & Bélanger, P. (2023). An alternative Rayleigh wave excitation method using an ultrasonic phased array. *Ultrasonics*, 135, 107121. doi: https://doi.org/10.1016/j.ultras.2023.107121.

Viktorov, I. A. (1967). *Rayleigh and Lamb waves: physical theory and applications*. New York: New York, Plenum Press, 1967.

Vu, B. Q. (1986). Diffraction of rayleigh waves in a half-space. II. inclined edge crack. *Journal of the Acoustical Society of America*, 79, 1688-1692. doi: 10.1121/1.393229.

Vu, B. Q. & Kinra, V. K. (1985). Diffraction of Rayleigh waves in a half-space. I. Normal edge crack. *Journal of the Acoustical Society of America*, 77, 1425-1430. doi: 10.1121/1.392036.

Wang, D. & Tang, J. (2022). Can we obtain the internal information of a surface crack from Rayleigh waves? *NDT & E International*, 132, 102714. doi: https://doi.org/10.1016/j.ndteint.2022.102714.

Wilcox, P. D., Croxford, A. J., Budyn, N., Bevan, R. L. T., Zhang, J., Kashubin, A. & Cawley, P. (2020). Fusion of multi-view ultrasonic data for increased detection performance in non-destructive evaluation. *Proceedings of the Royal Society A: Mathematical, Physical and Engineering Sciences*, 476(2243), 20200086. doi: 10.1098/rspa.2020.0086.

Wong, B. S., Low, Y. G., Wang, X., Ho, J.-H., Tan, C. & Ooi, J. B. (2010). 3D finite element simulation of magnetic particle inspection. *2010 IEEE Conference on Sustainable Utilization and Development in Engineering and Technology*, pp. 50–55.

Wu, J., Jiang, C., Fang, H. & Ng, C.-T. (2023). Damage detection in the T-welded joint using Rayleigh-like feature guided wave. *NDT & E International*, 135, 102806. doi: https://doi.org/10.1016/j.ndteint.2023.102806.

Xiang, L., Greenshields, D., Dixon, S. & Edwards, R. S. (2020). Phased Electromagnetic Acoustic Transducer Array for Rayleigh Wave Surface Defect Detection. *IEEE Transactions on Ultrasonics, Ferroelectrics, and Frequency Control*, 67(7), 1403-1411. doi: 10.1109/TUFFC.2020.2968151.

Xiao, J. & Cui, F. (2023). Machine learning enhanced characterization of surface defects using ultrasonic Rayleigh waves. *NDT & E International*, 140, 102969. doi: https://doi.org/10.1016/j.ndteint.2023.102969.

Xiao, J., Chen, J., Yu, X., Lisevych, D. & Fan, Z. (2022). Remote characterization of surface slots by enhanced laser-generated ultrasonic Rayleigh waves. *Ultrasonics*, 119, 106595. doi: https://doi.org/10.1016/j.ultras.2021.106595.

Xie, R., Chen, D., Pan, M., Tian, W., Wu, X., Zhou, W. & Tang, Y. (2015). Fatigue Crack Length Sizing Using a Novel Flexible Eddy Current Sensor Array. *Sensors*, 15(12), 32138–32151. doi: https://doi.org/10.3390/s151229911.

Xu, L., Wang, K., Su, Y., He, Y., Yang, J., Yuan, S. & Su, Z. (2022). Surface/sub-surface crack-scattered nonlinear rayleigh waves: A full analytical solution based on elastodynamic reciprocity theorem. *Ultrasonics*, 118, 106578. doi: https://doi.org/10.1016/j.ultras.2021.106578.

Yamada, H., Hasegawa, T., Ishihara, Y., Kiwa, T. & Tsukada, K. (2008). Difference in the detection limits of flaws in the depths of multi-layered and continuous aluminum plates using low-frequency eddy current testing. *Ndt & E International*, 41(2), 108–111. doi: https://doi.org/10.1016/j.ndteint.2007.08.004.

Yan, W.-B., Fan, Y.-X., Liu, H., Zhang, R.-Z. & Tao, Z.-Y. (2018). Mode conversion detection in an elastic plate based on Fizeau fiber interferometer. *Applied Acoustics*, 141, 234-239. doi: https://doi.org/10.1016/j.apacoust.2018.07.013.

Yang, X., Wang, K., Zhou, P., Xu, L. & Su, Z. (2022). Imaging damage in plate waveguides using frequency-domain multiple signal classification (F-MUSIC). *Ultrasonics*, 119, 106607. doi: https://doi.org/10.1016/j.ultras.2021.106607.

Yusa, N., Hashizume, H., Urayama, R., Uchimoto, T., Takagi, T. & Sato, K. (2014). An arrayed uniform eddy current probe design for crack monitoring and sizing of surface breaking cracks with the aid of a computational inversion technique. *NDT & E International*, 61, 29–34. doi: https://doi.org/10.1016/j.ndteint.2013.09.004.

Zeng, W., Qi, S., Liu, L. & Yao, Y. (2019). Research on laser-generated Rayleigh waves with angled surface crack by finite element method. *Optik*, 181, 57-62. doi: https://doi.org/10.1016/j.ijleo.2018.11.105.

Zhang, J., Drinkwater, B. W. & Wilcox, P. D. (2010). The use of ultrasonic arrays to characterize crack-like defects. *Journal of Nondestructive Evaluation*, 29(4), 222–232.

Zhang, S., Li, X. & Jeong, H. (2017). Measurement of Rayleigh wave beams using angle beam wedge transducers as the transmitter and receiver with consideration of beam spreading. *Sensors*, 17(6), 1449. doi: 10.3390/s17061449.

Zhang, S., Li, X., Jeong, H. & Hu, H. (2018). Experimental investigation of material nonlinearity using the Rayleigh surface waves excited and detected by angle beam wedge transducers. *Ultrasonics*, 89, 118-125. doi: https://doi.org/10.1016/j.ultras.2018.05.004.

Zhang, S., Cheng, C., Li, X. & Kundu, T. (2022). Fast Fourier transform method for determining velocities of ultrasonic Rayleigh waves using a comb transducer. *Ultrasonics*, 124, 106754. doi: https://doi.org/10.1016/j.ultras.2022.106754.

Zhang, Z., Zhao, J. & Pan, Y. (2020). Surface circular-arc defects interacted by laser-generated Rayleigh wave. *Ultrasonics*, 103, 106085. doi: https://doi.org/10.1016/j.ultras.2020.106085.

Zhou, Z., Zhang, K., Zhou, J., Sun, G. & Wang, J. (2015). Application of laser ultrasonic technique for non-contact detection of structural surface-breaking cracks. *Optics & Laser Technology*, 73, 173-178. doi: https://doi.org/10.1016/j.optlastec.2015.04.026.

Zhu, W. & Rose, J. (1999). Lamb wave generation and reception with time-delay periodic linear arrays: a BEM simulation and experimental study. *IEEE Transactions on Ultrasonics, Ferroelectrics, and Frequency Control*, 46(3), 654-664. doi: 10.1109/58.764852.

Zolfaghari, A., Zolfaghari, A. & Kolahan, F. (2018). Reliability and sensitivity of magnetic particle nondestructive testing in detecting the surface cracks of welded components. *Nondestructive Testing and Evaluation*, 33(3), 290–300.